UNIVERSITY OF CAPE TOWN

Faculty of Engineering and the Built Environment

Department of Civil Engineering

MSc. Dissertation

Ezekiel Arito

Assessment and prediction of chloride ingress and carbonation in patch repair mortars

Supervisor:

Associate Professor Hans Beushausen

February 2016

Assessment and Prediction of Chloride Ingress and Carbonation in Patch Repair Mortars

Ezekiel Arito

Submitted to the Faculty of Engineering and the Built Environment, University of Cape Town, on the 12th of February 2016, in partial fulfilment of the requirements for the degree of Master of Science in Civil Engineering

Cape Town, 2016

Declaration

This dissertation is being submitted for the degree of Master of Science in Engineering in the University of Cape Town, Cape Town, South Africa. It has not been submitted before for any degree in any other university. In addition, I know the meaning of plagiarism and declare that all the work in the document, save for that which is properly acknowledged, is my own.

(Signature of candidate)

12th Day of February 2016

Abstract

The specifications for concrete patch repair mortars usually entail mechanical properties such as compressive strength and tensile strength. However, these properties may not directly relate to the desired performance in relation to durability and prevention of reinforcement corrosion. In addition, the literature does not show any direct relationship between compressive strength and durability properties of concrete and mortars in natural exposure conditions. Relevant performance requirements, such as carbonation resistance and chloride resistance, are usually not considered despite the fact that they have a direct influence on the durability performance of concrete repair mortars. The widespread premature failure of patch repairs which meet the existing compressive strength criteria implies that the use of compressive strength as a performance indicator may not provide a reliable measure of the durability performance. Therefore it can be argued that modern concrete repairs should be based on durability considerations, rather than compressive strength.

In this study, an experimental investigation was conducted to determine the durability performance of patch repair mortars. Experimental results were analysed to investigate the correlations that exist between (i) electrical conductivity (Chloride Conductivity Index test) and rate of chloride-ion diffusion (bulk diffusion test), and (ii) gas permeability (Oxygen Permeability Index test) and rate of carbonation (accelerated carbonation test) in patch repair mortars. Eight mortar mixes were used in the investigation, including four commercially available repair mortars and four laboratory-made mortar mixes. To vary the pore structure of the laboratory mixes, different water/binder ratios (0.45 and 0.60) and binder types (100% Portland cement and 50/50 blend of Portland cement/blast furnace slag) were used to make the mortar specimens. Two curing conditions (dry and moist) were adopted with the aim of investigating the influence of curing on durability performance of patch repair mortars.

Test results indicate good correlations between electrical conductivity and rate of chloride diffusion (correlation coefficient of 0.9112), and between oxygen permeability and rate of carbonation (correlation coefficient of 0.6751). This correlation was mainly attributed to the fact that these material properties largely depend on the pore structure (specifically the size, connectivity and tortuosity of pores). The good correlation further implies that electrical conductivity and oxygen permeability of repair mortars as evaluated by the CCI and OPI tests may provide a reasonable measure of chloride resistance and carbonation resistance respectively. However, the prediction of chloride ingress and carbonation depth from the

electrical and gas permeability properties respectively, ought to be implemented within the range where reasonable correlation can be established. The results also showed that the durability performance of repair mortars in terms of chloride and carbonation resistance is sensitive to material factors, such as w/b ratio, curing type and binder type, which directly influence penetrability.

Service life models for predicting chloride ingress and carbonation in the patch repair mortars used in this study were developed based on modified Fickian equations. The prediction profiles for chloride penetration were developed from a modified solution to Fick's second law of diffusion, while the carbonation depth prediction profiles were developed from the square-root-of-time law. Chloride penetration and carbonation depth could be predicted using the developed profiles. Though several assumptions that should be verified and/or modified in future work were made, the modelling results of this study serve as useful framework for evaluating the resistance to chloride ingress and carbonation in patch repair mortars.

Acknowledgements

I would like to thank my supervisor, Associate Professor Hans Beushausen for his guidance and support throughout this study. It was great working together.

The contributions from Dr. Björn Höhlig and Mr. Philemon Arito, more so at the inception of this research were vital and are highly appreciated.

I would also wish to acknowledge with gratitude the following for financial support and materials for this research: The Cement and Concrete Institute, The National Research Foundation (NRF), PPC, Sika (SA) Pty Ltd., The Concrete Manufacturer's Association, The Tertiary Education Support Programme (TESP) of ESKOM, the Water Research Commission (WRC) and the University of Cape Town through the Concrete Materials and Structural Integrity Research Unit (CoMSIRU).

Special thanks also goes to the Civil Engineering laboratory staff at the University of Cape Town concrete laboratory for their support and technical assistance during my experiments.

I gratefully acknowledge my colleagues in CoMSIRU for making my experience at the University of Cape Town interesting and memorable.

Table of Contents

Declaration ii
Abstract iii
Acknowledgements v
List of Tables x
List of Figures xi
Notations xiv
CHAPTER 1: INTRODUCTION 1
1.1 Background 1
1.2 Problem statement 3
1.3 Research motivation and significance 4
1.4 Objectives 4
1.5 Scope and limitations 5
1.6 Thesis outline 5
CHAPTER 2: LITERATURE REVIEW 7
2.1 Introduction 7
2.2 Concrete durability 7
2.3 Reinforcement corrosion 9
2.3.1 Carbonation-induced reinforcement corrosion 11
2.3.2 Chloride-induced reinforcement corrosion 12
2.3.3 Influence of electrical resistivity on reinforcement corrosion 13
2.3.4 Influence of the environment on reinforcement corrosion 13
2.3.5 Influence of concrete cover on reinforcement corrosion 14
2.3.6 Influence of oxygen availability on reinforcement corrosion 14
2.3.7 Influence of cracks on reinforcement corrosion 15
2.4 Factors affecting penetrability of cement-based materials 15
2.4.1 Water/binder ratio 16
2.4.2 Binder type 16
2.4.3 Curing practice 17

2.4.4 Environmental factors 19

2.5 Chloride transport 20

2.5.1 Mechanisms of chloride-ion transport 20
2.5.2 Chloride diffusion coefficient 27
2.5.3 Chloride binding 29
2.5.4 Chloride binding isotherms 30
2.5.5 Reference tests for chloride ingress 31
2.5.6 Service life prediction models for chloride ingress 38

2.6 Carbonation 42

2.6.1 Carbonation reactions 43
2.6.2 Carbonation coefficient 45
2.6.3 Effects of carbonation on pore structure 45
2.6.4 Reference tests for carbonation 45
2.6.5 Service life prediction models for carbonation 51

2.7 Influence of aggregate size on penetrability 54
2.8 Performance of patch repair mortars 57

2.8.1 Cracking resistance 57
2.8.2 Penetration resistance in repair mortars 58
2.8.3 Relationship between porosity and permeability 58
2.8.4 Effects of self-sealing and autogenous healing 59

2.9 Summary 60

CHAPTER 3: EXPERIMENTAL METHODOLOGY 62

3.1 Introduction 62
3.2 Test materials 64

3.2.1 Laboratory mixes 64
3.2.2 Commercial repair products 66

3.3 Experimental variables 67

3.3.1 Water/binder ratio 67
3.3.2 Binder type 67
3.3.3 Curing conditions 67

3.4 Specimen preparation 68

3.4.1 Mix design 68
3.4.2 Casting and curing 69
3.4.3 Exposure conditions 72

3.5 Test methods 74

3.5.1 Bulk diffusion test 74
3.5.2 Chloride conductivity index test 75
3.5.3 Accelerated carbonation test 76
3.5.4 Oxygen permeability index test 77
3.5.5 Compressive strength test 78

3.6 Closure 78

CHAPTER 4: RESULTS AND DISCUSSION 79

4.1 Introduction 79
4.2 Chloride-ion resistance measurements 79

4.2.1 Chloride-ion diffusion 80
4.2.2 Chloride conductivity 82
4.2.3 General discussion of chloride-ion resistance results 83
4.2.4 Correlation between chloride diffusion and chloride conductivity 86

4.3 Carbonation resistance measurements 87

4.3.1 Accelerated carbonation depth 87
4.3.2 Oxygen permeability 88
4.3.3 General discussion of carbonation resistance results 89
4.3.4 Correlation between carbonation depth and oxygen permeability 91

4.4 Closure 93

CHAPTER 5: SERVICE LIFE PREDICTION 95

5.1 Introduction 95

5.2 Prediction of chloride ingress 95

5.2.1 Time-dependent chloride diffusion coefficient 95

5.2.2 Time-dependent surface chloride content 97

5.2.3 Chloride threshold values 99

5.2.4 Estimation of binder content in commercial mortars 100

5.2.5 Prediction profiles for chloride ingress 101

5.3 Prediction of carbonation 105

5.3.1 Carbon dioxide concentration 105

5.3.2 Relationship between accelerated and natural carbonation depths 106

5.3.3 Prediction profiles for carbonation depth 108

5.4 Closure 111

CHAPTER 6: CONCLUSIONS AND RECOMMENDATIONS 112

6.1 Introduction 112

6.2 Summary of the major findings 112

6.2.1 Effect of curing on penetration resistance 112

6.2.2 Effect of water/binder ratio on penetration resistance 113

6.2.3 Effect of binder type on penetration resistance 113

6.2.4 Correlations between material transport properties 114

6.2.5 Modelling of chloride penetration and carbonation 114

6.3 Recommendations 115

REFERENCES 117

Appendix A: Experimental results 132

Appendix B: Summarised procedures for tests and data analysis 144

Appendix C: Salient details of the commercial repair products used 146

Appendix D: EBE Faculty: Assessment of Ethics in Research Projects 147

List of Tables

Table 2.1: Environmental classes according to BS EN 206 42
Table 3.1: Typical composition of CEM II 64
Table 3.2: Chemical composition, in terms of oxides, of South African GGBS 65
Table 3.3: Description of the commercial repair products used in this study 66
Table 3.4: Summary of mix design and proportions 69
Table 4.1: Descriptions of names of the mortar mixes used 79
Table 4.2: Diffusion coefficients and surface chloride content of the mortar mixes 80
Table 4.3: Percentage increase in diffusion coefficients, surface chloride content and chloride conductivity with increase in w/b ratios in specimen with w/b ratios of 0.45 to 0.60. 83
Table 5.1: Values of aging coefficient, *m* as published in various literatures 96
Table 5.2: One-year predictions of the effective diffusion coefficients using Equation 5.2 ... 97
Table 5.3: Empirical coefficients for various exposure conditions 98
Table 5.4 One-year predictions of the surface chloride content using Equation 5.3 99
Table 5.5: Chloride threshold values as presented in various publications 100
Table 5.6: Estimated binder contents of the commercial mortars 101
Table 5.7: Equations for modelling chloride ingress for mortar mixes used in this study 102
Table 5.8: Carbon dioxide concentration in ppmv based on land use. 106
Table 5.9: A summary of one-month (31 days) accelerated carbonation depths and the corresponding natural carbonation depths 107
Table A.1: Compressive strength test results 133
Table A.2: Chloride conductivity values of the mortar mixes 134
Table A.3: Carbonation depth measurements of the laboratory-made mortar mixes after 12 weeks of exposure in the carbonation chamber. 139
Table A.4: Carbonation depth measurements of the commercial mortar mixes after 12 weeks of exposure in the carbonation chamber. 140
Table A.5: Carbonation coefficients of the mortar mixes 141
Table A.6: OPI results showing the OPI values and the corresponding permeability coefficients of the mortar mixes. 143

List of Figures

Figure 2.1: Schematic of the Duracrete 2000 probabilistic service life 8
Figure 2.2: Electrochemical reactions leading to steel corrosion 9
Figure 2.3: Three-phase deterioration model for steel reinforcement corrosion 10
Figure 2.4: Expansive products of corrosion and their effects on concrete-steel interface 11
Figure 2.5: Schematic of carbonation-induced steel corrosion 12
Figure 2.6: Schematic of chloride-induced steel corrosion 13
Figure 2.7: General relationship between carbonation depth and time to initiation of reinforcement corrosion 14
Figure 2.8: Effect of w/b ratio on the rate of carbonation 16
Figure 2.9: Effects of curing practice on strength and service life in carbonating conditions with reference to 6-day ponding 18
Figure 2.10: Effects of curing practice on strength and service life in chloride conditions with reference to 6-day ponding 18
Figure 2.11: Correlation between results of Torrent air permeability and method of curing 19
Figure 2.12: Mechanism of capillary absorption 24
Figure 2.13: Convection zone in concrete cover 25
Figure 2.14: Typical chloride profile fit 28
Figure 2.15: Effects of binder type on chloride transport in concretes of different strength grades tested 28 days after casting 30
Figure 2.16: Set up for salt ponding test 32
Figure 2.17: Set up for bulk diffusion test 33
Figure 2.18: Experimental arrangement for migration tests 34
Figure 2.19: Set up for rapid chloride permeability test 35
Figure 2.20: Set up for rapid migration test 36
Figure 2.21: Schematic diagram of the two-cell conduction rig for CCI test 36
Figure 2.22: Schematic of the Four-Point Wenner Probe. 38
Figure 2.23: Diffusion of CO_2 in partially filled pore system 43
Figure 2.24: Schematic of carbonation mechanism 44
Figure 2.25: Carbonation depth measurements 46
Figure 2.26: Typical set-up of a diffusion cell 47
Figure 2.27: Schematic diagram of the falling head permeameter 48
Figure 2.28: Schematic representation of the Cembureau pressure cell 50

Figure 2.29: Torrent permeability test apparatus 50
Figure 2.30: Schematic of Autoclam air permeability test 51
Figure 2.31: SEM images of (a) 90-day mortar containing 70% sand volume fraction, and (b) 90-day concrete containing 70% aggregate (coarse and fine) volume fraction 55
Figure 2.32: SEM image showing microcracks on concrete specimen subjected to a temperature of 105^0C, simulating those caused by drying shrinkage. 56
Figure 2.33: Schematic of porosity and permeability 59
Figure 3.1: Flowchart showing experimental set-up 63
Figure 3.2: Grading curve of 50/50 blend of dune and crusher sand 65
Figure 3.3: Specimens subjected to dry and moist curing conditions in an environmentally controlled room 68
Figure 3.4: (a) Illustration of the core-drilling process, and (b) obtained cylindrical discs 70
Figure 3.5: Cylindrical specimens used in the bulk diffusion test 70
Figure 3.6: Specimens used in the accelerated carbonation test 71
Figure 3.7: Cube specimens used in the compressive strength test 71
Figure 3.8: Oven-drying of the OPI and CCI disc specimens 72
Figure 3.9: (a) Specimen sealed with epoxy resin, and (b) specimens submerged in 3g/L calcium hydroxide solution 73
Figure 3.10: The Mettler Toledo DL50 potentiometric titrator 75
Figure 3.11: Apparatus used for CCI test 76
Figure 3.12: The falling head permeameter used in the OPI test 77
Figure 4.1: Diffusion coefficients of the mortar mixes 81
Figure 4.2: Surface chloride content of the mortar mixes 81
Figure 4.3 Chloride conductivity of the mortar mixes used in this study 82
Figure 4.4: Chloride conductivity versus diffusion coefficient of the mixes 86
Figure 4.5: Carbonation depth measurements of mortar mixes after 12 weeks of exposure in the carbonation chamber 87
Figure 4.6: OPI results of the mortar mixes used 88
Figure 4.7: Permeability coefficients obtained from the OPI values of the mixes 89
Figure 4.8: Carbonation coefficient after 12 weeks of exposure versus coefficient of permeability 92
Figure 4.9: Carbonation coefficient versus OPI for all the mortar mixes after 12 weeks of exposure 92
Figure 5.1: 28-day compressive strength versus w/b ratio for the CEM II specimens 101

Figure 5.2: Chloride penetration profiles showing the rate of accumulation of chloride ions at a cover depth of 30 mm, for all the mortar mixes used. 103
Figure 5.3: Chloride penetration profiles showing the rate of accumulation of chloride ions at a cover depth of 40 mm, for all the mortar mixes used. 104
Figure 5.4: Linear relationship between one-month natural carbonation depth and one-month accelerated carbonation depth 108
Figure 5.5: Carbonation depth profiles showing the predicted carbonation depths in the laboratory-made mortar mixes 109
Figure 5.6: Carbonation depth profiles showing the predicted carbonation depths in the commercial mortar mixes 110
Figure A.1: Grading curve of Philippi dune sand 132
Figure A.2: Grading curve of crusher sand 132
Figure A.3: 7-day and 28-day compressive strength results 134
Figure A.4: Chloride profiles for (a) PM45 specimens and (b) PM60 specimens 135
Figure A.5: Chloride profiles for (a) SM45 specimens and, (b) SM60 specimens 136
Figure A.6: Chloride profiles for (a) CM1 specimens and, (b) CM2 specimens specimens 137
Figure A.7: Chloride profiles for (a) CM3 specimens and, (b) CM4 specimens 138
Figure A.8: Variation of temperature in the carbonation chamber 142
Figure A.9: Variation of relative humidity in the carbonation chamber 142
Figure A.10: A plot of chloride content versus profile depth 145

Notations

Abbreviations:

ACT – accelerated carbonation test
BDT – bulk diffusion test
$CaCO_3$ – calcium carbonate
CCI – chloride conductivity index
CH – calcium hydroxide ($Ca(OH)_2$)
Cl^- – chloride ions
CO_2 – carbon dioxide
CSH – calcium silicate hydrate
DI – durability index
GGBS – ground granulated blast-furnace slag
ITZ – interfacial transition zone
OPI – oxygen permeability index
PC – Portland cement
PM45 – laboratory-made PC mortar with w/b of 0.45
PM60 – laboratory-made PC mortar with w/b of 0.60
RC – reinforced concrete
RH – relative humidity
SCM – supplementary cementitious materials
CM1 – Sika® MonoTop®-612 (commercial repair product from *Sika SA (Pty) Ltd*.)
CM2 – Sika® MonoTop®-615 HB (repair product from *Sika SA (Pty) Ltd*.)
CM3 – Sika® Rep LW (commercial repair product from *Sika SA (Pty) Ltd*.)
CM4 – Sikacrete®-214 (commercial repair product from *Sika SA (Pty) Ltd*.)
SM45 – laboratory-made PC/GGBS mortar in 50/50 ratio with w/b of 0.45
SM60 – laboratory-made PC/GGBS mortar in 50/50 ratio with w/b of 0.60
SSE – self-sealing effect
w/b – water-binder ratio

Letters and symbols:

A – carbonation coefficient

C_s – surface chloride content

C_x – chloride content at depth x from the surface

d_c – carbonation depth

D_{eff} – effective diffusion coefficient

erf – error function

k – coefficient of permeability

m – aging factor

n – empirical coefficient

CHAPTER 1: INTRODUCTION

1.1 Background

Reinforced concrete (RC) is the most extensively used construction material, primarily due to its exceptional resistance to water, the ease with which the structural elements can be cast into different shapes and sizes, and its availability in most parts of the world (Mehta and Monteiro, 2006). Concrete provides physical and chemical protection to the reinforcing steel against attack by aggressive chemical species such as chloride ions and carbon dioxide, thus making RC a durable construction material. Concrete structures are intended to last for decades or even centuries.

However, the problem of premature deterioration of RC structures, more specifically those exposed to harsh conditions such as marine environments, continues to be a serious issue in the concrete construction industry. Several researchers have acknowledged the gravity of the problem through developing and promoting the implementation of performance-based specifications approach over the prescriptive method, in order to facilitate quality control of concrete as well as enable service life prediction of RC structures (Bickley *et al.*, 2006a, 2006b; Beushausen and Alexander, 2008; Baroghel-Bouny *et al.*, 2011; Alexander and Thomas, 2015). Whether the proposed approach can be used to enhance a repair-free service life is a matter of particular interest to modern construction. For the existing RC structures facing premature deterioration, durable repair measures are needed. The deterioration of large reinforced concrete structures such as nuclear power plants and other structures built in aggressive environments, for example, calls for durable repairs.

There exist a variety of methods for concrete repair. Common among these is the use of repair mortars to replace damaged (cracked, delaminated or spalled) or contaminated (with chloride ions or carbonation) sections of concrete, as well as to restore the load-bearing capacity of concrete members (Beushausen and Alexander, 2009). Repair mortars play a significant role in the prevention of corrosion of steel reinforcement in repaired concrete structures. To enhance durable concrete repairs, patch repair mortars ought to (i) protect the embedded steel from the aggressive species which initiate steel corrosion, and (ii) restore passivity to steel by maintaining an alkaline environment that promotes steel passivation.

It is clear that deteriorating RC structures require durable repairs in order to realise their remaining service life. The durability of concrete and mortars is largely controlled by transport processes such as diffusion, permeation, capillary absorption and wick action, which occur within their pore system (Mackechnie and Alexander, 2002; Nilsson, 2003). The transport of fluids and aggressive chemical species play a significant role in reducing the service life of RC structures. The ease with which water, chloride ions and carbon dioxide penetrates the concrete determines the rate of deterioration of RC structures (Mehta and Monteiro, 2006). The key aspects of durability, which comprise resistance to chloride ingress and resistance to carbonation, therefore are vital in the design of durable repair mortars (Oh and Jang, 2007).

It has been reported that chloride ingress and carbonation are the main mechanisms that initiate reinforcement corrosion. Literature further suggests that reinforcement corrosion is the main cause of deterioration in RC structures (Martin-Perez, 1999; Saraswathy and Song, 2002; Glass, 2003; Roziere *et al.*, 2009). The damage to concrete members due to corrosion of steel is manifested in the forms of cracking, spalling and delamination, which emanate from the accumulation of corrosion products that occupy a volume greater than that of the original steel (Kovacs, 2000; Papadakis, 2000; Ballim *et al.*, 2009).

Service life prediction models are necessary for the assessment of service life of reinforced concrete structures in various exposure conditions (Rooij *et al.*, 2007). Several empirical and numerical models for predicting chloride penetration and carbonation in cement-based materials have been proposed for concrete. It is important to note that these models have not been verified for common types of patch repair mortars.

The diffusion of carbon dioxide in cement-based materials can be predicted by models based on Fick's law of diffusion, e.g. the DuraCrete model. These models predict carbonation depth development with time. They assume a constant diffusion coefficient for carbon dioxide, though studies have shown that the diffusion coefficient varies with time, depth and moisture content of the pores (Costa and Appleton, 2001; Czarnecki and Woyciechowski, 2015). The models however, provide reasonable estimation of concrete carbonation with time. Service life prediction models for chloride ingress have been developed to describe the performance of concrete in an environment containing chlorides, e.g. LIFE-365 and DuraCrete model for chloride ingress. The long-term prediction of chloride penetration in cement-based materials

takes into account the time-dependent diffusion coefficient and surface chloride concentration (Lindvall, 2000; Shukla and Pillai, 2015; Tang *et al.*, 2015).

1.2 Problem statement

Mechanical properties, such as compressive strength are often used to specify concrete patch repair mortars for various repair applications (Bickley *et al.*, 2006b). However, these properties may not directly relate to the desired performance. In addition, literature does not show any direct relationship between compressive strength and durability properties of concrete and mortars exposed to real environments. Thus, the compressive strength per se may not provide a reliable measure of the durability performance of patch repair mortars.

Research by several authors has established that there exists a direct relationship between penetration resistance (resistance to chloride ingress and carbonation) and durability of cement-based materials. This consequently implies that carbonation resistance and chloride resistance would provide a better measure of the durability performance of patch repair mortars. Thus, it is deemed beneficial that the specification of concrete patch repair mortars ought to take into account these key aspects that affect durability directly instead of material properties such as compressive strength. This approach is similar to the recently proposed performance-based design approach for concrete structures (Bickley *et al.*, 2006b).

Performance requirements for repair mortars have been addressed in the European Standard EN 1504-3:2005. From the provided specifications, it is evident that chloride-ion resistance and carbonation resistance have not been dealt with comprehensively. A limiting value of electrical conductivity, for example, might provide a more practical specification than chloride ion content since a majority of the methods commonly used to measure chloride-ion resistance, such as the CCI test and the Four-probe (Wenner) method, apply the principle of conductivity (or resistivity). Similarly, a limiting value of gas permeability may be applicable since a majority of the tests that measure carbonation resistance, for example the OPI test and the Torrent permeability test, use the principle of gas permeability.

In addition, there is a need to establish whether these commonly applied durability test methods can provide reasonable measures of the resistance of concrete patch repair mortars to chloride ingress and carbonation. This can be achieved by investigating the correlations between various test methods as outlined in the objectives of this study.

1.3 Research motivation and significance

Modern concrete repairs ought to be based on durability considerations rather than compressive strength. To predict the durability performance of patch repair mortars, the resistance to penetration of the aggressive chemical species must be evaluated. The evaluation ought to be based on more relevant material properties that directly or indirectly relate to transport processes of these species. Some of these material properties, as mentioned in the previous sections, include chloride conductivity, chloride diffusion coefficient, gas permeability and carbonation coefficient.

To predict the resistance of mortars to chloride ingress and carbonation, a better understanding of the transport processes and their governing laws is critical. In addition, an in-depth knowledge of concrete deterioration mechanisms such as reinforcement corrosion is essential since these mechanisms have a direct influence on the durability of RC structures. The durability of concrete repairs can be improved by developing and specifying patch repair mortars with tailor-made material properties, depending on the exposure conditions.

The prediction of chloride-ion resistance and carbonation resistance of patch repair mortars may provide reliable estimates of the potential durability of concrete repairs. With this in mind, a better understanding of the performance requirements for patch repair mortars will assist asset owners, manufacturers and engineers to plan and execute cost effective and durable concrete repairs. In addition, durability of concrete repairs will be improved owing to the fact that appropriate consideration will be given to (i) the exposure environment, and (ii) the choice of penetration-influencing parameters such as concrete quality and cover depth.

1.4 Objectives

The objectives of this research are:

i) To predict the service life of the mortars used in this study in terms of chloride ingress and carbonation using Fick's laws of diffusion.
ii) To investigate the correlations, for mortars, between:
    a) Chloride Conductivity Index (CCI) test and bulk diffusion test,
    b) Oxygen Permeability Index (OPI) test and accelerated carbonation test.
iii) To investigate the effects of varying parameters such as water/binder ratio, binder type and curing type on the penetration resistance of patch repair mortars.

1.5 Scope and limitations

The scope and limitations of this study can be summarized as follows:

i) Two aspects of durability were investigated, namely chloride resistance and carbonation resistance.
ii) The properties of uncracked mortars were studied; the effects of cracking on durability were not considered.
iii) Only a limited number of parameters affecting penetrability of mortars were considered. These comprised: (a) two water/binder ratios (0.45 and 0.60), two binder types (100% CEM II (A-L) 52.5N and 50/50 CEM II/GGBS), and (c) two curing types (dry curing and moist (wet hessian) curing).
iv) Tests were done on commercially available and laboratory-made mortar mixes.
v) Penetration resistance of mortars was evaluated by taking the following measurements: (a) diffusion coefficient (using bulk diffusion test), (b) chloride conductivity (using CCI test), (c) accelerated carbonation test (in the carbonation chamber), and (d) oxygen permeability (using OPI test).
vi) Specimens were exposed to controlled laboratory conditions (temperature, relative humidity and carbon dioxide concentration) in an environmental room and carbonation chamber.

1.6 Thesis outline

This thesis comprises six chapters. The contents of each chapter are as follows:

Chapter 1 presents an introduction to the study, covering the theoretical background of research. Also included are: the problem statement, research motivation and significance, objectives, and scope and limitations of the study.

Chapter 2 presents a review of literature in three main areas. Firstly, concrete durability is covered, with emphasis on corrosion of reinforcing steel and its influencing factors. In addition, processes that often lead to concrete deterioration (chloride transport and carbonation) are reviewed, including the commonly applied reference tests and service life prediction models. Lastly, a discussion on performance of patch repair mortars and its influencing factors is presented.

Chapter 3 presents a description of the experimental work performed in the laboratory. These include the test materials used, experimental variables, specimen preparation, exposure conditions and evaluation techniques. Furthermore, reasons for choice of materials and experimental variables are provided.

Chapter 4 presents the experimental results, analyses and discussions of the obtained results. In this Chapter, the effects of the experimental variables on penetration resistance are covered. In addition, the results of various tests as mentioned in objective (ii) are compared to determine the level of correlation.

Chapter 5 presents the service life prediction models for chloride-ion penetration and carbonation of patch repair mortars. The models are based on the experimental results presented in Chapter 4.

Chapter 6 presents the conclusions drawn from the experimental results, literature and the discussion presented in Chapter 4. Also included in this Chapter are recommendations for future work in this area.

Also included in this dissertation are detailed experimental results and procedures for some test methods. These are presented within the Appendices.

CHAPTER 2: LITERATURE REVIEW

2.1 Introduction

This chapter reviews durability and repair of RC structures. Reinforcement corrosion, viewed as the main cause of deterioration in RC structures, is briefly covered. In addition, decisive transport processes that lead to chloride-induced and carbonation-induced corrosion of steel reinforcement are reviewed. Also included in this chapter are reference tests and service life prediction models for chloride ingress and carbonation. Finally, a discussion on the actual performance of repair mortars and its influencing factors is presented.

2.2 Concrete durability

The subject of concrete durability has received particular attention in the recent past (Miyagawa, 1991; Polder, 2005; Bickley *et al.*, 2006a; Alexander *et al.*, 2008). This can be attributed to the increasing socio-economic challenges that emanate from the growing need for repair and maintenance of RC structures (Vanier, 2001). Durability refers to the ability of a concrete structure to withstand the exposure conditions of its environment. It is often described in terms of the resistance to the penetration of aggressive substances such as chloride ions and carbon dioxide (Hearn *et al.*, 2006; Bentur and Mitchell, 2008; Ballim *et al.*, 2009). Durability, in RC structures entails the protection of reinforcing steel against corrosion, which is caused by these aggressive substances (Ballim *et al.*, 2008).

The durability of RC structures can be quantified in terms of service life. Service life is the period during which a concrete structure is required to fulfil its performance requirements without non-intended maintenance (Nilsson, 2003). The 'structural limit state design philosophy' outlined in DuraCrete 2000, defines service life as the period in which the *resistance, R(t)* of a structure can withstand the environmental *load, S(t)* (Wegen *et al.*, 2012). Figure 2.1 illustrates this philosophy.

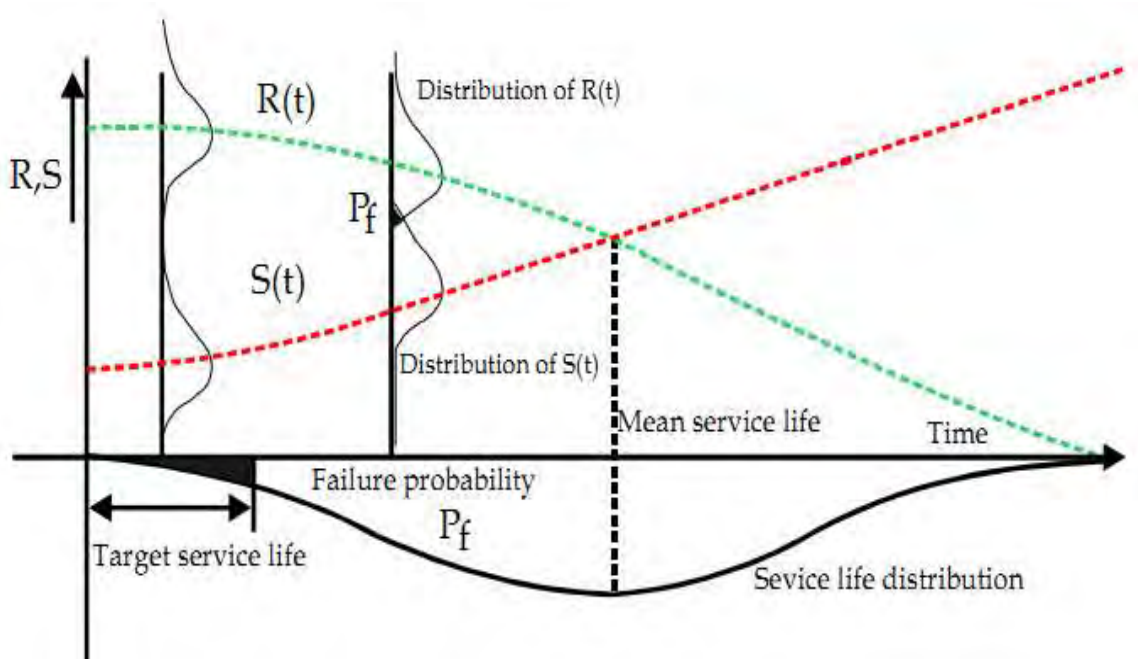

Figure 2.1: Schematic of the Duracrete 2000 probabilistic service life (Wegen *et al.*, 2012)

The initiation of reinforcement corrosion may be regarded as the *limit state*; the chloride content that increases at the level of steel may represent the *load*, *S(t)*; and the critical chloride threshold at steel level may signify *resistance*, *R(t)*. The prediction of performance of the structure is based on predetermined maximum probability of failure at the end of service life (Gjorv, 2009; Wegen *et al.*, 2012).

Service life design considers durability models as tools for predicting future deterioration of concrete structures. The prerequisites for service life design include relevant and quantifiable performance requirements; environmental conditions, including possible future changes; the deterioration mechanisms; and the prediction methods, which comprise performance tests and theoretical models (Nilsson, 2003). Due to high levels of uncertainty associated with modelling and prediction of corrosion propagation stage, most service life models assume a conservative approach, which defines the actual service life of RC structures as the end of the initiation phase (Savija, 2014). However, several researchers have argued that service life ought to take into account both initiation and propagation stages of reinforcement corrosion (Nilsson, 2003; Polder and Rooij, 2005; Otieno *et al.*, 2012).

2.3 Reinforcement corrosion

Steel that is embedded in concrete is often well protected against corrosion due to the formation of a thin protective film of γ iron oxide on its surface as a result of the high alkalinity during cement hydration. Corrosion, however, initiates when this protective film is destroyed as a result of concrete carbonation or accumulation of chloride ions at steel-concrete interface above a chloride threshold level. The electrochemical reactions that describe steel corrosion are (Papadakis, 2000; Gjorv, 2009; Ballim *et al.*, 2009; Savija, 2014):

Anodic reaction: $$Fe \rightarrow Fe^{2+} + 2e^{-} \quad (2.1)$$

Cathodic reaction: $$O_2 + 2H_2O + 4e^{-} \rightarrow 4OH^{-} \quad (2.2)$$

Figure 2.2 shows a schematic of these electrochemical reactions.

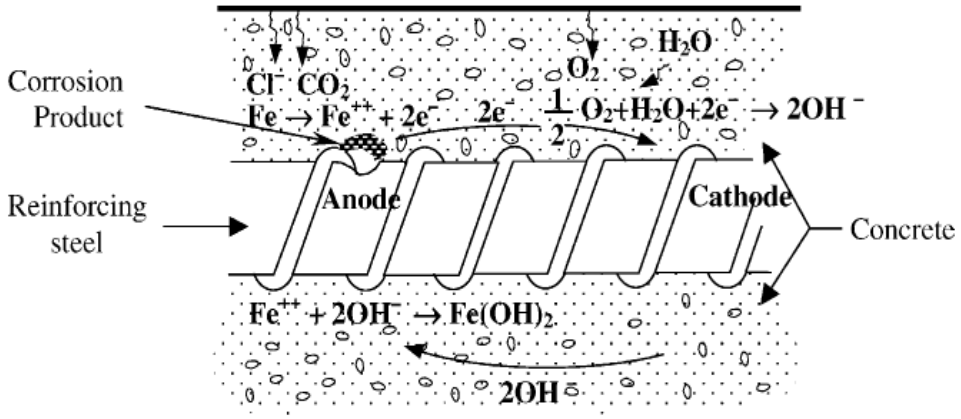

Figure 2.2: Electrochemical reactions leading to steel corrosion (Ahmad, 2003)

The two main stages of reinforcement corrosion are initiation and propagation. The steel surface becomes susceptible to corrosion during initiation stage whereas active corrosion occurs in the propagation stage (Arya and Wood, 1995). The effects of steel corrosion on durability can be summarised using a time-related deterioration model that takes into account the initiation, propagation and acceleration phases as illustrated in Figure 2.3.

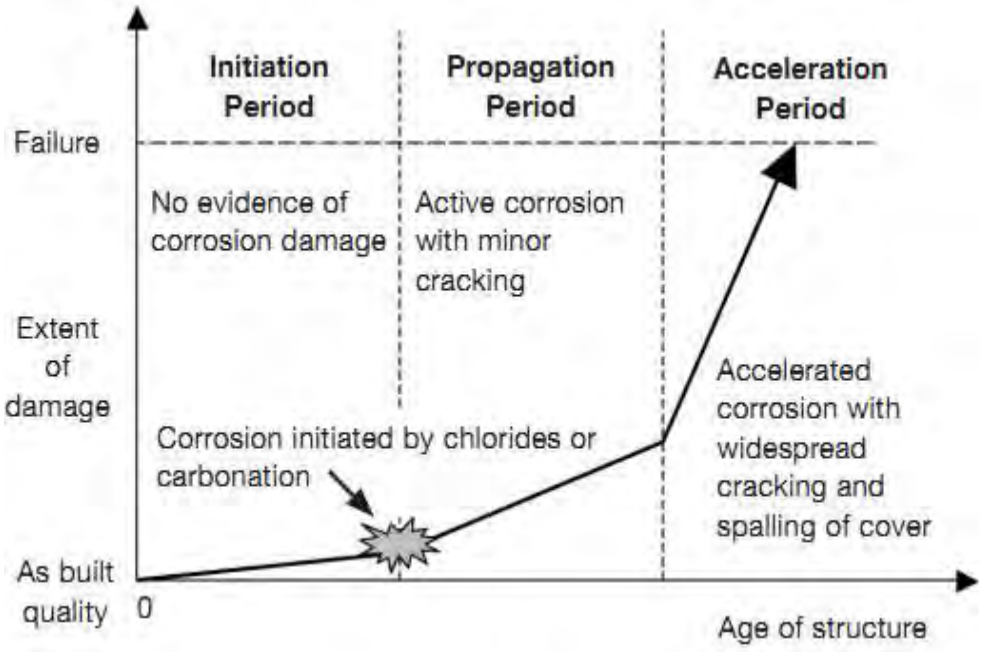

Figure 2.3: Three-phase deterioration model for steel reinforcement corrosion (Beushausen and Alexander, 2009)

The rate of reinforcement corrosion is generally influenced by the availability of oxygen and water, the number and size of voids and cracks, concrete resistivity and temperature (Taylor *et al.*, 1999; Ballim *et al.*, 2009). Other factors mentioned by Andrade *et al.* (2002) include the pH of pore solution and the concentration of chloride ions at the level of steel. The damage to concrete members due to corrosion of steel is manifested in the forms of cracking, rust staining, spalling and delamination, which result from the accumulation of expansive corrosion products that normally occupy a larger volume than the original steel (see Figure 2.4) (Kovacs, 2000; Papadakis, 2000; Glass, 2003). In addition, the loss of bond at the steel-concrete interface and the decrease in the cross sectional area of steel reduces the load-carrying capacity in structural members.

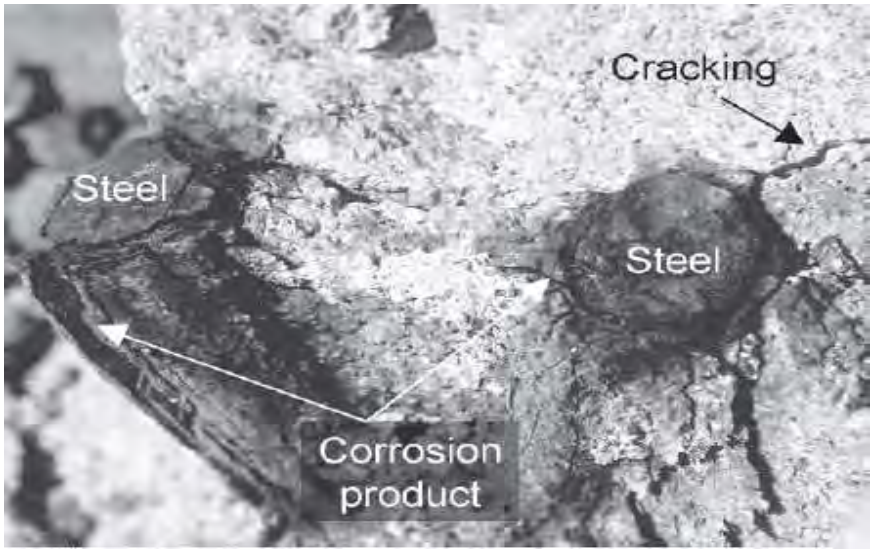

Figure 2.4: Expansive products of steel corrosion and their effects on concrete-steel interface (Glass, 2003)

The depassivation and subsequent corrosion of steel reinforcement is often initiated by the following factors (Papadakis, 2000; Ballim *et al.*, 2009):

i) Carbonation of concrete (to the level of steel-concrete interface) which lowers the high pH conditions essential for maintaining the protective gamma ferric-oxide film on the surface of steel.
ii) Penetration of aggressive chemical species to the steel-concrete interface which attacks the passive oxide film thus destroying it.

Carbonation-induced and chloride-induced steel corrosion and their influencing factors are presented in the subsequent sub-sections.

2.3.1 Carbonation-induced reinforcement corrosion

The carbonation of concrete is a common phenomenon in RC structures that are located in industrial and urban environments where the concentration of carbon dioxide in the atmosphere is high. Corrosion of steel in concrete is initiated when the high pH environment around the steel decreases due to the diffusion of carbon dioxide into the pore structure and the subsequent chemical reactions with cement hydrates (mainly portlandite and silica gel) in the presence of moisture. Lower pH conditions disrupts the protective ferric-oxide film on the steel surface resulting in depassivation and subsequent corrosion of steel (RILEM

Recommendations CPC-18, 1988; Roziere *et al.*, 2009). Figure 2.5 illustrates carbonation-induced steel corrosion. A detailed discussion on carbonation is presented in Section 2.6.

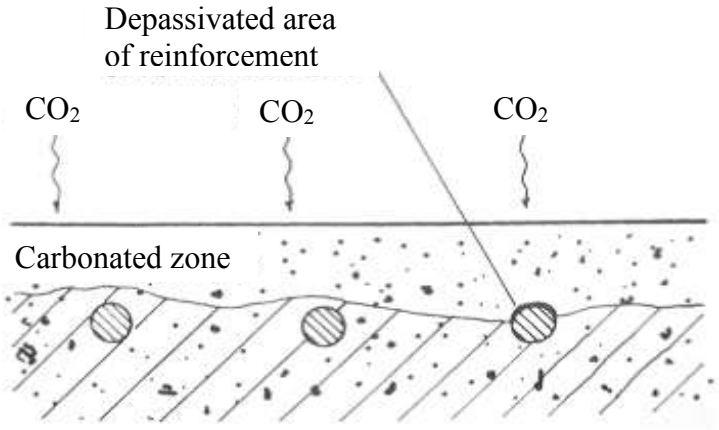

Figure 2.5: Schematic of carbonation-induced steel corrosion (Richardson, 2002)

The time to corrosion initiation depends on the rate at which the carbonation front progresses. Factors that govern the rate of movement of the carbonation front include carbon dioxide concentration, ambient temperature, moisture content and the amount of cement hydrates (Mackechnie and Alexander, 2002; Atis, 2003).

2.3.2 Chloride-induced reinforcement corrosion

The deterioration of RC structures due to chloride-induced reinforcement corrosion is predominant in marine environments. The ingress of chloride ions, e.g., from sea sprays and de-icing salts, is enhanced by transport processes such as capillary absorption and diffusion. Figure 2.6 shows the schematics of chloride-induced steel corrosion. A comprehensive discussion on chloride transport is presented in Section 2.5. Corrosion of steel reinforcement is often initiated by the accumulation of chloride ions at the steel-concrete interface beyond a critical chloride threshold value. When the amount of accumulating chloride ions exceed the critical threshold level, the protective oxide film is destroyed resulting in corrosion initiation (Ballim *et al.*, 2009).

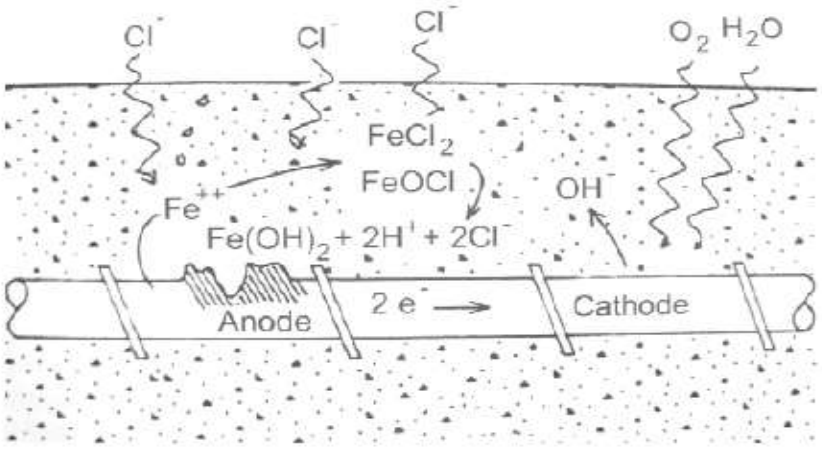

Figure 2.6: Schematic of chloride-induced steel corrosion (Richardson, 2002)

2.3.3 Influence of electrical resistivity on reinforcement corrosion

The resistivity of concrete has a considerable influence on the rate of steel corrosion. Resistivity is influenced by permeability, temperature, relative humidity, cover depth and the presence of aggressive and deleterious chemical species e.g. chloride ions (Building Research Establishment, 1998). When the electrical resistivity of concrete is low, galvanic cells develop along the embedded steel, resulting in the flow of current. The amount of current flowing determines the rate at which the steel will corrode.

In concrete of sufficiently high electrical resistivity, the rate of steel corrosion is very low or negligible. Factors that determine the amount of current flow in steel reinforcement include the size and geometry of the anodic and cathodic areas in the galvanic cells (Gjorv, 2009). The electrical current is transmitted through concrete by the charged ions. The electrical conductivity of concrete, therefore, depends on permeability, amount of pore solution and the concentration of ions in the pore solution (Gjorv, 2009).

2.3.4 Influence of the environment on reinforcement corrosion

Environmental conditions play a significant role in dictating the rate at which reinforcement corrodes, since carbon dioxide, oxygen, chlorides and moisture originate from the exposure environment. Under certain environmental conditions, the penetration of one or more of these aggressive species may be prevented or slowed, thus delaying corrosion (Arya and Wood, 1995). The aggressiveness of the environmental conditions also determines the severity of attack by chloride ions or carbonation. BS EN-1:2000 provides classification of environmental aggressiveness (Ballim *et al*., 2009).

2.3.5 Influence of concrete cover on reinforcement corrosion

Concrete cover refers the zone between the concrete surface and the reinforcing bar. Durability performance is highly sensitive to deficiencies in concrete cover. The quality of concrete cover determines its protective capacity against chloride penetration or carbonation. The premature deterioration of most RC structures can be attributed to failure to achieve the specified thickness and quality of concrete cover (Marsh, 2003b; Luco *et al.*, 2007; Theodosiou, 2009). Figure 2.7 shows the relationship between cover depth and time to initiation of reinforcement corrosion.

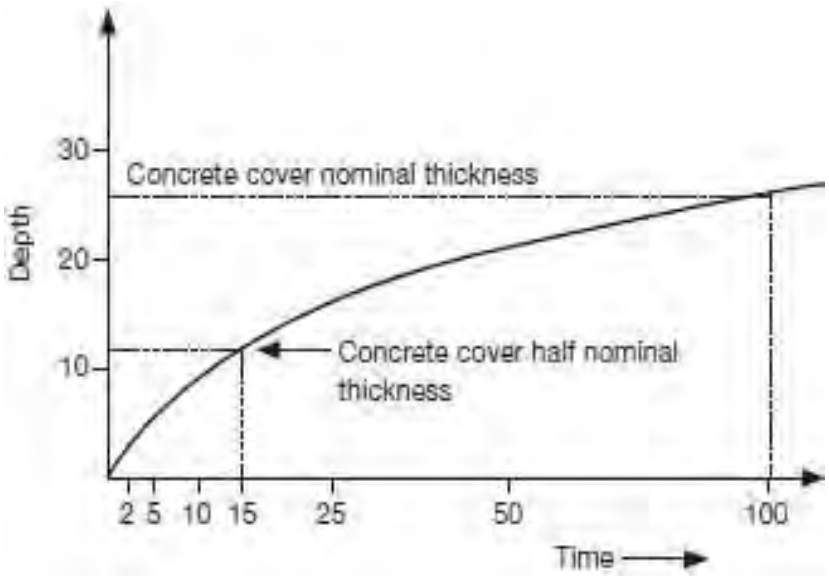

Figure 2.7: General relationship between carbonation depth and time to initiation of reinforcement corrosion (Theodosiou, 2009)

The specifications for minimum cover depths depends on the exposure conditions that have been stipulated in various codes of practice. The cover depth that meets the required thickness for the particular design is expected to provide adequate protection to the embedded steel (Martin-Perez, 1999). The thickness of the concrete cover also influences the crack width. The specifications for maximum cover depth is a measure that controls cracking (Marsh, 2003b; Luco *et al.*, 2007).

2.3.6 Influence of oxygen availability on reinforcement corrosion

The availability of oxygen has significant influence on the rate of steel corrosion, particularly during the propagation stage. In the presence of oxygen, the alkaline pore solution forms a thin oxide film on the surface of embedded steel, which protects it from corrosion. However,

when the integrity and protective quality of this film is destroyed by the presence of chlorides, corrosion initiates (Gjorv, 2009). The propagation stage of steel corrosion (see Figure 2.3) is characterised by active corrosion. The controlling factor at this stage is the rate of reaction, which is determined by, among other factors, the availability of oxygen (Pease, 2010).

The state of available oxygen (gas or dissolved in water) also determines its rate of diffusion through the pore structure of concrete. Corrosion of embedded steel reinforcement may not be a problem in submerged RC structures due to lack of dissolved oxygen. However, for structures exposed to the air in a marine environment, oxygen is readily available and it has an influence on the rates of corrosion. It is also important to note that oxygen must be in a dissolved state (moisture) for the electrochemical cathode reaction to take place (Gjorv, 2009).

2.3.7 Influence of cracks on reinforcement corrosion

The sources of cracks in concrete include shrinkage, chemical reactions (e.g. alkali-aggregate reaction), mechanical loading and reinforcement corrosion (Blagojevic *et al.*, 2012). Cracks may create preferential pathways and subsequently increase the penetration of aggressive substances (such as moisture, oxygen, carbon dioxide and chloride ions), thus aggravating the corrosion of steel (Ballim *et al.*, 2009)

The penetrability of cracked concrete depends on crack characteristics such as crack width, crack density and frequency, crack orientation (relative to steel reinforcement), degree of connectivity and whether the cracks are active or dormant (Arya and Ofori-Darko, 1996; Poursaee and Hansson, 2008; Djerbi *et al.*, 2008; Marsavina *et al*., 2009; Otieno *et al.*, 2009; Pease, 2010).

2.4 Factors affecting penetrability of cement-based materials

Factors that affect the durability of cement-based materials can be broadly classified into three main categories: material factors, factors related to workmanship and environmental factors (Dinku and Reinhardt, 1997; Stanish *et al*., 2000). These factors are briefly discussed in the following subsections.

2.4.1 Water/binder ratio

The water/binder ratio (abbreviated as w/b) largely determines the porosity of cement-based materials. A number of studies have shown that reducing the w/b ratio decreases porosity, and consequently reduces penetrability (Halamickova *et al.*, 1995; Dinku and Reinhardt, 1997; Roziere *et al.*, 2009; Wong *et al.*, 2009). A study undertaken by Khunthongkeaw *et al.*, (2006) established a link between w/b ratio and carbonation resistance. The results indicate higher carbonation resistance with decreasing w/b ratio, due to densification of the pore structure. Figure 2.8, for example, shows that increasing the w/b ratio will increase capillary porosity and rate of carbonation.

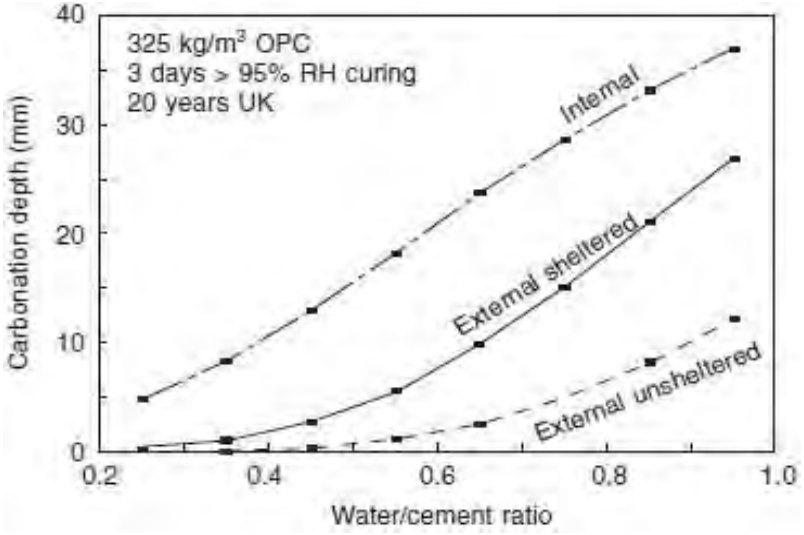

Figure 2.8: Effect of w/b ratio on the rate of carbonation (Hassanein, 1997)

During the mixing stage, the w/b ratio controls the initial spacing of cement particles (Glass, 2003), thus a lower w/b ratio would result in reduced spacing between cement particles and therefore, a denser microstructure. A dense microstructure is made up of a less connected pore system containing capillary pores of reduced sizes, which impede the transport of substances. Given the low penetrability, the difficult transport of aggressive chemical species would delay the deterioration processes.

2.4.2 Binder type

Concretes (and mortars) containing cements extenders have been shown to generally display improved resistance to the penetration of fluids and ionic species, particularly in the long term (Baroghel-Bouny *et al*., 2009). Several factors promote this beneficial effect of cement

extenders, also known as supplementary cementitious materials (SCMs). Firstly, the products of the pozzolanic reaction of SCMs such as blast furnace slag (GGBS) fills up the pores and voids resulting in a refined pore structure (Khunthongkeaw *et al.*, 2006; Pack *et al.*, 2010). Secondly, the fine particles from SCMs such as silica fume fills up the spaces and voids between larger particles, thus blocking the potential pathways of transport. Furthermore, experimental evidence shows that blast furnace slag (GGBS) increases the chloride binding capacity of cement-based materials, thereby reducing the amount of chloride ions involved in depassivation of steel (Luo *et al.*, 2003)

On the contrary, studies have shown that carbonation depth increases with the addition of cement extenders. The substitution of Portland cement with SCMs such as GGBS significantly reduces the alkaline reserves. The alkaline reserves refer to the hydration products (calcium hydroxide and calcium silicate hydrate), which take part in the chemical reactions that lead to carbonation. A reduction in the alkaline reserves would result in an increase in the rate of carbonation, and consequently accelerate the deterioration of RC structures (Papadakis, 2000; Glass, 2003; Khunthongkeaw *et al.*, 2006; Penttala, 2009).

2.4.3 Curing practice

Most deficiencies and damage in RC structures can be directly linked to site operations during repairs. One of the most important factors that relates to the quality of work done on site is curing practice (Marsh, 2003b). The duration and type of curing plays an important role in developing the pore structure of cement-based materials. Curing enhances the steady progress of cement hydration reaction to form calcium silicate hydrate gel, which binds the aggregate leading to a dense microstructure. The densification of the microstructure consequently decreases the porosity and enhances durability. In addition, a dense microstructure protects concrete from losing moisture and maintains a reasonable temperature range, resulting in increased strength and decreased penetrability (Atis, 2003; Glass, 2003; Marsh, 2003).

To protect steel reinforcement from corrosion, the cover layer ought to be as impermeable as possible. Inadequate curing reduces the degree of cementing reactions resulting in cover of poor quality and with a high permeability (Kellerman, 2009). The overall effect of reduced cementing reactions is increased size and connectivity of the pores and therefore, reduced

resistance to penetration by fluids and aggressive chemical species (Halamickova *et al.*, 1995; Grassl *et al.*, 2010).

A study by Bentur and Mitchell (2008) reports on the effects of curing on the durability performance of concrete specimens. The durability performance was quantified by chloride diffusivity and rates of carbonation, from which service life was calculated. The two researchers found that improved curing practice increases the service life of concrete as shown in Figure 2.9 and Figure 2.10.

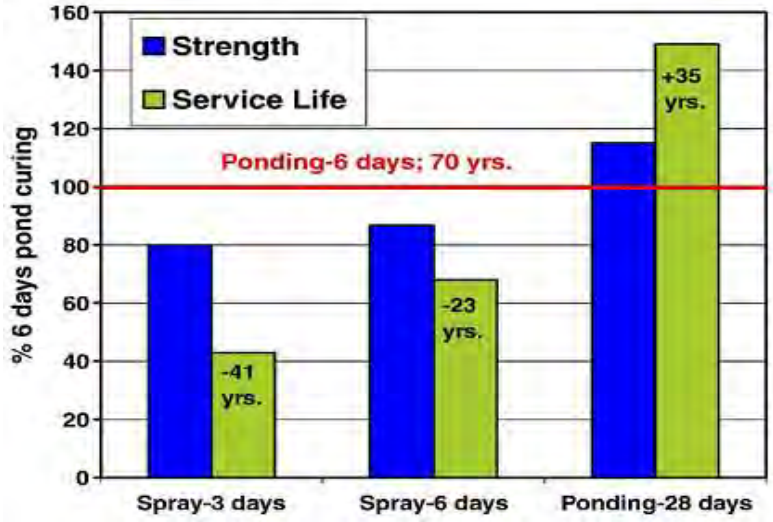

Figure 2.9: Effects of curing practice on strength and service life in carbonating conditions with reference to 6-day ponding (Bentur and Mitchell, 2008)

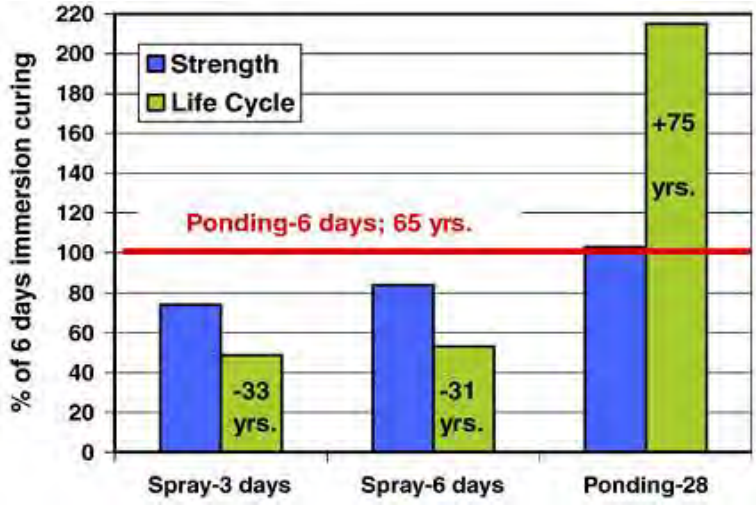

Figure 2.10: Effects of curing practice on strength and service life in chloride conditions with reference to 6-day ponding (Bentur and Mitchell, 2008)

Based on the experimental results, the researchers further mention that deficient curing would reduce the service life of RC structures by 30 to 60%, which translates to as much as 20 to 40 years. Kubens *et al*. (2003) correlated air permeability results obtained from Torrent air permeability with different methods of curing as shown in Figure 2.11. The methods of curing were as follows: A – continuous exposure to air after demoulding at 1 day; B – 3 days of alternating water curing; C – 7 days of alternating water curing; D – 7 days of curing in water bath; and E – 28 days of curing in water bath.

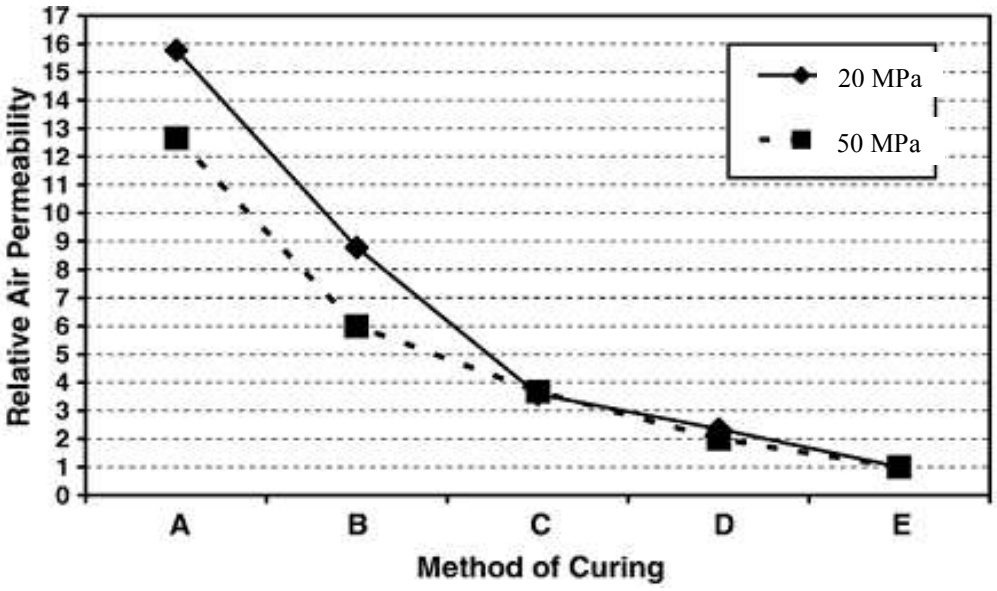

Figure 2.11: Correlation between results of Torrent air permeability test and method of curing (Kubens *et al*., 2003)

It can be seen that air permeability decreases with better curing practice. The researchers also found a good correlation between air permeability and chloride penetration, as well as carbonation. Similar results were observed by Dinku and Reinhardt (1997) who found that prolonged curing resulted in a decrease in carbonation depth. Martys and Ferraris (1997) also observed that chloride diffusivity decreases with prolonged curing. These results support the idea that better curing practice can delay deterioration mechanisms such as chloride-induced or carbonation-induced corrosion of reinforcement.

2.4.4 Environmental factors

The environmental factors that influence the performance of patch repair mortars include temperature, humidity, precipitation, chlorides (from de-icing salt or sea water) and carbon dioxide concentration (Lindvall, 2000). Factors related to the exposure environment have

been shown to influence deterioration processes. Figure 2.8 (in Section 2.4.1), for example, shows that carbonation rate is lower in external unsheltered environment probably due to effects of drying and wetting. The abovementioned environmental factors influence degradation in the following ways (Lindvall, 2000):

i) The temperature play an important role in the diffusion of chloride ions and carbon dioxide into cement based materials.
ii) The transport properties (diffusion coefficient) of mortar depends on moisture and temperature conditions.
iii) The rate of corrosion in concrete is also influenced by moisture and temperature conditions.

2.5 Chloride transport

In marine environments and structures exposed to de-icing salts (e.g. bridges), chloride transport is a decisive factor for service life design. Chloride attack is not a concern in unreinforced concrete, since it does not affect the concrete, but initiates corrosion of steel, which consequently affects concrete. The main processes that transport chloride ions in uncracked concrete include, inter alia, capillary absorption, diffusion, permeation, wick action and migration (Martin-Perez, 1999; Glass, 2003; Gjorv, 2009; Savija, 2014). The following sections deal with these transport processes and their influencing factors.

2.5.1 Mechanisms of chloride-ion transport

Studies have shown that the transport of chloride ions in concrete is a complex process involving an interaction of several transport processes, accompanied by physical or chemical binding of these ions (Alexander and Mackechnie, 2004; Andrade *et al.*, 2007; Gjorv, 2009). The following subsections present these transport processes for chloride ingress and its influencing factors.

2.5.1.1 Chloride diffusion

Diffusion is the principal mechanism that drives the transport of chloride ions in concrete exposed to a marine environment (Hearn *et al.*, 2006; Gjorv, 2009). It is defined as the process through which fluids and ionic species move through materials, due to concentration gradient (Stanish *et al*., 2000; Beushausen and Alexander, 2008; Pack *et al.*, 2010). Dissolved

chloride ions require continuous liquid pathways in order to diffuse through materials (Nilsson, 2003). The key factors that influence the rate of diffusion are moisture content, temperature, characteristics of the diffusing substance and the diffusivity of the material (Roziere *et al.*, 2009; Ballim *et al.*, 2009).

Fick's first law of diffusion (Equation 2.3) governs the diffusion of chloride ions in concrete (Costa and Appleton, 1999):

$$J = -D_{eff} \frac{dC}{dx} \tag{2.3}$$

where: J is the rate of diffusion (g/m^{2}s),
D_{eff} is the effective diffusion coefficient (m^2/s),
dC/dx is the concentration gradient (g/m^3/m),
C is the concentration of ions or gases (g/m^3),
x is the distance (m).

Fick's First Law describes the steady state diffusion of gases and ionic species in a porous material, usually in one dimension. Steady state condition implies absence of changes in concentration over time (Martin-Perez *et al.*, 2000; Stanish *et al.*, 2000; Hamilton *et al.*, 2007). In this model, the rate of diffusion is directly proportional to the concentration gradient. The negative sign indicates that flow of ions take place from high to low concentration.

The model for prediction of chloride ingress in concrete structures is based on Fick's Second law. This model incorporates the effect of varying concentration with time (Poulsen, 1995; Costa and Appleton, 1999; Stanish *et al.*, 2000; Tamimi *et al.*, 2008). The rate of change of concentration with time is directly proportional to the rate of change of concentration gradient with distance, as expressed by the Equation 2.4. The symbols in this equation are similar to those of Equation 2.3.

$$\frac{\partial C}{\partial t} = D_{eff} \frac{\partial^2 C}{\partial x^2} \tag{2.4}$$

If the surface concentration is assumed constant, initial concentration in concrete assumed zero, and the concentration at an infinite point from the surface assumed zero, then Crank's

solution to Fick's Second Law of diffusion is expressed as shown in Equation 2.3 (Nokken *et al.*, 2006; Hamilton *et al.*, 2007):

$$\frac{C(x,t)}{C_0} = 1 - erf\left(\frac{x}{\sqrt{4 \times D_{eff} \times t}}\right) \tag{2.5}$$

where *erf* is the error function expressed as (Tamimi *et al.*, 2008):

$$erf(z) = \frac{2}{\sqrt{\pi}} \int_0^z e^{-u^2} du \tag{2.6}$$

Equation 2.5 is often used in the curve-fitting of chloride profiles of laboratory test specimens after an exposure time, *t* using a regression analysis (Kropp and Alexander, 2007). The rate of chloride diffusion decreases with time due to continued cementing reactions (hydration) that densifies the pore structure as well as physical and chemical binding of chloride ions (Nokken *et al.*, 2006).

2.5.1.2 Permeation

Permeation refers to the process by which fluids move in saturated pores due to pressure gradients. In view of chloride transport in concrete, water is the most essential fluid (Poulsen, 1995; Kropp, 2005; Hamilton *et al.*, 2007; Kropp and Alexander, 2007). The ingress of chloride ions particularly in the tidal zones of concrete structures depends on water permeability, and diffusion coefficient (Tang *et al.*, 2015). Wave action on partially submerged structures or retained mass of water, for example, may provide the external hydrostatic pressure that moves water containing chloride ions by permeation, through the pores of submerged concrete member.

The empirical approach developed by Darcy (Equation 2.7) governs the permeation of water in cement-based materials and is used in the evaluation of permeation experiments (Hearn *et al.*, 2006; Kropp and Alexander, 2007).

$$K_w = \frac{Q}{t}\frac{L}{A}\frac{1}{\Delta h} \tag{2.7}$$

where: K_w is the coefficient of water permeability (m/s),

Δh is pressure head applied (m),
Q is volume of flow (m^3),
t is time (s),
L is thickness of penetration section (m),
A is permeated area (m^2).

The coefficient of water permeability, K is essentially controlled by the pore structure (Hearn *et al.*, 2006). It indicates the ease with which permeation occurs in materials. A higher value of K indicates higher permeability (Mehta and Monteiro, 2006). While the intrinsic permeability relies on characteristics of the porous medium, it is independent of fluid characteristics such as viscosity, which describes the shear resistance of the fluid. In the case of gases, compressibility is a vital consideration (Basheer *et al.*, 2001).

Gas permeability has been shown to exceed water permeability particularly in low porosity materials. When comparing these two, the Klinkenberg correction shown in Equation 2.8, is used to correct the slippage of gas (Bentz *et al*., 1999; Webb and Pruess, 2003; Hearn *et al.*, 2006):

$$K_a = K\left(1 + \frac{b}{P_m}\right) \tag{2.8}$$

Where: K_a is gas permeability (m^2),
K is actual intrinsic permeability (m^2),
b is constant (m),
P_m is mean pressure (m).

2.5.1.3 Capillary absorption

In the absence of pressure gradients, porous materials such as concrete can take up liquids by capillary absorption (Kropp and Alexander, 2007). The absorption of water containing chloride ions has significant implications on durability of RC structures. Capillary suction facilitates the absorption of fluids containing chloride ions into partially saturated concrete, under the action of moisture gradients. The key factors that influence capillary absorption include the pore sizes and connectivity, the sequence and duration of cyclic wetting and drying, and the degree of saturation of concrete (Hong and Hooton, 1999; Basheer *et al.*, 2001).

The Laplace equation (Equation 2.9) describes the capillary pressure of water (also known as pore water pressure). The parameters used in the equation are illustrated in Figure 2.12 (Kropp and Alexander, 2007):

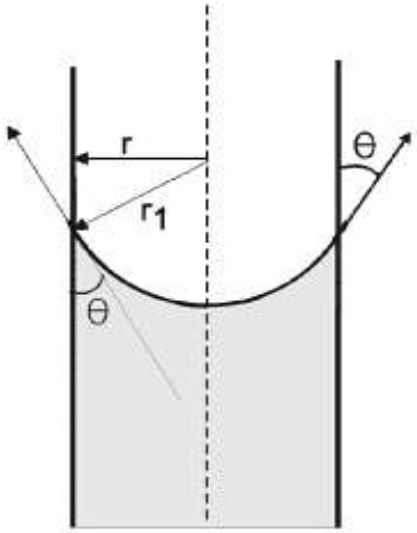

Figure 2.12: Mechanism of capillary absorption (Kropp and Alexander, 2007)

$$p_{cap} = p_l - p_g = \frac{2\sigma}{r_1} \qquad (2.9)$$

With r_1 as $r_1 = \frac{r}{\cos\theta}$, then

$$p_{cap} = \frac{2\sigma\cos\theta}{r} \qquad (2.10)$$

where: p_{cap} is capillary pressure (N/m^2),
p_l is pressure in liquid (N/m^2),
p_g is pressure in gaseous phase above liquid column (N/m^2),
σ is surface tension (N/m),
θ is wetting angle,
r is radius of capillary (m),
r_1 is radius of curvature of meniscus (m).

Equation 2.11 (Kropp and Alexander, 2007) gives the penetration depth for water (or absorbed water):

$$M_1(t) = D + Ct^n \text{, } n < 0.5 \qquad (2.11)$$

where: $M_1(t)$ is the mass of liquid absorbed at time t per unit area of surface exposed to liquid (g/m^2),
D is the initial absorption (g/m^2),
C is absorption rate (g/m2√t).

2.5.1.4 Convection

Convection plays an important role in the transport of chloride ions in concrete exposed to drying-wetting cycles. The continuous cycles of wetting and drying, for example in the tidal zones of marine structures, lead to penetration and accumulation of chloride ions in concrete. The evaporation of water during the drying cycle concentrates these ions. The depth of wetting and drying is referred to as the convection zone (DuraCrete, 1998; Hong and Hooton, 1999). Figure 2.13 shows the convection zone in concrete.

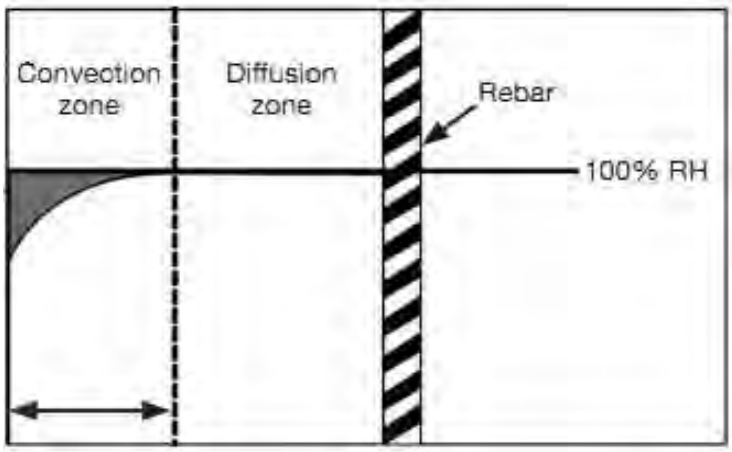

Figure 2.13: Convection zone in concrete cover (Ballim *et al*., 2009)

Below the convection zone, the concrete remains moist during the drying period, thus chlorides penetrate by diffusion irrespective of the external conditions (Hong and Hooton, 1999; Ballim *et al*., 2009). Literature suggests that convection on its own cannot transport chlorides to the level of steel due to the small depth of wetting and drying, unless the concrete is of extremely poor quality. However, it reduces the distance that the chloride ions must diffuse to reach the level of steel reinforcement (Martys and Ferraris, 1997; Stanish *et al*., 2000).

2.5.1.5 Migration

Migration refers to the movement of ions under the influence of an electrical field. This technique is commonly applied in laboratory accelerated chloride tests to evaluate conductivity or resistivity of materials (Ballim *et al.*, 2009). In a concrete pore solution containing various ions, an electrical field is initiated when the transport of cations is not balanced by a corresponding counter flow of anions (Stanish *et al.*, 2000; Nilsson, 2003; Kropp and Alexander, 2007).

The Nernst-Plank equation (Equation 2.12) describes the flow of ions due to the combined mechanisms of diffusion, migration and convection (Kropp and Alexander, 2007).

$$q_i = D_i \frac{\partial C_i(x)}{\partial x} + \frac{z_i F}{RT} DC_i \frac{\partial E(x)}{\partial x} + C_i v_i(x) \qquad (2.12)$$

where q_i is the mass flux (g/m^{2}s),
D_i is the diffusion coefficient (m^2/s),
$C_i(x)$ is the concentration of ions (g/m^3),
x is the distance (m),
z_i is the valence of the ionic species i,
F is Faraday's constant (J/V mol),
R is the universal gas constant (J/mol K),
T is the absolute temperature (K),
$E(x)$ is the applied electrical potential (V),
$v_i(x)$ is the velocity of capillary flow (m/s).

2.5.1.6 Wick action

Wick action occurs when one side of a relatively thin concrete is exposed to ionic solution while the opposite side remains dry, for example, in tunnel liners and slabs. This causes drawing of the ionic solution towards the dry surface, resulting in increased concentration of ions in concrete. The combined action between wicking and diffusion increases chloride ingress. Also, exposure of a concrete surface to wetting and drying cycles may promote wick action, which may result in the accumulation of chloride ions near the drying face of concrete (Boddy *et al.*, 1999; Hearn *et al.*, 2006). The analytical and empirical relationships for wick action have not yet been well established, thus an in-depth study of this process is still

needed. However, efforts aimed at improving understanding in this area includes studies by Boddy *et al*. (1999) and Buenfeld *et al*. (1997).

2.5.1.7 Combined transport

The real transport process of chloride ions in concrete involves a combination of several mechanisms. Isolation of a single transport process may therefore be an over-simplification of the actual transport process (Nilsson, 2003; Andrade *et al.*, 2007; Ballim *et al.*, 2009). The interaction of several transport mechanisms in chloride transport has been highlighted in Section 2.5.1.2 to 2.5.1.6.

2.5.2 Chloride diffusion coefficient

The diffusion coefficient provides an indication of the ease with which the diffusion process occurs in a material. It provides a measure of a material's resistance to chloride penetration. Factors that influence the diffusion coefficient include the size, connectivity and tortuosity of the pores (Nilsson, 2003; Wegen *et al.*, 2012). Several test methods attempt to estimate the diffusion coefficient of cement-based materials. A typical method is the bulk diffusion test discussed in Section 2.5.5.1, in which the diffusion coefficient is determined from the chloride profiles of concrete specimens (Stanish and Thomas, 2003).

The diffusion coefficient of concrete decreases with time due to continued cementing reactions, chloride binding and evaporation (Nilsson *et al.*, 2003; Stanish and Thomas, 2003; Wegen *et al.*, 2012). For this reason, the diffusion coefficient at early age may not accurately represent the actual chloride resistance for concretes in service (ASTM C1556-04, 2004). As mentioned by Hamilton *et al.* (2007), extended exposure of test specimens may yield diffusion coefficients that provide a better representation of concrete in service.

A number of service life prediction models for RC structures in marine environments take into account the diffusion coefficient of chloride ions. Literature suggests two types of diffusion coefficients used in these service life models, namely the average (also referred to as apparent or effective) diffusion coefficient and the instantaneous diffusion coefficient (Stanish and Thomas, 2003; Nokken *et al.*, 2006). In the first approach, the diffusion coefficient at any age is considered the average diffusion coefficient from the beginning of exposure to the time of its estimation. The instantaneous diffusion coefficient approach is rather time dependent. It involves the application of finite difference method on Fick's First

Law to describe the diffusion coefficient at each moment (Hearn, 1998; Hearn *et al.*, 2006; Pack *et al.*, 2010). Equation 2.13 shows the applied exponential function.

$$D(t) = D_{ref}\left(\frac{t_{ref}}{t}\right)^{m} \qquad (2.13)$$

where: $D(t)$ is the diffusion coefficient at time, t,
D_{ref} is the diffusion coefficient at reference time, t_{ref} (usually 28 days),
m is a variable that describes the rate of change of diffusivity (depending on variables such as type of cementitious material and mix proportions).

Standard test procedures such as the ASTM C1556-04 (2004) consider the average diffusion coefficient. Due to the complex nature of chloride transport process, an empirical model is used to determine the apparent chloride diffusion coefficient. This model is based on curve-fitting the measured chloride profiles. Figure 2.14 shows a typical chloride profile using the solution to Fick's Second law of diffusion (Equation 2.5).

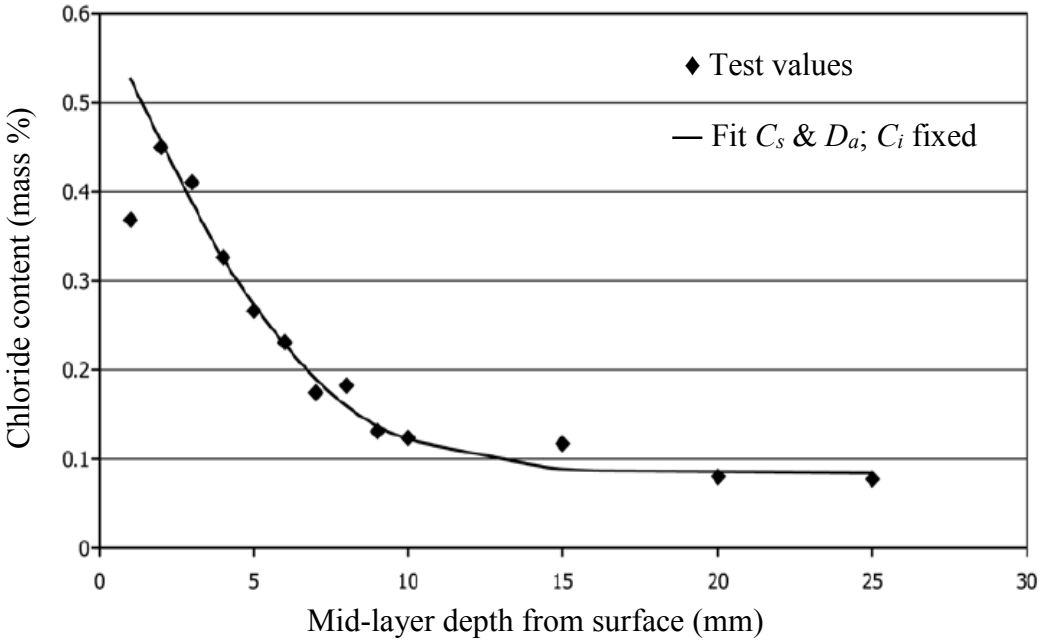

Figure 2.14: Typical chloride profile fit (ASTM C1556-04, 2004)

The parameters obtained from the curve fitting are the apparent diffusion coefficient (D_{eff}) and the surface chloride concentration (C_s) (Nilsson, 2003). As reported by Tang and

Sorensen (2001) and Hearn *et al*. (2006), D_{eff} value can be used as an input parameter for service life prediction of chloride ingress in RC structures.

2.5.3 Chloride binding

Chloride binding can be defined as the interaction between the chloride ions and the porous matrix in cement-based materials (Poulsen, 1995; Tang and Nilsson, 1995). Chloride ions in the pore structure of cement-based materials may exist as dissolved ions in the pore solution (free chlorides) or chemically (or physically) bound to cement hydrates (bound chlorides). The total chloride content constitutes both bound and free chlorides. (AFREM Technical report, 1999; Martin-Perez *et al.*, 2000; Tang, 2007). Chloride binding thus removes the free chlorides that take part in diffusion process, from the pore solution. However, from a theoretical perspective and in most experiments, the total chloride content is assumed to take part in the diffusion process (Tang and Nilsson, 1995; Zibara, 2001; Hearn *et al.*, 2006).

The service life predictions for chloride ingress in concrete ought to consider chloride binding due to the following reasons (Savija, 2014):

i) Removal of free chlorides from the pore solution prolongs the initiation of reinforcement corrosion,
ii) Formation of Friedel's salt in the pore structure reduces the size and connectivity of the pores thus slowing down the transport of chloride ions,
iii) The rate of chloride diffusion slows down when the free chloride ions are removed from the diffusion flux.

Chloride binding alters the ionic concentration of the pore solution and subsequently the concentration gradient that drives chloride diffusion. This reduces the rate of diffusion. The result is reduced penetration depth in a given time (Glass, 2003; Nilsson, 2003; Kropp, 2005). It is presumed that chloride binding occurs prior to attaining the steady state conditions, after which its influence is insignificant (Stanish *et al.*, 2000; Loser *et al.*, 2010).

The chloride binding capacity of concrete depends on the type of binder or cement extender used (Ballim *et al.*, 2009). Literature shows a higher chloride binding capacity in cements containing high amounts of calcium aluminate (C_3A). This has been attributed to the chemically binding reaction between C_3A and chloride ions to form Friedel's salt (also referred to as calcium choro-aluminate hydrate) (Martin-Perez, 1999; Stanish *et al.*, 2000;

Pack, 2010). In addition, experimental evidence has shown a higher binding capacity in concretes containing cement extenders such as blast-furnace slag than concretes containing Portland cement only. Alexander *et al*. (1999), for example, have shown the effects of various binders on chloride transport (Figure 2.15). The low chloride conductivity in concretes containing SCMs can be attributed to increased interaction between SCMs and chloride ions due to higher amounts of C_3A.

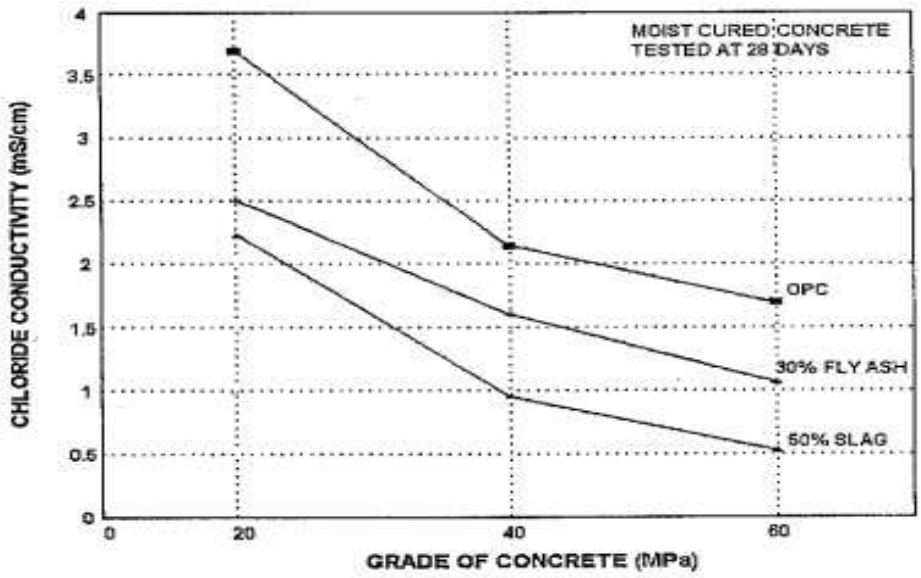

Figure 2.15: Effects of binder type on chloride transport in concretes of different strength grades tested 28 days after casting (Alexander *et al.*, 1999)

2.5.4 Chloride binding isotherms

Chloride binding isotherms describe the relationship between free and bound chlorides at a given temperature. It expresses the amount of bound chlorides as a function of free chlorides. The various types of chloride binding isotherms mentioned in literature include (Zibara, 2001; Savija, 2014):

Linear binding isotherm: $C_b = \alpha C_f$

Langmuir isotherm: $C_b = \frac{\alpha C_f}{\left(1+\beta C_f\right)}$

Freundlich isotherm: $C_b = \alpha C_f^b$

Brunauer, Emmett, Teller isotherm:

$$\frac{C_b}{C_{bm}} = \frac{\alpha \frac{C}{C_s}\left[1-(1-\beta)\left(1-\beta\frac{C}{C_s}\right)^2\right]}{\beta\left(1-\beta\frac{C}{C_s}\right)\left(1-\beta\frac{C}{C_s}+\alpha\frac{C}{C_s}\left(1-\beta\frac{C}{C_s}+\frac{C}{C_s}\right)\right)}$$

The parameters α and β are empirical constants experimentally determined for a given concrete, while C_b and C_f denote bound and free chlorides respectively. The linear binding isotherm is generally considered an oversimplification of this relationship. In addition, studies have shown a good fit of experimental data for lower chloride concentrations (0.005M) when using Langmuir isotherm. For higher chloride concentrations (0.01-1M), the Freundlich isotherm has been found to better describe chloride binding (Tang and Nilsson, 1993; Glass and Buenfeld, 2000; Zibara, 2001; Savija, 2014). As mentioned by Martin-Perez *et al.* (2000) and Savija (2014) it is necessary to consider chloride binding when calculating the service life of RC structures. Neglecting binding or assuming linear binding may underestimate the service life.

2.5.5 Reference tests for chloride ingress

The laboratory test methods for evaluating chloride penetration are generally based on ionic diffusion, chloride conductivity or concrete resistivity. These tests characterise the micro- and macro-structural properties of early-age concrete, which relate to its durability performance (Alexander *et al.*, 2008). To reduce the duration of testing, measures that increase the rate of penetration of chloride ions such as imposing an electrical field are applied (Stanish *et al.*, 2000; Loser *et al.*, 2010). Tests for chloride penetration can be broadly categorized into diffusion tests, migration tests and indirect tests (based on material resistivity). The following sections present a discussion of the commonly applied test methods.

2.5.5.1 Ion diffusion methods

Ionic diffusion methods follow the principles of chloride diffusion already discussed in Section 2.5.1.1. These methods include, inter alia, the 90-day salt ponding test and the bulk diffusion test (NT Build 443).

a) 90-day salt ponding test

The ponding test evaluates the ingress of chloride ions under non-steady state conditions in accordance with AASHTO T259. The method involves ponding the test specimen with 3%

sodium chloride solution (NaCl). After an exposure period of 90 days, the penetration of chloride ions is observed by determining the penetration profiles on cored and sliced (10-12 mm interval) specimens. Fick's second law of diffusion (Equation 2.3) and regression analysis are then applied to derive the diffusion coefficient (Hearn *et al.*, 2006; Hamilton *et al.*, 2007; Kropp and Alexander, 2007). Figure 2.16 illustrates the set up for ponding test.

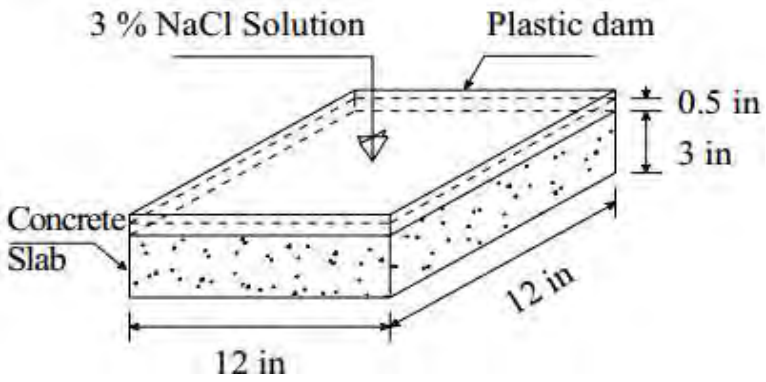

Figure 2.16: Set up for salt ponding test (Hamilton *et al.*, 2007)

Several limitations of ponding test have been reported. Firstly, literature suggests that chloride ingress occurs not only through diffusion, but also through capillary absorption and wicking. Capillary absorption occurs in the initial stage of exposure (on dry sample), whereas wicking occurs from the wet face to the drier face of the sample during exposure (Stanish *et al.*, 2000; Hamilton *et al.*, 2007). Therefore, several transport processes influence the diffusion coefficient derived. Secondly, it has been reported that this method estimates the average chloride content in specimens, rather than the profile of chloride penetration (Stanish *et al.*, 2000). In addition, chloride penetration has been found to be insufficient, especially in concretes of high quality, which have low penetrability. An extended period of ponding may therefore be necessary to ensure sufficient chloride penetration. The bulk diffusion test (NTBuild 443) attempts to address the abovementioned limitations associated with salt ponding test.

b) Bulk diffusion test (NT Build 443)

Bulk diffusion test is used to determine the apparent chloride diffusion coefficient of specimens in accordance with the NordTest NTBuild 443. Cylindrical test specimens saturated with calcium hydroxide solution are submerged in 16.5% sodium chloride solution for at least 35 days. To enhance unidirectional ionic diffusion, the specimen is sealed on all faces except on one circular face. After the exposure period, chloride penetration is

determined by evaluating the penetration profiles on cored and sliced specimens. The chloride content at each profile is determined by potentiometric titration method, after which the derivation of the apparent chloride diffusion coefficient can be accomplished by curve fitting the chloride profiles to Fick's second law of diffusion (Tang and Sørensen, 2001; Hearn *et al.*, 2006; Kropp and Alexander, 2007). Figure 2.17 illustrates the set up for bulk diffusion test.

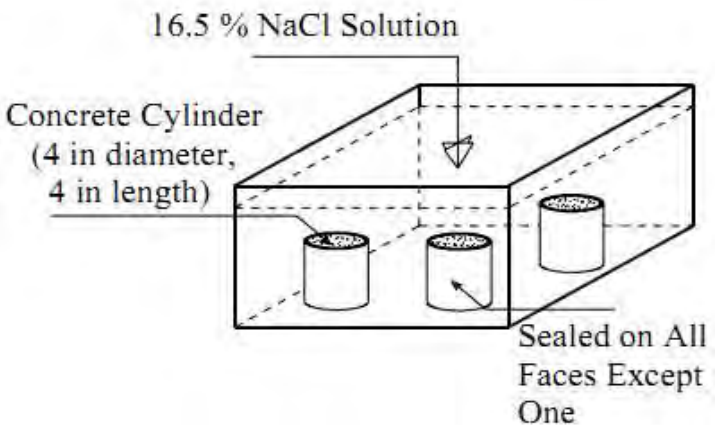

Figure 2.17: Set up for bulk diffusion test (Hamilton *et al.*, 2007)

In bulk diffusion test, chloride-ion transport by capillary absorption and wicking mechanisms are eliminated, thereby, achieving a diffusion process that is better controlled. Another advantage of bulk diffusion test over ponding test is that it can be applied for both laboratory samples and cored samples from existing concrete structures (Stanish and Thomas, 2003; Hamilton *et al.*, 2007).

2.5.5.2 Ion migration methods

Ionic migration methods impose an external electrical field to accelerate the transport of ions. The material transport properties are then evaluated using the Nernst-Planck equation (Kropp and Alexander, 2007). The general set up of a migration test cell is shown in Figure 2.18.

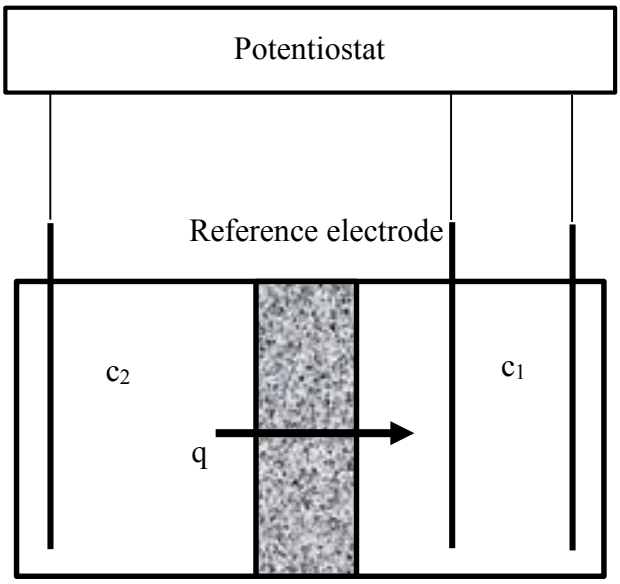

Figure 2.18: Experimental arrangement for migration tests (Kropp and Alexander, 2007)

The test specimen of a given thickness separates the cell into two chambers containing media of known concentrations (c_1 and c_2). The two electrodes connected to a potentiostat introduce the electrical field into the cell. The resistivity of the specimen can be evaluated with the same set up. As shown in Equation 2.14 the Einstein relation can be used to relate resistivity to the diffusion coefficient (Kropp and Alexander, 2007). The instructions on resistivity measurement have been documented, for example by Polder *et al*. (2000) and Polder (2001).

$$D_{eff} = \frac{k_{cl}}{\rho_{sat}} = k_{cl} \cdot \sigma \qquad (2.14)$$

where: D_{eff} is the effective diffusion coefficient,
k_{cl} is test parameter depending on external ionic concentration,
ρ_{sat} is the resistivity of saturated concrete,
σ is conductivity of saturated concrete.

a) Rapid chloride permeability test (ASTM C1202)

The rapid chloride permeability test (RCPT) evaluates the chloride conductivity of specimens in accordance with ASTM C1202. An externally applied direct current of 60 Volts provides the driving force which accelerates chloride ion transport (Stanish *et al.*, 2000; Hearn *et al.*, 2006). Figure 2.19 illustrates an RCP test set-up

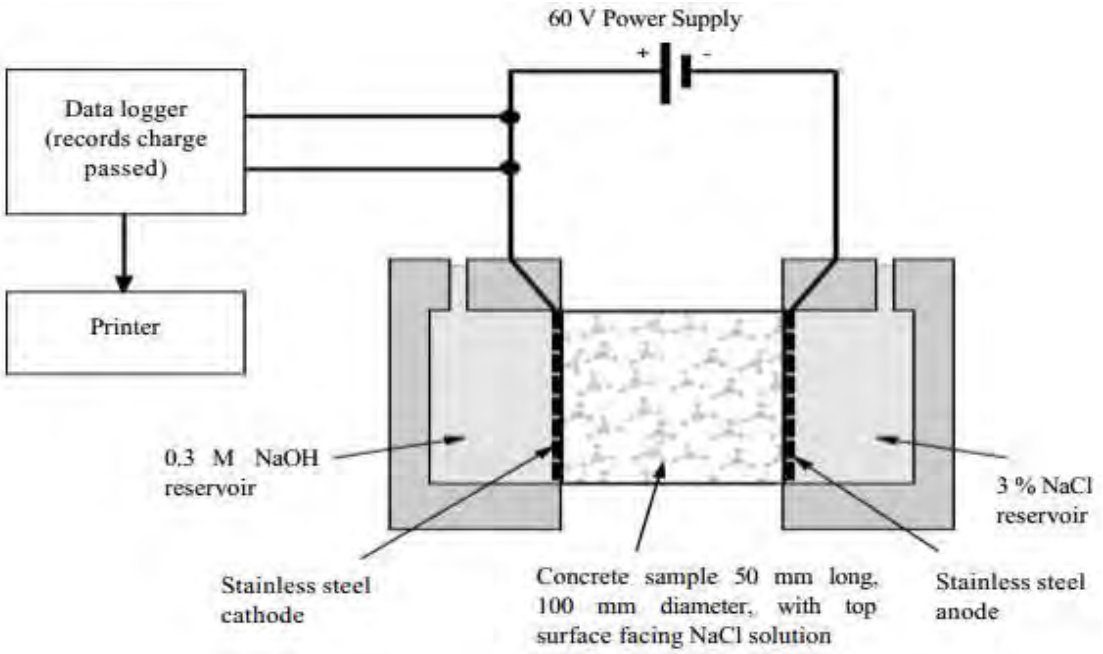

Figure 2.19: Set up for rapid chloride permeability test (Stanish *et al.*, 2000)

Several limitations of RCPT have been pointed out by a number of researchers. First, the high current flow during the 6 hours of testing heats the sample and pore solution, thus raising the measured conductivity (Stanish *et al.*, 2000; Young and Cho, 2003; Hearn *et al.*, 2006). Second, it has been mentioned that RCPT does not provide a reliable measure of permeability or chloride diffusion; it rather measures electrical conductivity, which is largely influenced by the chemistry of the pore solution (Yang and Cho, 2003). Thus, a change in the chemistry of the pore solution would alter electrical conductivity. For example, a reduction in charge passed would be recorded in fly ash concrete specimen due to reduction in alkalinity rather than reduction in permeability, even though permeability decreases at a slow rate in fly ash concrete (due to slow rate of hydration). Inconsistent results have been observed with samples containing pozzolans (Hearn *et al.*, 2006; Hamilton *et al.*, 2006; Hamilton *et al.*, 2007). In an attempt to improve RCPT, Hamilton *et al.* (2007) suggest reduced duration of testing and linear extrapolation of the results to 6 hours.

b) Rapid migration test

The rapid migration test (RMT) uses an electric field of lower intensity than RCPT (Stanish *et al.*, 2000). An external electrical potential applied to the specimen causes the migration of chloride ions in the sample. The depth of chloride penetration is determined on split samples by colorimetric analysis (Hamilton *et al.*, 2007). Figure 2.20 illustrates the test set up for

RMT. The main limitation of RMT as reported in literature is the long duration of testing (up to 4 days), as well as the wide range of voltage that is applied to the specimen. (Hamilton *et al.*, 2007).

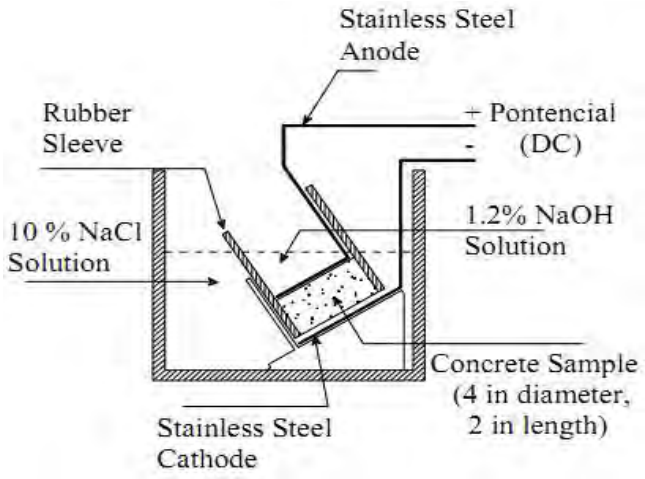

Figure 2.20: Set up for rapid migration test (Hamilton *et al.*, 2007)

c) Chloride conductivity index test

The chloride conductivity index (CCI) test uses the principle of migration to characterize ion conduction properties of materials. Chloride transport through the specimen is driven by an externally applied potential difference of approximately 10 Volts (Mackechnie and Alexander, 2002; Alexander *et al.*, 2006). Figure 2.21 shows a schematic of the two-cell conduction rig used in CCI test.

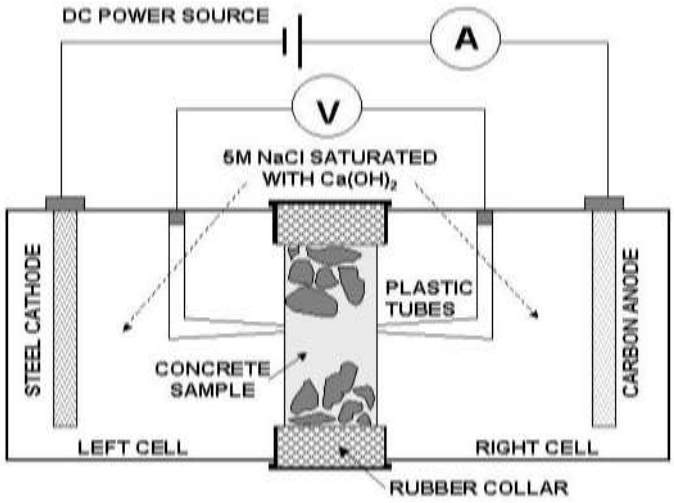

Figure 2.21: Schematic diagram of the two-cell conduction rig for CCI test (Alexander, 2004)

The conductivity values have been shown to provide reliable measures of chloride penetration in concrete. Streicher and Alexander (1995) and Mackechnie and Alexander (2004) observed good correlations between chloride conductivity and diffusivity. The output parameters of the CCI test (applied voltage, measured current and sample dimensions) are used in Equation 2.15 to calculate chloride conductivity of the specimen.

$$\sigma = \frac{it}{VA} \tag{2.15}$$

where: σ is chloride conductivity (mS/cm),
i is the current (A),
t is thickness of the specimen (cm),
V is voltage (V),
A is the cross-sectional area of specimen (cm^2).

2.5.5.3 Surface resistivity measurement

Surface resistivity method uses electrical resistivity property of materials as an indirect measure of chloride ingress. It is governed by the relationship between diffusivity of ions (and permeability of fluids) and electrical conductivity of concrete (Stanish *et al*., 2000). Concrete resistivity depends on porosity, the chemical composition (conductivity) of the pore solution and the degree of saturation in the pore structure. Electrical current is transmitted by ions dissolved in the pore liquid. Therefore, more pore liquid (wet concrete) as well as large and connected pores with lower degree of tortuosity would result in lower resistivity (higher conductivity). Carbonation and drying, particularly in Portland cement concrete, increases concrete resistivity (Building Research Establishment, 1998; Andrade *et al*., 2007). Both processes remove ions from the pore solution thus lowering electrical conductivity.

The Four-Point Wenner Probe is often used to determine the surface resistivity of materials. It consists of four equally spaced electrodes as shown in Figure 2.22. During testing, the four electrodes are pressed onto the concrete surface as illustrated. The two outer electrodes induce the current while the two inner electrodes measure the resulting potential difference (Andrade *et al.*, 2007).

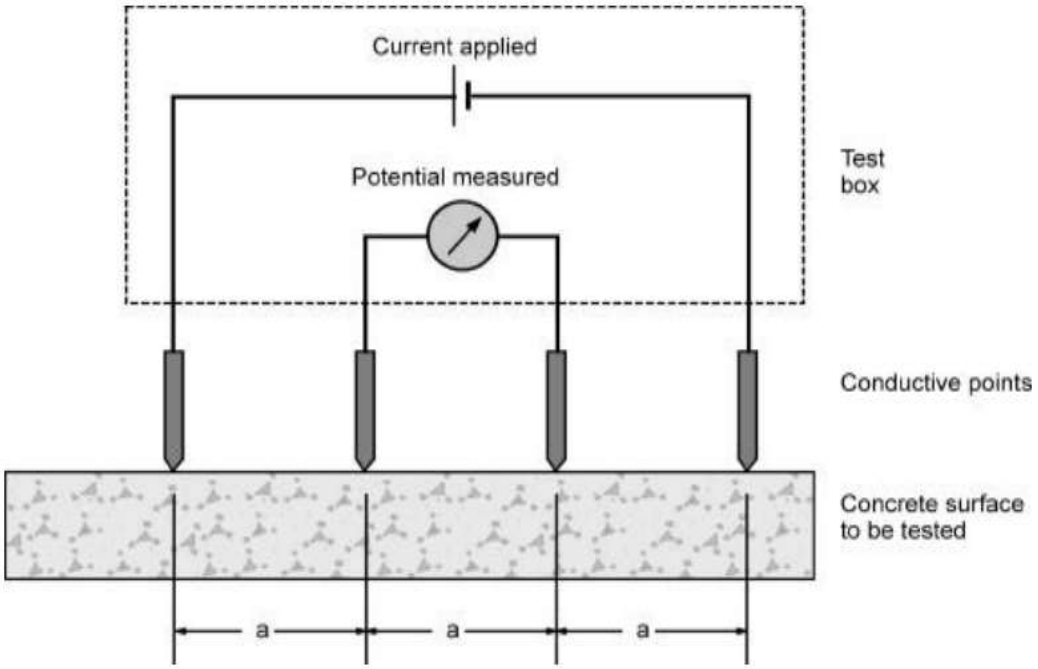

Figure 2.22: Schematic of the Four-Point Wenner Probe (Stanish *et al.*, 2000).

To calculate concrete resistivity from the resistance value, ***R***, a cell constant (Equation 2.16) based on theoretical considerations is applied (Andrade *et al*., 2007).

$$\rho = 2\pi aR \tag{2.16}$$

where: ρ is resistivity,
a is the electrode spacing
R is resistance

2.5.6 Service life prediction models for chloride ingress

Service life models for chloride ingress have been developed to describe the performance of concrete in an environment containing chlorides. These models take into account the exposure conditions and material characteristics in evaluating the performance of concrete. The diffusion coefficient is a commonly used input parameter in most of the chloride resistance models (Lindvall, 2000; Shukla and Pillai, 2015; Tang *et al.*, 2015). In the following sections, some chloride prediction models that are widely used or cited in literature will be discussed, namely the Collepardi model, ClinConc model, LIFE-365 model, DuraCrete model for chloride ingress and the South African chloride prediction model.

2.5.6.1 Collepardi (ERFC) model

The ERFC model (abbreviation denoting the mathematical Error Function Complement) was first proposed as a model for chloride ingress in concrete by Collepardi in the early 1970's. It has since been significantly improved into more sophisticated models. It is based on an erfc solution to Fick's 2nd law of diffusion (Tang, 2007; Nilsson, 2009).

$$C(x,t) = C_1 + (C_s - C_i) \cdot erfc\left(\frac{x}{2 \cdot \sqrt{D_a \cdot t}}\right) \qquad (2.17)$$

The key parameters of this model are surface chloride concentration (C_s) and diffusion coefficient (D_a), which are determined by curve-fitting the chloride ingress profiles obtained from specimens. Experimental evidence shows that this model, however, can only describe chloride ingress in the short term (the period during which the input parameters are determined) (Tang, 2007).

2.5.6.2 ClinConc model

ClinConc (denoting Chlorides in Concrete) is a numerical model initially developed by Tang and Nilsson (2000) for submerged environment. For concrete structures above water, certain modifications have to be implemented. It is based on chemical and physical processes involved in chloride transport and binding in concrete. This model takes into account the effects of temperature, curing age and concrete cover on diffusivity. The diffusion coefficient, measured at six months using chloride migration tests such as NTBuild 492 is the main input parameter for ClinConc. The diffusion coefficient is defined as shown in Equation 2.18. Other input data include concrete mix design, workmanship and exposure conditions (Lindvall, 2000; Tang and Nilsson, 2000; Tang, 2007; Shukla and Pillai, 2015).

$$D_0 = \frac{\left(0.8\alpha_1^2 - 2\alpha_1 + 2.5\right)\left(1 + 0.59K_b\right) \times k_{TD}}{1 + k_{OH} \times K_b \times k_{Tb} \times f_b \times \beta_b \left(\frac{c_s}{35.45}\right)^{\beta_b - 1}} \times D \qquad (2.18)$$

where: D_0 is the initial apparent diffusion coefficient,
α_1 is the time dependent factor for chloride binding,
K_b is the binding factor,
k_{TD} and k_{Tb} are the temperature factors for diffusion coefficient and chloride binding respectively,

k_{OH} is the factor describing the effects of alkalinity,

f_b and β_b are chloride binding coefficients,

c_s is the free chloride concentration in the surrounding environment.

D is the diffusion coefficient from laborstory tests 6 months after starting the experiment

The ClinConc model uses two main procedures in modelling chloride penetration in concrete. First, the penetration of free chlorides through the pore solution is simulated using a flux equation that is based on of Fick's second law of diffusion. The free chlorides provide the driving potential. Second, the distribution of the total chloride content in concrete is calculated using a combination of the mass balance equation and nonlinear chloride binding (Tang and Nilsson, 2000; Tang, 2007; Shukla and Pillai, 2015). In addition to diffusion process, ClinConc model takes into account convection and ionic migration in modelling the ingress of chloride ions (Shukla and Pillai, 2015).

2.5.6.3 Life-365 model

Life-365 is an empirical model developed by the American Concrete Institute, which integrates chloride ingress, initiation and propagation of corrosion, repair schedule and life cycle cost together. It is based on Fick's second law of diffusion (Equation 2.4) with the total chloride content considered as the source of the driving force. It takes into account the effect of temperature on diffusion coefficient (Tang, 2007; Shukla and Pillai, 2015). Details about this model can be found in *Life-365 Service Life Prediction Model*™ (2008).

The diffusion coefficient is considered time and temperature dependent and is modelled as shown in Equation 2.19. In order to minimise the effects of continually decreasing diffusion coefficient with time, the relationship shown in Equation 2.2 is considered valid up to 30 years, beyond which the value at 30 years (D_{30y}) calculated from the equation is assumed constant during the rest of the period. A special software is needed for the application of the model (Tang, 2007; Shukla and Pillai, 2015).

$$D(t,T) = D_{ref} \times \left(\frac{t_{ref}}{t} \right)^{m} \times e^{\frac{U}{R}\left(\frac{1}{T_{ref}} - \frac{1}{T}\right)} \qquad (2.19)$$

where: $D(t,T)$ is the diffusion coefficient at time, t and temperature T,

m is the age factor,

D_{ref} is the diffusion coefficient at reference time (t_{ref} = 28 days),

T_{ref} is the reference temperature (293 K),

U is the activation energy of the diffusion process (35000 $Jmol^{-1}$),

R is the universal gas constant.

Life-365 is widely used due to its user friendly interface, free availability and comprehensiveness. In addition to predicting service life, it also generates maintenance and repair plans. The limitations of this model include simplifications and assumptions made during its application, and limited use outside North America, where it was developed for use (Shukla and Pillai, 2015).

2.5.6.4 DuraCrete model

The DuraCrete model for chloride ingress is a probabilistic service life prediction model developed within the Brite-EuRam (DuraCrete) project, which defines a serviceability limit state and calculates the probability of attaining that limit state. It uses the 28-day diffusion coefficient measured using chloride migration tests governed by Fick's second law of diffusion. Alternatively, a time dependent variation of the apparent diffusion coefficient can be modelled using a power function shown in Equation 2.20 (Lindvall, 2000; Tang, 2007; Shukla and Pillai, 2015).

$$D_0(t) = D_0(t_{ex}) \times \left(\frac{t_{ex}}{t} \right)^n \qquad (2.20)$$

where: $D_0(t)$ is the time dependent variation of the apparent diffusion coefficient,

t_{ex} is the time of first exposure,

t is the time of inspection,

n is the aging factor.

The aging factor (n) depends on the rate of hydration and extent of drying, thus, it relies on binder type and exposure environment. The input parameters for the DuraCrete model comprise chloride concentration at the exposed surface, measured chloride diffusion coefficient of concrete and exposure time (Lindvall, 2000; Polder and Rooij, 2005; Wegen *et al.*, 2012). An extensive review of this model is presented in DuraCrete (1998).

2.5.6.5 South African chloride prediction model

The South African prediction model (also referred to as UCT Service Life Model) for chloride ingress allows for the determination of expected service life of concrete structures based on environmental conditions, concrete quality and cover thickness. It characterises chloride resistance of concrete using early-age (28-35 days) chloride conduction properties. Depending on type of binder, allowance is made for continued cementing reactions and chloride binding, thus the model is sensitive to long-term effects. Therefore, it can be used to predict long-term performance of RC concrete in terms of chloride resistance. The environmental classes relate to the EN 206 classes, modified with additional sub-clauses to suit the South African coastal conditions as shown in Table 2.1. Chloride conductivity index obtained from the CCI test is used in the prediction model (Mackechnie, 2001; Mackechnie and Alexander, 2002; Alexander and Beushausen, 2009; Heiyantuduwa and Alexander, 2009).

Table 2.1: Environmental classes according to BS EN 206 (Ballim *et al.*, 2009)

EN206-1 Class	**Description of environment**
XS1	Exposure to airborne salt but not in direct contact with sea water
XS2a	Permanently submerged
XS2b*	XS2a + exposed to abrasion
XS3a	Tidal, splash and spray zones
XS3b*	XS3a + exposed to abrasion

**Sub-clauses added for South African coastal conditions*

The South African chloride model takes into account the main influencing factors from the material, construction practices and the environment. Factors such as binder type, initial curing, marine exposure zone and concrete maturity are considered in evaluating chloride resistance. The non-steady state migration of chloride ions in specimens follows the Einstein and Nernst-Planck equations (Alexander and Mackechnie, 2004; Alexander and Beushausen, 2009).

2.6 Carbonation

Concrete carbonation is predominant in environments with high concentration of CO_2 (e.g. urban and industrial areas). Carbonation process involves the diffusion of atmospheric CO_2

through partially filled pore system (see Figure 2.23), and subsequent chemical reactions that lower the pH of concrete (Chang and Chen, 2006; Roziere *et al.*, 2009).

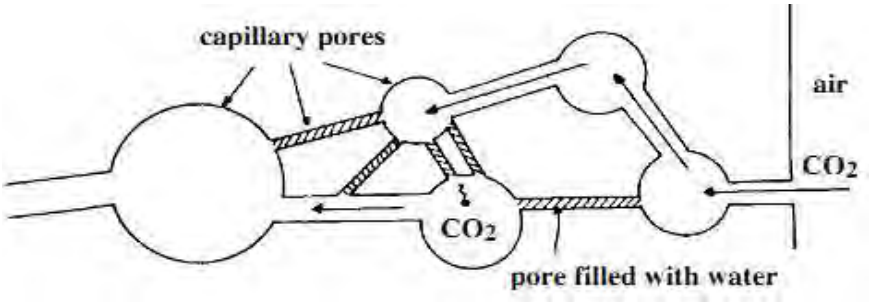

Figure 2.23: Diffusion of CO_2 in partially filled pore system (Houst, 1996)

The factors affecting carbonation in cement-based materials include penetrability, CO_2 concentration, temperature, relative humidity and the amount of carbonatable components (Atis, 2003; Sisomphon and Franke, 2007). Carbonatable components refer to the cement hydrates (portlandite ($Ca(OH)_2$) and calcium silicate hydrates (C-S-H)) that maintain the alkaline conditions in concrete (Nilsson, 2003).

2.6.1 Carbonation reactions

The reactions leading to carbonation take place in the pores of the cement paste. The cement paste of hardened concrete contains hydrates such as silicates, aluminates and calcium hydroxide in varying amounts depending on the type of cement used. The pore solution contains ions such as sodium (Na^+), potassium (K^+), calcium (Ca^{2+}), hydroxyl (OH^-), and dissolved oxygen, which enhance alkalinity in concrete, thus creating a protective passive film on the surface of steel (Papadakis and Vayenas, 1991; DuraCrete, 1998; Badaoui *et al*., 2013).

The diffusion and dissolution of atmospheric carbon dioxide in the pore solution results in the formation of carbonic acid (H_2CO_3), which lowers the high pH of the pore solution (Glass, 2003; Thiery *et al.*, 2007; Penttala, 2009).

$$CO_2 + H_2O \rightarrow H_2CO_3 \qquad (2.21)$$

Figure 2.24 illustrates the interactions among gaseous, fluid and solid phases during carbonation of cement paste.

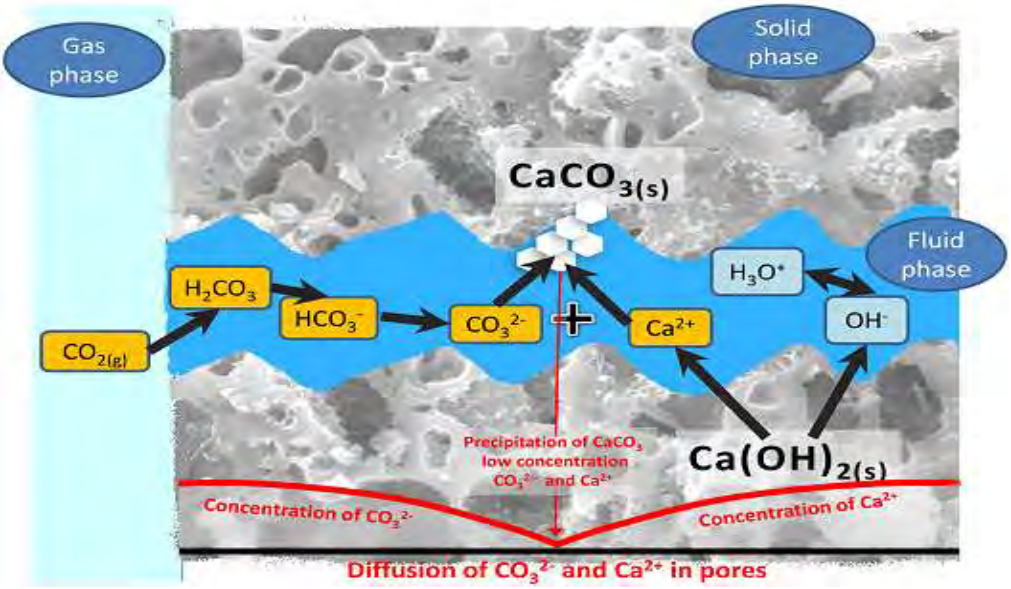

Figure 2.24: Schematic of carbonation mechanism (Czarnecki and Woyciechowski, 2015)

The dissociation of carbonic acid into HCO_3^- and CO_3^{2-}, the subsequent dissolution of solid $Ca(OH)_2$ to release Ca^{2+} and OH^- ions, and the precipitation of Ca^{2+} and CO_3^{2-} to form calcium carbonate ($CaCO_3$), can be combined in the overall chemical equation (Hearn *et al.*, 2006; Thiery *et al.*, 2007):

$$Ca(OH)_2 + CO_2 \rightarrow CaCO_3 + H_2O \qquad (2.22)$$

Similarly, the chemical reaction between CO_2 and calcium silicate hydrates (C-S-H) yields $CaCO_3$, with hydrous silica gel (Hearn *et al.*, 2006; Papadakis and Vayenas, 2012):

$$3CaO \cdot 2SiO_2 \cdot 3H_2O + 3CO_2 \rightarrow 3CaCO_3 \cdot 2SiO_2 \cdot 3H_2O \qquad (2.23)$$

The relative humidity (RH) plays a key role in the diffusion of CO_2 and the kinetics of carbonation reaction. Maximum depths of carbonation at 21 ± 1°C have been recorded in the range of 55 – 75% RH (Russell *et al.*, 2001; Thiery *et al.*, 2008; Houst, 1996; Russell *et al.*, 2001). Experimental evidence shows that at RH values above 75%, the saturated pores impede the diffusion of CO_2, thus slowing down carbonation. At relative humidity below 55%, the moisture is insufficient for chemical reactions (Equations 2.22 and 2.23) to proceed (Basheer *et al.*, 2001; Nilsson, 2003; Thomas and Skalny, 2006; Badaoui *et al.*, 2013). As carbon dioxide reacts with cement hydrates a carbonated zone of pH progresses into the concrete. A decrease in pH distroys the passive film, thus exposing steel to the aggressive

chemical species that initiate corrosion (Basheer *et al.*, 2001; Glass, 2003; Thiery *et al.*, 2007).

2.6.2 Carbonation coefficient

The carbonation coefficient determines the rate of carbonation in concrete. Factors that influence the carbonation coefficient include carbon dioxide concentration, penetrability of the surface layer, relative humidity and thickness of the cover. As carbonation proceeds, the carbonation coefficient decreases due to precipitation of calcium carbonate ($CaCO_3$) on the pore wall (thus reduction in size of pores).

2.6.3 Effects of carbonation on pore structure

The product of carbonation reaction ($CaCO_3$) has larger mass compared to the initial reactant ($Ca(OH)_2$). Therefore, the precipitation of $CaCO_3$ on the pore walls reduces the pore volume. This slows down the rate of carbon dioxide diffusion and subsequently reduces carbonation reaction (Bentz *et al.*, 1999; Sisomphon and Franke, 2007; Penttala, 2009). In unreinforced concrete, carbonation enhances durability by refining and improving the pore structure of the cover zone (Ballim *et al*., 2009).

2.6.4 Reference tests for carbonation

The general principles for laboratory test methods that evaluate concrete carbonation are gas permeability and testing under accelerated conditions. Factors that ought to be controlled by the test methods when applying these principles include aging of concrete due to continued hydration, reactivity of concrete with penetrating substances, pore water composition and its effect on transport processes, effects of preconditioning on the pore structure, e.g. microcracking upon drying (Kropp and Alexander, 2007). The following sections present a discussion on some of the commonly used methods.

2.6.4.1 Accelerated carbonation test

The accelerated carbonation test is used to evaluate depths of carbonation after exposure of specimens to conditions that accelerate the carbonation process, in accordance with NT Build 357. The specimens are placed in a carbonation chamber, set to maintain 2-3% CO_2 concentration at 20 ± 2 ˚C and 55-75% RH during the exposure period. After exposure, the specimen is split and phenolphalein indicator solution applied on the surface to indicate

carbonated sections (DuraCrete, 1998). Non-carbonated zones are shown by a change in colour of the indicator to pink, while no colour change is observed on carbonated areas. The depth of carbonation is then measured as illustrated in Figure 2.25.

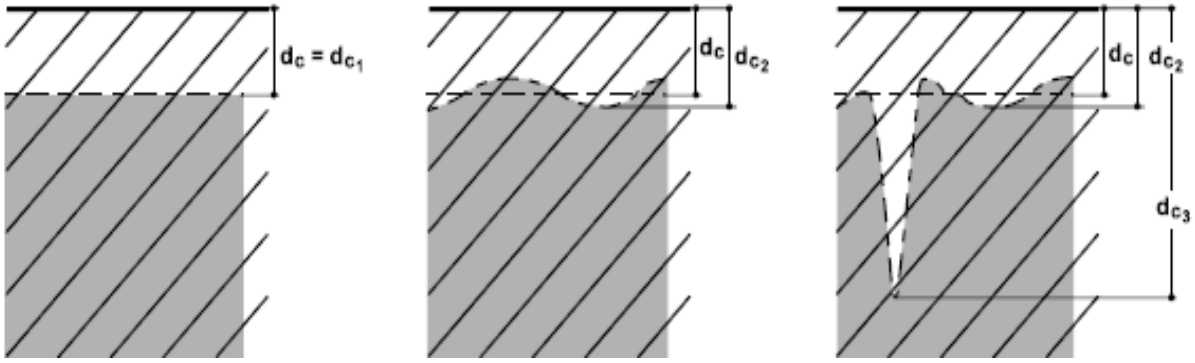

(a) (b) (c)

Figure 2.25: Carbonation depth measurements (DuraCrete, 1998)

When the carbonation front is approximately parallel to the surface, the depth of carbonation, d_c, is reported as shown in Figure 2.19(a). If the carbonation front is uneven but without distinctly deeper penetration depth as shown in Figure 2.19(b), both the average carbonation depth, d_c, and maximum carbonation depth, d_{c2}, are considered. When there are isolated areas of distinctly deeper carbonation fronts as shown in Figure 2.19(c), the maximum depth, d_{c2}, and average depth, d_c, are considered separately. However, the deeper isolated depths are not considered while calculating the average value (RILEM recommendations CPC-18, 1988; DuraCrete, 1998).

2.6.4.2 Gas permeability tests

The gas permeability characteristics are of particular importance in predicting the carbonation resistance of cement-based materials. Experiments on gas permeability are based on the application of a pressure gradient across the specimen and monitoring the flow rate at steady state. The general set up of gas permeability apparatus consists of a diffusion cell separated by the test specimen into two chambers which contain gases of known pressure (see Figure 2.26) (Bentz *et al.*, 1999; Kropp and Alexander, 2007; Beushausen and Alexander, 2008).

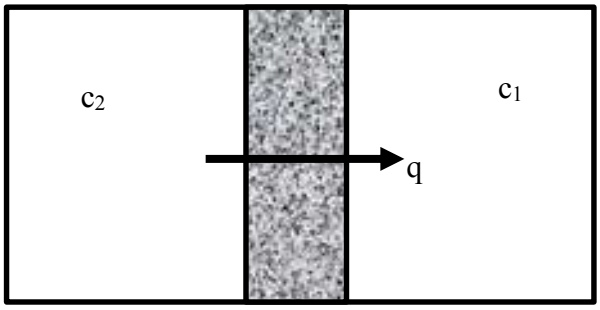

Figure 2.26: Typical set-up of a diffusion cell (Kropp and Alexander, 2007)

Experiments on gas permeability take reasonably short time and can be performed on laboratory specimens, cored samples or even existing concrete structures (DuraCrete, 1998; Bentz *et al.*, 1999). The specimen is mounted in a pressure cell with distinct difference in gas pressure in each chamber. Due to concentration gradient, gas will flow from the chamber of higher pressure (c_2) through the specimen and into the chamber of lower pressure (c_1). Gas flow in the capillary pores of the specimen is assumed to be laminar. Gas permeation is evaluated according to the Hagen-Poiseuille relation (Equation 2.24) for laminar flow of Newtonian fluids (Kropp and Alexander, 2007).

$$K_i = \frac{2P_a Q_i L \mu}{A\left(P_i^2 - P_a^2\right)} \qquad (2.24)$$

where: A is the cross-sectional area of the specimen (m^2),
L is the thickness of the specimen (m),
K_i is gas permeability coefficient at pressure stage i (m^2),
μ is the dynamic viscosity of the fluid at test temperature (N s m^{-2}),
Pa is atmospheric (absolute) pressure (1 bar = 10^5 Pa),
P_i is the applied (absolute) test pressure (Pa),
Q_i is the flow rate at pressure stage I (m^3/s)

a) Oxygen permeability index test

The oxygen permeability index (OPI) test is based on pressure-induced flow of oxygen through disc specimens (typically 70 ± 2 mm diameter and 30 ± 2 mm thick). The falling head permeameter (shown in Figure 2.27) measures the pressure decay of oxygen gas passed through the test specimens. The gas flow through the sample follows Darcy's law (Equation 2.25), which characterizes the porous material by the intrinsic permeability coefficient, K

(Alexander *et al.*, 2006; Beushausen and Alexander, 2008). Instructions for OPI test are provided in the DI Testing Procedure Manual (2010).

$$\frac{dq}{dt} = KA\frac{\rho g}{\mu}\frac{dh}{dL} \tag{2.25}$$

where: ρ is density of the permeating fluid (kg/m^3),
g is acceleration due to gravity (9.81 m/s^2),
μ is viscosity of the permeating fluid (Pa·s),
K is intrinsic permeability coefficient (m^2).

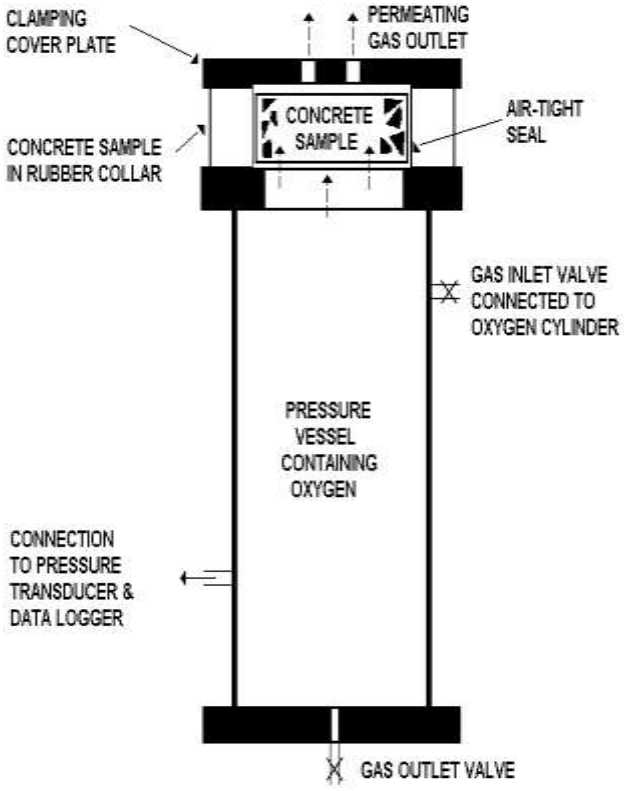

Figure 2.27: Schematic diagram of the falling head permeameter (Alexander, 2004)

The key factors affecting the intrinsic permeability coefficient are pore structure (size, connectivity and tortuosity) and moisture content. The presence of moisture in the pores substantially reduces gas permeability. Thus, the test samples ought to be conditioned to constant moisture content through drying, though with caution to avoid microstructure damage through cracking (Hearn *et al.*, 2006; Bentur and Mitchell, 2008; Wong *et al.*, 2009).

The OPI test is sensitive to the volume and connectivity of larger pores and voids where the transport processes occur. Research indicates that the gas permeability characteristics of concrete and mortars may provide a reliable indication of carbonation resistance in RC structures in service (DuraCrete, 1998; Alexander *et al.*, 2006; Hearn *et al.*, 2006; Ballim *et al.*, 2009). The design against carbonation considers the empirical relationships between 28-day OPI values and carbonation depth measurements obtained from built structures or samples subjected to accelerated carbonation test conditions.

The OPI values range from 8 to 11 and are taken as negative logarithm of the *k*-value. The higher the OPI the lower the permeability of specimen. The Darcy coefficient of permeability (*k*-value) is derived from the plot of the natural log of the ratio of initial pressure to pressure at a given time versus time, as expressed in Equation 2.26 (Alexander *et al.*, 2006; Ballim *et al.*, 2008, 2009).

$$k = \left(\frac{\omega V g d}{R A \theta}\right)\left(\frac{\ln P_0}{P}\right)\frac{1}{t} \qquad (2.26)$$

where k is the coefficient of permeability (m/s),
ω is the molecular mass of permeating gas (kg/mol),
V is the volume of pressure cylinder (m^3),
g is acceleration due to gravity (m/s^2),
d is sample thickness (m),
R is the universal gas constant (N m/k mol),
A is the cross-sectional area of the sample (m^2),
θ is the absolute temperature (K),
t is time (s),
P_0 is the initial pressure (kPa),
P is pressure at any given time t (kPa).

b) RILEM-Cembureau method

The RILEM-Cembureau method is used to measure gas permeability of disk specimens (typically 150 mm diameter and 50 mm thick). A constant pressure gradient is applied to initiate gas flow (Kollek, 1989; DuraCrete, 1998; RILEM TC 116-PCD, 1999). Figure 2.28 shows a schematic of the set up with details of the pressure cell. The procedures for the test

as well as preconditioning measures have been documented by Kropp (1999a, 1999b) and Carcasses *et al*. (2002).

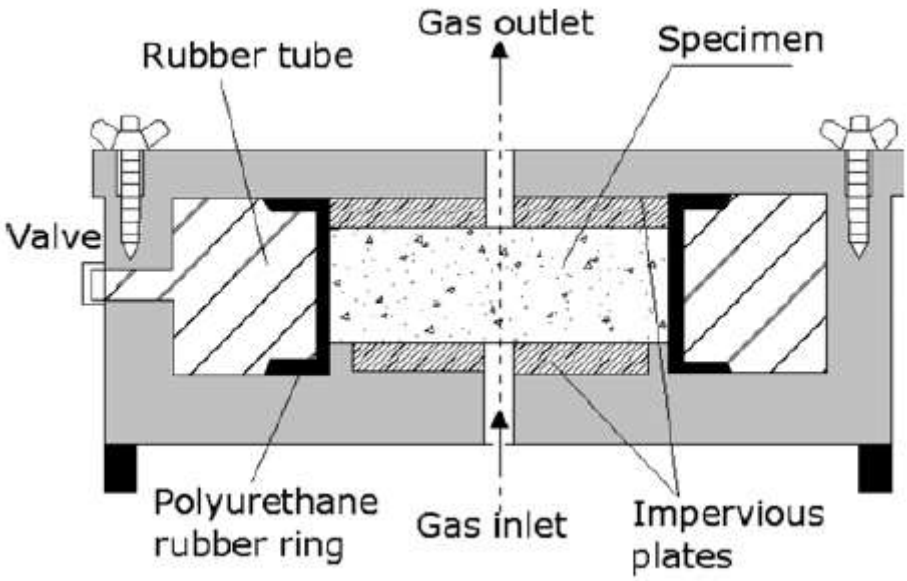

Figure 2.28: Schematic representation of the Cembureau pressure cell (Guneyisi *et al.*, 2012)

c) Torrent permeability test

The Torrent permeability test (TPT) method measures the oxygen permeability of concrete cover using a two-chamber vacuum cell. It can be applied on both laboratory specimens and in-situ concrete (DuraCrete, 1998; Beushausen and Alexander, 2008). Figure 2.29 shows the TPT apparatus.

Figure 2.29: Torrent permeability test apparatus (Ballim *et al.*, 2009)

To evaluate gas permeability, the cell is placed on the concrete surface and air in the chambers is evacuated using a pump to create a vacuum. A regulator is used to balance pressure in the inner and outer chambers. As air is drawn from the underlying concrete, pressure increases in the inner chamber. The rate of increase in pressure is then recorded (Torrent *et al.*, 2007b)

d) Autoclam Permeability test

The Autoclam permeability test method can be used to measure water and air permeability of concrete. This method involves bonding or sealing a bond ring onto the test surface using a rubber ring, which isolates the test area with a diameter of 50. The body of the Autoclam containing the pressure transducer is bolted to the base ring with an O-ring sealing the ring and the body during the test as shown in Figure 2.30 (Torrent *et al.*, 2007b). To perform the Autoclam permeability test, relative pressure inside the apparatus is increased to slightly above 0.5 bars, after which the test begins automatically. The decay in pressure is monitored every 15 minutes or until it has diminished to zero (Torrent *et al*., 2007b).

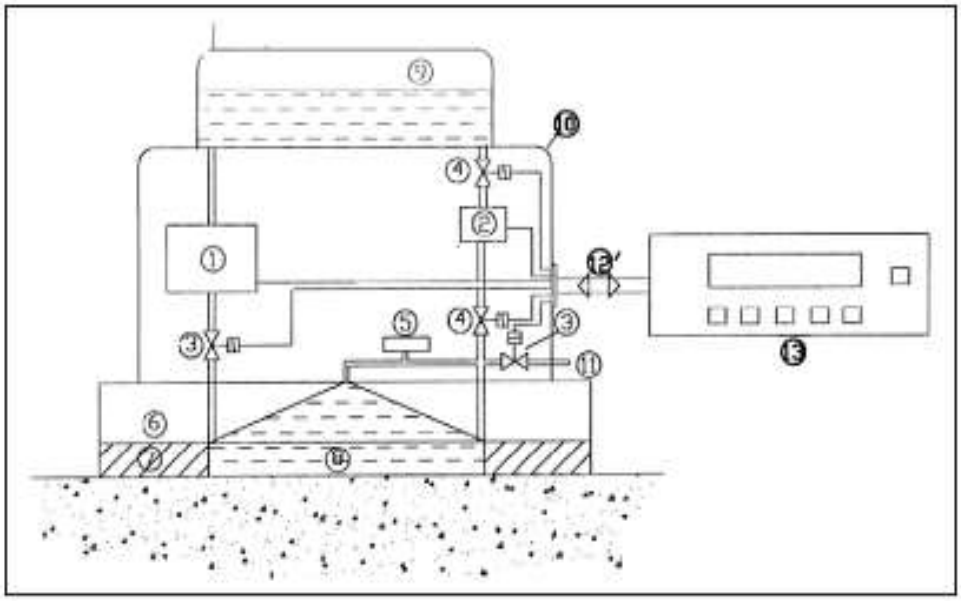

Figure 2.30: Schematic of Autoclam air permeability test (Torrent *et al.*, 2007b)

2.6.5 Service life prediction models for carbonation

Carbonation process involves the diffusion of carbon dioxide from the atmosphere into the pore structure and the subsequent reaction of carbon dioxide with cement hydrates. Deterioration of concrete through carbonation is often quantified in terms of carbonation

depth by applying phenolphthalein indicator solution, which can detect a change in pH value of about 9 (Nilsson, 2003; Tang, 2007). Prediction models for carbonation assume that corrosion occurs when the carbonation front reaches the steel reinforcement. Most of these models are based on modified Fick's first law of diffusion, expressed as (Tang, 2007):

$$X_c = \sqrt{\frac{2D_c(c_1 - c_2)}{a}} \cdot \sqrt{t} = A \cdot \sqrt{t} \qquad (2.27)$$

where: X_c is the depth of carbonation,
D_c is the diffusion coefficient of CO_2,
C_1 is the CO_2 concentration at concrete surface,
C_2 is the CO_2 concentration at the front,
a is the amount of carbonatable materials,
t is the exposure period,
A is the carbonation coefficient.

In the following sections, some frequently used and/or well documented carbonation prediction models will be discussed. These include the DuraCrete model for carbonation, the RILEM-Cembureau model and the South African carbonation prediction model.

2.6.5.1 DuraCrete model

The DuraCrete model for carbonation prediction is an empirical relationship proposed in the EU project DuraCrete in 1996. The prediction of carbonation depths is based on material composition, exposure conditions, curing regime and age of concrete (Tang, 2007; Badaoui *et al.*, 2013; Decatoire *et al.*, 2014). In DuraCrete model, the carbonation coefficient A in Equation 2.27 is expressed as (Tang, 2007; Badaoui *et al.*, 2013).

$$A = \sqrt{\frac{2k_{e,ca} \cdot k_{c,ca} \cdot D_{eff,ca} \cdot c_{s,ca}}{a}} \cdot \left(\frac{t_0}{t}\right)^{n_{ca}} \qquad (2.28)$$

where: $k_{e,ca}$ and $k_{c,ca}$ are constants accounting for the influence of environment and curing conditions respectively on carbonation process,
$D_{eff,ca}$ is the effective diffusion coefficient of CO_2,
$C_{s,ca}$ is the CO_2 concentration at the surface of concrete,
t_0 is the reference period (28 days),
n_{ca} is the aging factor which relies on environmental conditions

The parameter *a* is expressed as:

$$a = 0.75 \cdot C \cdot [CaO] \cdot \gamma_h \cdot \frac{M_{CO_2}}{M_{CaO}} \quad (2.29)$$

where: C is the cement content in concrete,
$[CaO]$ is calcium oxide (CaO) content in cement,
γ_h is the degree of hydration,
M denotes the respective molar masses.

2.6.5.2 RILEM-Cembureau model

In the Cembureau method, the coefficient of permeability is calculated according to the Hagen-Poiseuille relation (Equation 2.24). The average flow rate is evaluated at each pressure stage using the Cembureau permeameter, after which the average coefficient is calculated. The model assumes laminar flow though the flow rate shows a non-linear behaviour, thus making the permeability coefficient a function of applied pressure (RILEM TC 116-PCD, 1999; Bjegovic *et al.*, 2015).

2.6.5.3 Square-root-of-time model

The square root of time model relates the carbonation depth and the rate of advance of the carbonation front using the expression (Ballim *et al*., 2009):

$$x = Dt^n \quad (2.30)$$

where: x is the depth of carbonation,
t is the time of exposure,
n is a constant typically varying from 0.4 - 0.6 depending on exposure conditions,
D is the carbonation coefficient.

Assuming a constant diffusion coefficient, this model assumes a direct proportionality between the progression of carbonation front and the square root of time as shown in Equation 2.27. The coefficient of diffusion, however, varies with carbonation depth; it also depends on the moisture content of the pore system. For these reasons, the use of constant

parameters while applying Fick's law for CO_2 diffusion in concrete is limited (Papadakis and Vayenas, 1991; Basheer *et al.*, 2001; Sisomphon and Franke, 2007).

2.6.5.4 South African carbonation prediction model

The South African carbonation model utilizes the oxygen permeability index determined at early age to predict the long term performance of RC structure in terms of carbonation resistance. The model is derived from the correlation of the results of the short-term OPI test and actual carbonation depths monitored in aggressive environments over periods of up to ten years (Alexander and Beushausen, 2009; Ballim *et al.*, 2009).

The carbonation prediction model may also be used to determine the required OPI value based on predetermined values for cover thickness, exposure environment and expected service life. If the quality of concrete is known from a given OPI value, a corrosion-free design life can be estimated (Alexander and Beushausen, 2009). In addition to material properties, this model takes into account construction practices such as initial curing. Characterization of gas permeability of specimens is governed by Darcy's law (Alexander *et al.*, 2006).

2.7 Influence of aggregate size on penetrability

The service life prediction models discussed in Sections 2.5.6 and 2.6.5 have not been verified for common types of patch repair mortars. Clearly, concrete and mortar have different microstructures, thus different transport properties. This difference mainly arises from their dissimilar mix compositions. For example, mortar does not contain coarse aggregate. Moreover, it has a higher paste content compared to concrete. The differences in microstructures is primarily manifested in the size, tortuosity and volume of the pores. Thus, the variation in transport properties between concrete and mortar can be attributed to the differences in their pore structures. To compare the durability performance of concrete and mortar, a better understanding of the differences in their pore structures is essential.

The interfacial transition zone (ITZ) is the region of cement paste that surrounds each aggregate particle. Mehta and Monteiro (2006) describe the ITZ as the bridge between mortar matrix and coarse aggregate particles, which contains voids and microcracks. It has significant influence on the transport properties of both concrete and mortar. The ITZ contains greater volume of capillary pores compared to the cement paste matrix, thus the

higher local penetrability in the ITZ. Numerous studies have attributed the porous nature of the ITZ to the 'wall effect'; which occurs when cement particles cannot pack together near aggregate (Delagrave *et al.*, 1997; Yang and Su, 2002; Wong *et al*., 2009).

Literature shows that the volume and distribution of ITZ in cement-based materials depends on the size and volume fraction of aggregates (Garboczi and Bentz, 1996; Ballim *et al.*, 2009; Wong *et al*., 2009). The scanning electron microscopy (SEM) images in Figure 2.31 show the distribution of aggregates of mortar and concrete.

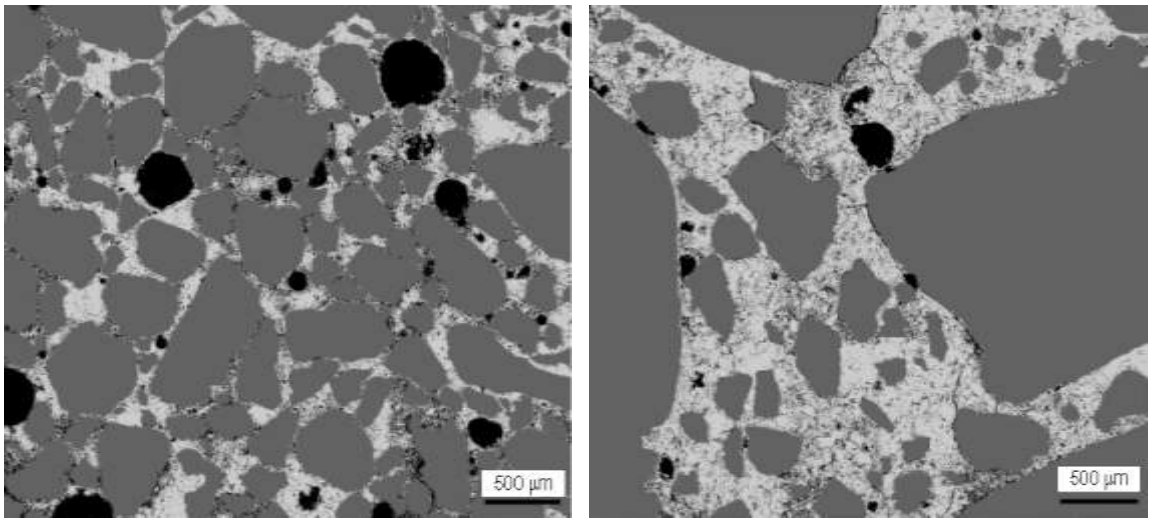

(a) (b)

Figure 2.31: SEM images of (a) 90-day mortar containing 70% sand volume fraction, and (b) 90-day concrete containing 70% aggregate (coarse and fine) volume fraction (Wong *et al*., 2009)

From Figure 2.31, it can be seen that at a constant aggregate volume fraction, the cement paste matrix is thicker in concrete than in mortar. In addition, the volume of ITZ is greater in mortar compared to concrete. Based on the presented SEM images, mortar can thus be assumed to be more penetrable than concrete since the ITZs appear to be interconnected, thus creating continuous pathways that enhance penetration. Wong *et al*. (2009), in contrast, observed lower penetrability in mortar than in concrete, at a constant aggregate volume fraction. A study by Grassl *et al*., (2010), also found that increasing the size of aggregate while keeping its volume fraction constant increases penetrability of cement-based materials. Both researchers attributed the increase in penetrability to increase in the average width of microcracks induced when the aggregate restrains the shrinkage (drying) of cement paste.

Thus, an increase in size of aggregate seems to increase the average width of microcracks when the cement paste is drying, which results in higher penetrability.

These microcracks are generally wider than the capillary pores in the cement paste matrix. The propagation of microcracks establishes interconnectivity, which significantly lowers the penetrability of materials (Mehta and Monteiro, 2006). The two main types of microcracks reported by Wong *et al*. (2009) are *bond cracks* and *matrix cracks*. *Bond cracks* develop along the ITZ while *matrix cracks* develop from the surface of the aggregate and propagate into the cement paste matrix. On reaching the surface of the adjacent aggregate particle, cracking may either stop or proceed around the aggregate. Though unusual, the microcrack may also traverse the intercepting aggregate. The SEM image in Figure 2.32 shows the two types of microcracks.

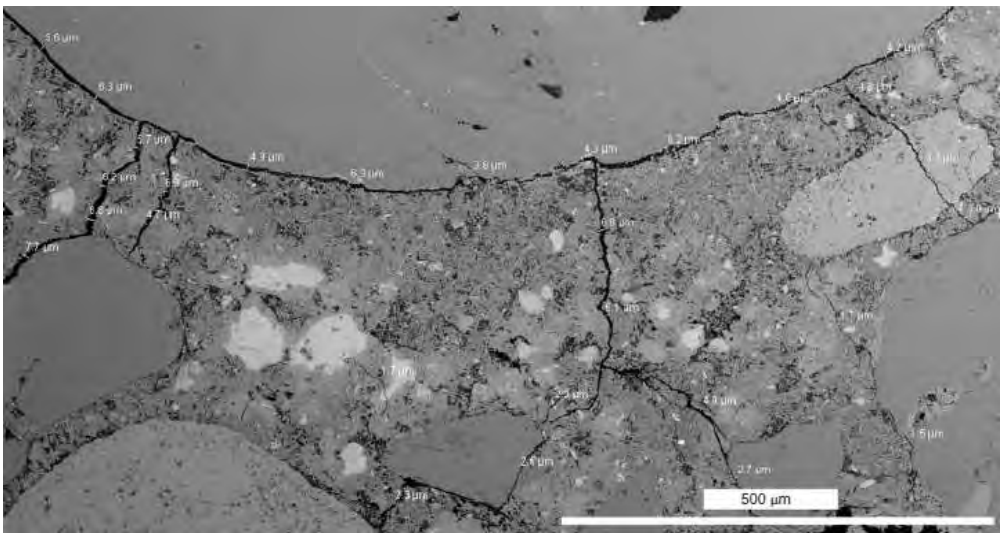

Figure 2.32: SEM image showing microcracks on concrete specimen subjected to a temperature of 105^0C, simulating those caused by drying shrinkage (Wong *et al*., 2009).

The tortuosity of microcracks is determined by their effective length. Factors influencing the tortuosity of microcracks include the volume fraction and size distribution of aggregates. In cement-based materials containing more aggregate particles per unit volume such as mortar, microcracks have tortuous paths, since they are either intercepted or compelled to circumvent the aggregate particles. Under similar drying conditions and same aggregate fraction, the microcracks in concrete would therefore be expected to be less tortuous than in mortar due to fewer intercepting aggregate particles in concrete (Wong *et al.*, 2009). This implies a higher penetrability in concrete than in mortars.

2.8 Performance of patch repair mortars

Patch repair mortars (PRMs) are used to replace damaged (cracked, delaminated or spalled) or contaminated (with chloride ions or carbonation) sections of concrete. In structural applications, PRMs have an additional role of restoring the load-bearing capacity of concrete members. Although the literature covers a wide variety of performance requirements for PRMs (BS-EN 1504-3, 2005; Beushausen and Chilwesa, 2013), this review will focus on resistance to cracking, penetration of chloride ions, and carbonation.

2.8.1 Cracking resistance

Cracking resistance of repair mortars is an important consideration in the durability performance of concrete repairs. Studies suggest that volume changes in cement-based repair materials is the main cause of cracking (ICRI Technical Guidelines, 1996). Cracks offer easier pathways, which allow a more rapid ingress of the aggressive chemical species to the surface of steel, thus accelerating the deterioration of concrete structures (Glass, 2003). Repair mortars with high crack resistance would adequately protect the steel reinforcement from corrosion. Several studies mention drying shrinkage and tensile strength as the key factors that influence the cracking resistance of patch repair mortars (Decter, 1997; Rao, 1998; Itim *et al.*, 2011). However, the results from a study by Beushausen and Chilwesa (2013) showed that the cracking resistance of repair mortars depends on the interaction of several material properties that include tensile relaxation, elastic modulus, tensile strength and shrinkage.

As already mentioned in Section 2.7, mortars and concretes usually contain microcracks (fine cracks) within the cement matrix due to restrained shrinkage deformations within the cement paste. When these microcracks connect to form a continuous network, the penetrability of the mortar increases. This could lead to reinforcement corrosion, consequently reducing the durability of RC structures. Cracking in RC structures ought to be minimised due to the following reasons (Savija, 2014):

i) Cracks form preferential pathways for the penetration of aggressive and deleterious chemical substances such as chlorides, carbon dioxide and oxygen.
ii) By reducing the protection offered by concrete cover, cracks reduce the duration of corrosion initiation.

iii) The different conditions within concrete created by cracks may result in varied electrochemical potentials, which may lead to the formation of electrochemical cells.
iv) Aesthetically, cracks are undesirable and may reduce confidence in safety and integrity of the structure.

2.8.2 Penetration resistance in repair mortars

Studies on penetration behavior of cement-based materials have been conducted for over 100 years, with one of the early publications on permeability of cement and mortars by Hyde and Smith (1889) dating back to 1889. Penetrability can be defined as the ease with which the transport of fluids and ionic species occur in the pores of a material. It is mainly influenced by the volume, size and connectivity of the pores (Hearn *et al.*, 1994; Basheer *et al.*, 2001; Nilsson, 2003; Hearn *et al.*, 2006; Ballim *et al.*, 2009). Dense microstructures with narrow and less connected pores will display low penetrability.

2.8.3 Relationship between porosity and permeability

Porosity and permeability are often used to characterize the resistance to penetration of substances in concretes and mortars (Lafhaj *et al.*, 2006). These two parameters are closely related. Permeability of concretes and mortars is mainly controlled by capillary porosity (Bentz *et al.*, 1999). Pores are entrapped voids in the cement paste, through which the transport of fluids and chemical species occur. The rate of transport in cement-based materials is therefore dependent on cement paste characteristics, which includes pore size distribution, essentially controlled by the water-cement ratio. Porosity influences concrete properties such as compressive strength, permeability, shrinkage and creep. In the light of durability, porosity has a significant influence on transport properties (Hearn *et al.*, 1994; Lafhaj *et al.*, 2006; Alexander and Thomas, 2015).

The total pore volume consists of gel and capillary pores. The capillary pores are instrumental in the transport of ionic species, more so, if they are interconnected and filled with pore solution (Pack *et al*., 2010). Figure 2.33 illustrates the various pore systems in materials.

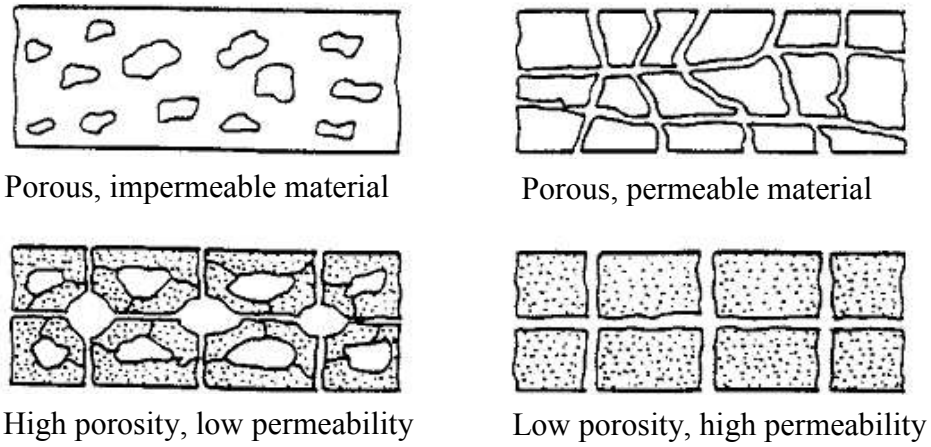

Figure 2.33: Schematic of porosity and permeability (Hearn *et al.*, 1994)

Continuous conduits in cement-based materials may result from insufficient hydration or microcracking in the bulk paste or along the ITZ. Microcracking may be caused by drying shrinkage, thermal shrinkage, carbonation shrinkage, and applied loads. Microcracks are generally larger than capillary pores, thus they provide continuous and easy pathways for the flow of substances through concrete (Glass, 2003; Hearn *et al.*, 2006; Wong *et al.*, 2009).

The volume fraction and interconnectivity of the pores largely affects the permeability of materials. Factors that control these two parameters include the water-cement ratio, binder content, binder type and degree of hydration (Mehta and Monteiro, 2006; Pack *et al.*, 2010). At low porosity, on the one hand, the pores are distinct and isolated from each other, thereby, reducing the permeability of concrete or mortars (Glass, 2003). Moreover, further hydration results in disconnected and isolated capillary pores and thus the gel pores control the permeability (Hearn *et al*., 2006). On the other hand, large interconnected pores (and cracks) may significantly increase permeability (Mehta and Monteiro, 2006).

2.8.4 Effects of self-sealing and autogenous healing

The decrease in permeability of cement-based materials is caused by continued hydration as well as self-sealing mechanism and autogenous healing of cracks. Self-sealing effect (SSE) is attributed to the dissolution and redeposition of hydrates. The self-sealing mechanisms fall under two categories (Hearn, 1998):

i) Mechanisms that cause temporary reduction in permeability.
ii) Mechanisms that permanently change the permeability of cement-based materials.

The temporary self-sealing effect (SSE) may occur when the permeating water contains dissolved gases. This may be due to, for example, gas pressurization of water. A decrease in pressure across the specimen is accompanied by the release of air bubbles from permeating water, which blocks the pores. This SSE is, however, reversible and can be eliminated when the permeating liquid is de-aired. In addition, the inflow and outflow of water in the cement paste results in swelling and shrinkage respectively. These changes in the volume of cement paste have been attributed to expansion and shrinkage of C-S-H gel layers, which cause corresponding constriction and dilation of flow paths (Decter, 1997; Hearn, 1998).

The permanent SSE is mainly caused by the chemical interaction of water and cement paste (continued hydration), and physical clogging. Continued hydration causes swelling and subsequent reduction in size of pores, thus reducing permeability. Physical clogging may result from silting of cement particles due to high pressure, such as during gas permeability tests (Lafhaj *et al.*, 2006).

Autogenous healing refers to the sealing of cracks in fractured concrete through chemical reactions that involve the cement paste. This mechanism is common in water retaining structures and pipes made with concrete. The chemical reaction between the pore solution (containing calcium hydrogen carbonate, $Ca(HCO_3)_2$) and calcium hydroxide in the cement paste, or the carbonation process (discussed in section 2.7.1), results in white crystalline precipitate that fills up the cracks (Hearn, 1998). As reported by Hearn (1998), the main differences between autogenous healing and SSE are: (a) SSE does not necessarily involve cracks, and (b) SSE does not involve carbonation reactions. However, some mechanisms such as continued hydration and transport of loose particles may be common in both processes.

2.9 Summary

An overview of the main deterioration processes reported to reduce the service life of RC structures have been presented in this literature review. In addition, factors influencing these processes, reference tests and the service life models commonly used to measure and predict penetration resistance of materials are covered. All these were discussed to provide a holistic understanding of the deterioration processes that influence concrete durability, along with its influencing factors. A better understanding of these will assist in:

i) development of the experimental procedures in Chapter 3, which includes tests and experimental variables,
ii) understanding the principles that govern the various measurement techniques used in this study,
iii) prediction of chloride ingress and carbonation depths in patch repair mortars using the existing service life prediction models,
iv) analysis and interpretation of experimental data in Chapter 4,
v) generating service life prediction models for chloride penetration and carbonation in patch repair mortars

In light of performance-based specification of construction materials, much research has been conducted in the recent past and knowledge of this subject continues to improve. The review covered chloride resistance and carbonation resistance, which are the foci of this study. These properties have significant influence on the durability of RC structures. Factors influencing the rate of chloride diffusion such as chloride binding were reviewed, and those affecting the rate of carbonation were discussed. The next chapter presents details of the experiments carried out as part of this study.

CHAPTER 3: EXPERIMENTAL METHODOLOGY

3.1 Introduction

The following sections in this chapter describe the experimental investigations carried out as part of this study. The aim of conducting the experiments was to obtain and compare measures of material properties that relate to durability performance of repair mortars. This was in tandem with research objective (ii) presented in Chapter 1. The material properties evaluated included gas permeability, electrical conductivity, carbonation resistance and chloride diffusion behaviour. Mortar specimens with varying material properties were prepared and used in order to obtain varying results for better comparison. A flow chart summarising the experimental set up is presented in Figure 3.1.

A comparison was made between the results of (i) Oxygen Permeability Index (OPI) test and accelerated carbonation test, and (ii) Chloride Conductivity Index (CCI) test and bulk diffusion test. The OPI and CCI tests were selected because they are the commonly used tests in South Africa for performance-based design. In addition, previous results from these tests on concrete specimens have shown good correlations with carbonation under natural exposure and chloride diffusion coefficients after several years of marine exposure respectively (Ballim *et al.*, 2009). The accelerated carbonation test and bulk diffusion test are universally accepted methods for evaluating the rate of carbonation and chloride ingress in the laboratory. Comparing the results of these tests would therefore indicate the suitability of gas permeability (OPI test) and electrical conductivity (CCI test) in evaluating the carbonation resistance and chloride resistance of patch repair mortars.

The test materials are discussed in Section 3.2, followed by descriptions of the experimental variables and specimen preparation methods in Sections 3.3 and 3.4 respectively. A summary of procedures and test methods is presented in Section 3.5.

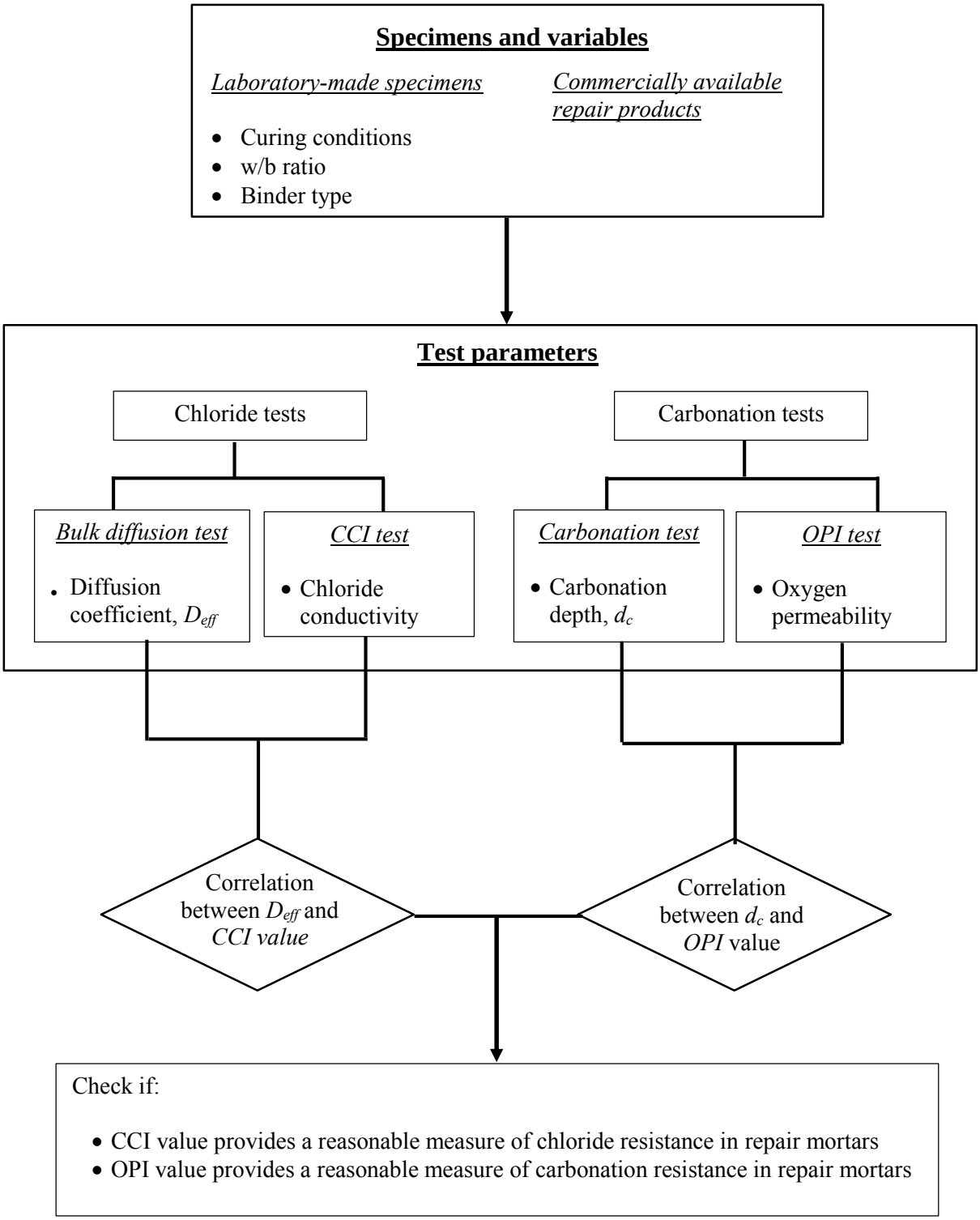

Figure 3.1: Flowchart showing experimental set-up

3.2 Test materials

Experimental investigations were performed on commercially available repair mortars supplied by Sika SA (Pty) Ltd and mortar mixes prepared in the laboratory. Details of the materials used to prepare test specimens are presented in the following subsections.

3.2.1 Laboratory mixes

The materials used to prepare the laboratory mortar mixes include Portland cement (CEM II (A-L) 52.5N), ground granulated blast-furnace slag (GGBS), crusher sand and Philippi dune sand. The following subsections provide detailed descriptions and reasons for selecting these materials.

a) Portland cement

Class 52.5N Portland cement (CEM II (A-L)) conforming to SANS 50197-1 was used in the manufacture of the laboratory mortar mixes. In some of the mixes (slag mortars), 50% of Portland cement was replaced by blast-furnace slag. CEM II (A-L) 52.5N was selected because it does not contain supplementary cementitious materials (see Table 3.1 for typical composition of CEM II). All the cement was obtained from Riebeek West PPC cement factory in the Western Cape Province, South Africa.

Table 3.1: Typical composition of CEM II (PPC)

Constituent	CaO	SiO_2	Al_2O_3	MgO	TiO_2	Fe_2O_3	MnO	K_2O	Na_2O	SO_3
% composition	66.17	21.1	4.58	1.24	0.30	3.45	0.10	0.66	0.09	1.96

b) Ground granulated blast-furnace slag

Ground granulated blast-furnace slag (GGBS) is a by-product of iron smelting. In the presence of water, it hydrates at a slow rate to form cementing compounds. However, it is more reactive in an alkaline environment (C&CI, 2009). The main reason behind the incorporation of GGBS into the mixes was their contribution to pore refinement and chloride binding (see Section 2.5.3). Table 3.2 presents the chemical composition, in terms of oxides, of the South African GGBS used.

Table 3.2: Chemical composition, in terms of oxides, of South African GGBS (Grieve, 2009a)

Oxide	SiO_2	CaO	Al_2O_3	MgO	FeO	MnO	K_2O	S	TiO_2
% by mass	34-40	32-37	11-16	10-13	0.3-0.6	0.7-1.2	0.8-1.3	1.0-1.7	0.7-1.4

The GGBS used in this study was obtained from AfriSam. It was used to replace 50% of Portland cement in some of the mixes (slag mortars). This ratio of blending lies within the range that has been reported to produce concretes and mortars with adequate resistance to chloride ingress and carbonation (Zibara, 2001; C & CI, 2009).

c) Fine aggregate

The fine aggregates used in this study were Philippi dune sand from the Cape Flats, and crusher sand obtained from crushed Cape granite near Malmesbury. The two types of fine aggregate were mixed at a ratio of 50/50 to produce a blend with good particle size distribution that would improve the workability of fresh mortar mixes. The grading curve for the 50/50 blend of dune and crusher sand is shown in Figure 3.2 (see Appendix A for particle size distribution of Philippi dune sand and crusher sand). To maintain the effective water/binder ratios of the laboratory mortar mixes, the aggregates were oven dried at 50°C for 48 hours and cooled to 23°C before casting of the test specimens in order to minimise the moisture content.

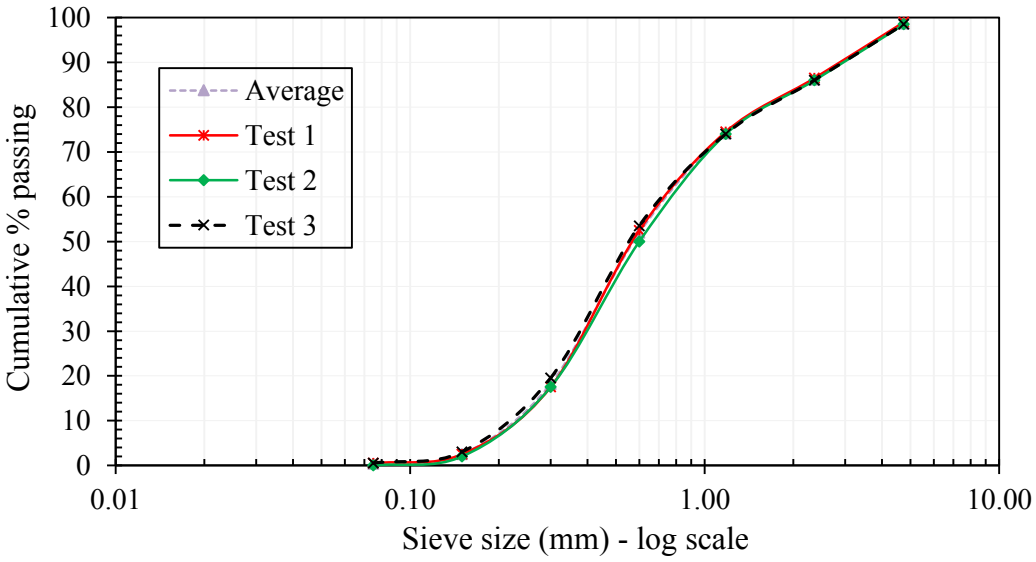

Figure 3.2: Grading curve of 50/50 blend of dune and crusher sand

d) Superplasticizer

Incremental dosage of a polycarboxylic ether-based superplasticizer was added to the fresh laboratory-made mortar mixes with lower water/binder ratio (0.45) to enhance their consistency. The consistency of the fresh mortar mixes was assessed using the slump test. To minimise the changes in pore structure which arise from treatments such as compaction on fresh mortars (with large variations in consistency), it was deemed beneficial to maintain a slump of 85 ± 5mm in all the laboratory-made mixes.

3.2.2 Commercial repair products

Four commercially available repair products from Sika SA (Pty) Ltd were used in this study, namely: Sika® MonoTop®-612, Sika® MonoTop®-615 HB, Sika® Rep LW and Sikacrete®-214. These products were selected because they best represent the range of products available in the South African market for patch repairs (Chilwesa, 2012). Table 3.3 provides a brief description of these commercially available repair products.

Table 3.3: Description of the commercial repair products used in this study

Product ID	Brief description
Sika® MonoTop®-612	Cementitious, polymer modified mortar containing silica fume and synthetic fibre reinforcement
Sika® MonoTop®-615 HB	Cementitious, polymer modified, one component repair mortar containing silica fume
Sika® Rep LW	A one component, non-sag, cement-based patching and repair mortar
Sikacrete®-214	A one component, free-flowing, cement-based concrete with maximum aggregate size of 9 mm

The salient details of the commercial repair products, from the manufacturer's data sheets, are provided in Appendix C. Information on the constituents of the commercial repair products were not made available. Specimens made from the commercial repair mortars were prepared according to the manufacturer's instructions as provided in the product data sheets.

3.3 Experimental variables

In order to manufacture specimens of varying penetrability, the water/binder ratio, binder type and curing conditions were varied in the mortar mixes that were designed and produced in the laboratory. A discussion on these parameters and reasons for altering them is presented in the following sections.

3.3.1 Water/binder ratio

Water/binder ratios (w/b) of 0.45 and 0.60 were used. The porosity of mortars largely depends on the w/b ratio (Dinku and Reinhardt, 1997; Roziere *et al.*, 2009). Thus varying the w/b ratio would result in specimens of varying penetrability, thereby resulting in a variation in their resistance to carbonation and chloride ingress. The use of specimens with varying penetrability was expected to provide a useful comparison of results from tests which measure different material properties. As mentioned by Masuku (2009), both ratios are within the range of w/b ratios commonly used in preparing patch repair mortars.

3.3.2 Binder type

CEM II (A-L) 52.5N and GGBS were used to prepare the specimens. Some mixes had 100% CEM II while others had 50/50 CEM II/GGBS blend. The 50% slag replacement is the common replacement at which durability of concrete is significantly increased (with respect to chloride ingress). In addition, the two binder types were used in order to produce specimens of varying pore structures.

3.3.3 Curing conditions

Two curing regimes were adopted in this study. In the first regime, the specimens were placed in an environmentally controlled room at 22 ± 1°C and 50 ± 4% RH within a timeframe of 15 minutes after demoulding, for a period of 27 days (see Figure 3.3). In the second regime, the specimens were moist cured in wet hessian within a timeframe of 15 minutes after demoulding, as shown in Figure 3.3.

Figure 3.3: Specimens subjected to dry and moist curing conditions in an environmentally controlled room

The hessian was kept continually damp by sprinkling water (22 ± 1°C) twice a day. After 7 days, the specimens were uncovered and left in the environmentally controlled room for the next 20 days. A 7-day curing regime is the suggested minimum period for moist curing in areas of hot weather with drying winds such as the Western Cape Province (especially during summer) (Kellerman, 2009). The selected curing regimes simulate the range of curing that may be expected in practice, with the dry curing representing the worst and moist curing being the best. Thus, the results obtained from this study would be a representative of what happens in practice.

3.4 Specimen preparation

The specimens were prepared using the mix proportions presented in Table 3.4. The following subsections give details of the mix design, casting and curing procedures.

3.4.1 Mix design

A summary of the mix design and proportions used to prepare the laboratory mixes is presented in Table 3.4.

Table 3.4: Summary of mix design and proportions

Mix ID	**PM45**	**PM60**	**SM45**	**SM60**
Water/binder ratio	0.45	0.60	0.45	0.60
CEM II (kg/m^3)	556	417	278	209
GGBS (kg/m^3)	-	-	278	209
Water content (l/m^3)	250	250	250	250
Philippi dune sand (kg/m^3)	745	803	745	803
Crusher sand (kg/m^3)	745	803	745	803
Slump (mm)	85	90	90	85
Superplasticizer (ml/m^3)	750	650	700	625

Note: -CEM II/GGBS ratio is kept constant at 50/50 for the last two mixes
-Philippi dune sand/crusher sand ratio is also kept constant at 50/50 for all mixes

3.4.2 Casting and curing

The mixes were prepared using a pan mixer, as per the mix proportions presented in Table 3.4. Fresh mortar mixes were placed in moulds and compacted using a vibrating table for a period of approximately 45 seconds until no air bubbles could be seen at the surface. The freshly cast mortar in the moulds was thereafter covered with a black polythene sheet and left for 24 ± 2 hours in the laboratory at 21 ± 2°C. The specimens were then cured as per the descriptions provided in Section 3.3.3, after which they were subjected to various exposure conditions depending on the test method. The number and sizes of the specimens for the test methods performed in this investigation are discussed in the subsequent sections.

a) OPI and CCI test specimens

In each test, 4 No. 100 x 100 x 100 mm cube specimens were cast for each mix. After 27 days, a core of 70 ± 2 mm diameter was extracted from each cube specimen using a core drill and thereafter wet-cut using a concrete cutter to obtain two cylindrical discs of approximately 70 ± 2 mm diameter × 30 ± 2 mm thickness in accordance with the Durability Index Testing manual (2010). Figure 3.4(a) and 3.4(b) illustrate the core-drilling process and the obtained cylindrical discs respectively.

(a) (b)

Figure 3.4: (a) Illustration of the core-drilling process, and (b) obtained cylindrical discs

b) Bulk diffusion test specimens

For each mortar mix, 3 No. 100 mm diameter × 200 mm long cylinders were cast and then cured for a period of 7 days as described in Section 3.3.3. Each of the aforementioned cylinders was thereafter wet-cut into two equal halves using a concrete cutter to produce 6 No. 100 mm diameter × 100 mm long specimens in accordance with the ASTM C1556-04 test standards. Figure 3.5 shows the cylindrical specimens used in the bulk diffusion test.

Figure 3.5: Cylindrical specimens used in the bulk diffusion test

c) Accelerated carbonation test specimens

For each mortar mix, 6 No. 100 × 100 × 100 mm cubes were cast and cured as described in Section 3.3.3. Each of the aforementioned cubes was thereafter dry-cut using a concrete cutter into two equal halves to produce twelve specimens per mix. Figure 3.6 shows the specimens used in the accelerated carbonation test.

Figure 3.6: Specimens used in the accelerated carbonation test

d) Compressive strength test specimens

For each mortar mix, 3 No. 100 × 100 × 100 mm cubes were cast. The freshly cast specimens were left in their moulds for a 24 ± 2 hours while covered with a black plastic bag. Thereafter, the specimens were demoulded and then cured in a water bath maintained at a temperature of (23 ± 2°C) for 27 days. Figure 3.7 shows the specimens used in the compressive strength test.

Figure 3.7: Cube specimens used in the compressive strength test

3.4.3 Exposure conditions

The controlled environmental conditions (22 ± 1 °C and 50 ± 5% RH) was kept constant for all the mortar mixes. After 27 days, the specimens were exposed to various environmental conditions in accordance with their respective test methods. The exposure conditions for each test are discussed in the following sections.

a) OPI and CCI test specimens

Conditioning of the OPI and CCI test specimens was performed in accordance with the DI Testing Manual (2010). Mortar disc specimens were preconditioned in an oven (see Figure 3.8) maintained at a temperature of 50°C for 7 days ± 4 hours. Oven-drying was done immediately after coring and cutting. The oven-drying conditions were assumed to be capable of establishing a minimal uniform moisture content in the specimens, with minimum degree of micro-structural alteration (DI Testing Procedure Manual, 2010). The specimens were thereafter placed in a desiccator (23 ± 2°C) for 3 hours to cool down prior to testing for OPI and CCI.

Figure 3.8: Oven-drying of the OPI and CCI disc specimens

b) Bulk diffusion test specimens

Testing for bulk diffusion was done in accordance with the ASTM C1556-04. A 20 mm thick slice was wet-cut - with minimal wetting to reduce the chances of washing out traces of chlorides which would have been in the mortar specimens - from each specimen. The 20 mm thick slice was used to determine the initial chloride content. The remaining specimens - from which the 20 mm thick slice were cut - were left to air dry under controlled environmental

conditions (22 ± 1°C and 55 ± 5% RH) for 24 ± 2 hours. To minimise the effects of wick action (Hong and Hooton, 1999) and to ensure unidirectional penetration of chloride ions, all sides were sealed with Sikadur-30 epoxy resin except for the surface from which the 20 mm thick slice was cut (see Figure 3.9(a)). The specimens were thereafter immersed in an airtight plastic container containing 3g/L calcium hydroxide solution as shown in Figure 3.9(b).

(a) (b)

Figure 3.9: (a) Specimen sealed with epoxy resin, and (b) specimens submerged in 3g/L calcium hydroxide solution

The change in mass in each specimen was monitored daily. The saturation of the specimens with calcium hydroxide solution was stopped when the change in mass within an individual specimen in three successive mass measurements was less than 0.1%. The calcium hydroxide-saturated specimens were thereafter rinsed with tap water. The specimens were immersed in plastic containers containing sodium chloride solution (NaCl) - with a concentration of 165 ± 1g NaCl per litre of solution - and sealed for 35 days.

c) Accelerated carbonation test specimens

Accelerated carbonation test specimens were conditioned as specified in the RILEM recommendations CPC-18 (1988). All sides except two opposite faces of accelerated carbonation test specimens were treated with a coat of Sikafloor-264 resin system (see Figure 3.6). The specimens were thereafter placed in an environmentally controlled room (22 ± 1°C and 55-75% RH) for two weeks before transferring them into a carbonation chamber. The reason for keeping the specimens in the room for two weeks was to minimize environmental fluctuations in the carbonation chamber in the initial period of exposure.

3.5 Test methods

The procedures for the test methods used in this investigation are summarised in the following subsections.

3.5.1 Bulk diffusion test

The bulk diffusion test was performed under controlled environmental conditions of 23 ± 2˚C and 50 ± 4% RH, in accordance with ASTM C1556-04 (2004). The main test procedures included profile grinding and chloride profiling.

a) Profile grinding

The cylindrical test specimens were rinsed with tap water and left to dry for 24 ± 3 hours after their removal from the 165g/L of sodium chloride solution. 6 No. 10 mm thick discs whose surfaces were parallel to that of the exposed surface were sliced from each cylindrical specimen. To avoid interference from the epoxy coating that was used to seal the surfaces of the specimens, a 5 mm slice was sawn around the edges of each disk. The SIEB crusher was then used to grind the profiles in order to obtain at least 10 g of powder samples from each layer. The powder samples were placed in an appropriately marked watertight resealable and transparent plastic bags in readiness for potentiometric titration.

b) Chloride profiling

The Mettler Toledo DL50 potentiometric titrator with a silver nitrate ($AgNO_3$) electrode (Figure 3.10) was used to determine the acid-soluble chloride-ion content of the powdered mortar specimens from each profile to an accuracy of 0.0001% (see Appendix B for a summary of the potentiometric titration test procedure). The chloride content was expressed in percentage by mass of mortar for all the mixes for the purpose of uniformity since the binder content of the commercial mortars was unavailable. However, for laboratory-made mixes the chloride content was separately expressed in percentage by mass of binder.

Figure 3.10: The Mettler Toledo DL50 potentiometric titrator

The parameters used to estimate the profile for chloride diffusion are (Poulsen, 1995):

i) Initial chloride content, C_i obtained from the 20 mm slice cut before exposure to sodium chloride solution,
ii) Chloride content at the surface of specimens, C_s, obtained from regression analysis
iii) Apparent diffusion coefficient, D_{eff}.

Fick's second law of diffusion (Equation 3.1) was used to generate the equation for each chloride profile using the non-linear curve fitting method.

$$C_x = C_0\left(1 - erf\frac{x}{2\sqrt{D_a t}}\right) \qquad (3.1)$$

3.5.2 Chloride conductivity index test

The oven-dried specimens were vacuum saturated in a 5.0 M sodium chloride solution (NaCl) before testing. Vacuum saturation helped to promote uniform conductivity in the pore solution, allowing instantaneous testing (Alexander and Mackechnie, 2004). The CCI test was conducted using a chloride conduction cell filled with sodium chloride (5.0 M NaCl) solution, in accordance with the DI Testing Procedure Manual (2010). Figure 3.11 shows the apparatus used to for CCI test.

Figure 3.11: Apparatus used for CCI test

Electrical conductivity was measured on 4 No. 70 ± 2 mm diameter × 30 ± 2 mm thick disc specimens from each mix, in a room whose temperature was maintained at (23 ± 2°C). With the conduction cell in a horizontal position, the DC power supply was adjusted until the voltage applied across the specimen was approximately 10 V. The current and voltage readings were simultaneously recorded within a timeframe of 15 minutes from the time of removing the specimens from the 5.0 M NaCl solution. An average of the four chloride conductivity readings (CCI values) from each specimen was reported. Equation 2.13 was used to calculate chloride conductivity.

3.5.3 Accelerated carbonation test

Accelerated carbonation testing was performed after exposure to a carbonation chamber that was capable of controlling temperature, humidity, and carbon dioxide concentration, in accordance with the RILEM recommendations CPC-18 (1988). The durations of exposure in the carbonation chamber were 6 and 12 weeks.

a) Conditions in the carbonation chamber

The carbonation chamber was set to maintain a concentration of 2 ± 0.01% CO_2, at 20 ± 1 ˚C during the 6- and 12-week exposure period. Saturated solutions of sodium nitrite ($NaNO_2$) and hydrated potassium carbonate ($K_2CO_3 \cdot 2H_2O$) salts were placed in the chamber with the aim of maintaining a relative humidity of 55 - 75% (O'Brien, 1947). The chamber was tightly closed to prevent disturbance from the external environment. The specimens were exposed to these conditions for periods of 6 weeks and 12 weeks, after which carbonation depths were measured.

b) Carbonation depth measurement

The depths of carbonation were measured after 6 and 12 weeks of exposure in the carbonation chamber. Test specimens were removed from the chamber, dry-cut across the opposite unsealed surfaces and air-blown to remove dust particles. After 24 hours, the cut surfaces were sprayed with 1% phenolphthalein solution to determine its depth of carbonation. The depth of carbonation was measured after another 24 hours, at four locations on each specimen, and perpendicular to the surface to an accuracy of 0.5 mm. An average of three readings from each specimen was recorded and reported as the mean carbonation depth.

3.5.4 Oxygen permeability index test

The OPI test was conducted using the falling head permeameter (see Figure 3.12), in accordance with the DI Testing Procedure Manual (2010). Oxygen permeability was measured on 4 No. 70 ± 2 mm diameter × 30 ± 2 mm thick disc specimens from each mix, in a room with controlled temperature (23 ± 2°C). Each specimen was tested within a timeframe of 30 minutes after its removal from the desiccator. According to the DI Testing Procedure Manual (2010), the test may be terminated when the pressure has dropped to 50 ± 2.5 kPa or after 6 hours ± 15 minutes, whichever occurs first. The 50 ± 2.5 kPa rule did not apply, thus testing was terminated after 6 hours ± 15 minutes. Pressure readings registered in the data logger were downloaded and all the data points used to calculate the OPI values. A custom-made MS Excel spreadsheet was used to calculate the OPI value and the permeability coefficient, *k* of each individual mix. An average of four OPI readings from each specimen was reported as the mean OPI value.

Figure 3.12: The falling head permeameter used in the OPI test

3.5.5 Compressive strength test

The compressive strength test was performed to characterise the 7- and 28-day strength of the mortar mixes. The Amsler compressive strength test machine was used to determine the 7-day and 28-day compressive strength of specimens after curing in water bath (23 ± 2°C), in accordance with SANS 5863 (2006). Surface dry specimens were weighed using an electronic balance to determine their density. Thereafter each specimen was tested until failure under a compressive load to determine its characteristic strength. The testing of each specimen was done within a timeframe of 20 minutes from the time of its removal from the water bath. An average of three readings from the three specimens of each mix was reported as the mean compressive strength (see Appendix A).

3.6 Closure

Durability of concrete repairs with patch repair mortars depend on the resistance to chloride ingress and carbonation. Information on the materials used, specimen preparation, experimental variables and the testing conditions have been given. The test methods presented in this chapter aim to investigate how the resistance to carbonation and chloride penetration influence the durability of concrete repairs with patch repair mortars. Tests on the chemical and physical properties of the binders, such as mineral composition and heat of hydration were not considered in this study, but should be taken into account in future investigation. In addition, measurement of fundamental material properties that govern the bulk properties of materials to some extent, such as porosity and pore size distribution are recommended to shed more light on the transport properties of the test materials. The results of the tests presented in this chapter are discussed in Chapter 4.

CHAPTER 4: RESULTS AND DISCUSSION

4.1 Introduction

This chapter presents the analysis and discussions of the experimental results obtained from the test methods outlined in Section 3.5 of Chapter 3. The tests comprised: bulk diffusion, Chloride Conductivity Index (CCI), accelerated carbonation and Oxygen Permeability Index (OPI) tests. The results for compressive strength test are presented in the Appendix. Table 4.1 shows the names of the mixes as used in this chapter (see Table 3.3 and 3.4 for descriptions of the mortar mixes).

Table 4.1: Descriptions of names of the mortar mixes used

Laboratory-made mixes		
Mix ID	**Water/cement ratio**	**Binder content**
PM45	0.45	100% PC*
PM60	0.6	100% PC
SM45	0.45	50/50 blend of PC/GGBS**
SM60	0.6	50/50 blend of PC/GGBS
Commercial mortar mixes		
Mix ID	**Description**	
CM1	Commercial mortar-1 (Sika® MonoTop®-612)	
CM2	Commercial mortar-2 (Sika® MonoTop®-615 HB)	
CM3	Commercial mortar-3 (Sika® Rep LW)	
CM4	Commercial mortar-4 (Sikacrete®-214)	

** Portland cement - CEM II (A-L) 52.5N*

*** Ground granulated blast furnace slag*

4.2 Chloride-ion resistance measurements

The results of bulk diffusion test (BDT) and CCI test are discussed in the following sections. The experimental results that will be primarily dealt with are chloride diffusion coefficient (D_{eff}) for bulk diffusion test and chloride conductivity index (*CCI value*) for CCI test.

4.2.1 Chloride-ion diffusion

Bulk diffusion testing was carried out to determine the diffusion coefficient and surface chloride content of the mortar mixes, in accordance with ASTM C1556-04. Though a close relation exists between diffusion coefficient and surface chloride content, the two parameters are distinct. The diffusion coefficient gives an indication of the ease of chloride penetration, while surface chloride content is a theoretical ratio of the mass of chloride ion at the interface of exposure liquid and test specimen, to the mass of concrete.

Saturated mortar samples sealed on all faces with the exception of one face were submerged in 165 ± 1g/L sodium chloride solution for a period of 35 days, after which six 10 mm thick profiles were sliced and ground from each sample, and the chloride content (C_x) determined as a function of the depth (x) from the exposed surface into the specimen. C_x was expressed in percentage by mass of mortar for all the mixes due to the absence of information on the binder content of the commercial mortars. The chloride diffusion coefficient (D_{eff}) and the surface chloride content (C_s) were estimated by regression analysis (see Appendix B for a summarized procedure). C_s is the projected chloride content at zero depth, which is determined by regression analysis. The chloride profiles for all the mortar mixes used in this study are presented in Appendix A. Table 4.2 presents the D_{eff} and C_s values obtained from regression analysis.

Table 4.2: Diffusion coefficients and surface chloride content of the mortar mixes

Mix	Surface chloride content, C_s		Diffusion coefficient, D_{eff}	
	Mean C_s (%)	Std. dev of C_s	D_{eff} ($\times 10^{-12}$ m²/s)	Std. dev of D_{eff}
PM45	1.20	0.26	7.79	0.12
PM60	1.53	0.06	8.36	0.25
SM45	0.93	0.32	7.60	0.12
SM60	0.98	0.06	7.90	0.12
CM1	1.07	0.05	7.64	0.23
CM2	2.27	0.06	7.63	0.14
CM3	1.05	0.02	7.72	0.12
CM4	0.61	0.02	7.64	0.20

Note: Each of C_s and D_{eff} value is an average of 3 readings

The profile interval used for chloride profiling in this investigation was quite coarse, thus the C_s values obtained by back-extrapolating may be rough estimates. For improved results and minimum errors in future work, finer profile interval (e.g. 2 mm) and longer duration of testing (e.g. 90 days) are recommended. Figure 4.1 and Figure 4.2 present the diffusion coefficients and the surface chloride content of the mortar mixes as calculated by an MS Excel spreadsheet template.

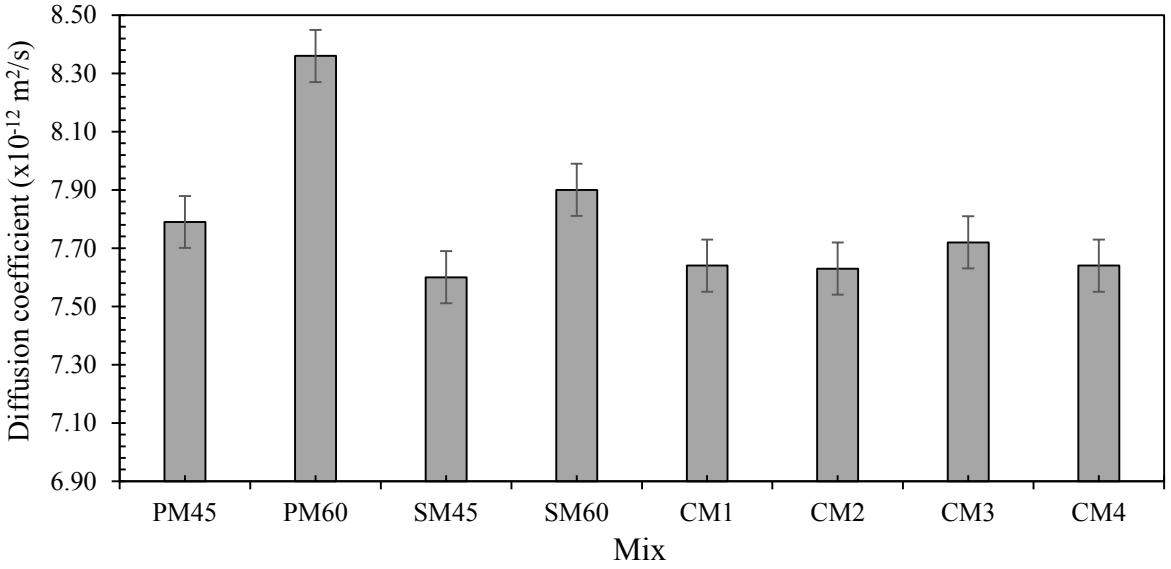

Figure 4.1: Diffusion coefficients of the mortar mixes (error bars indicate standard deviations)

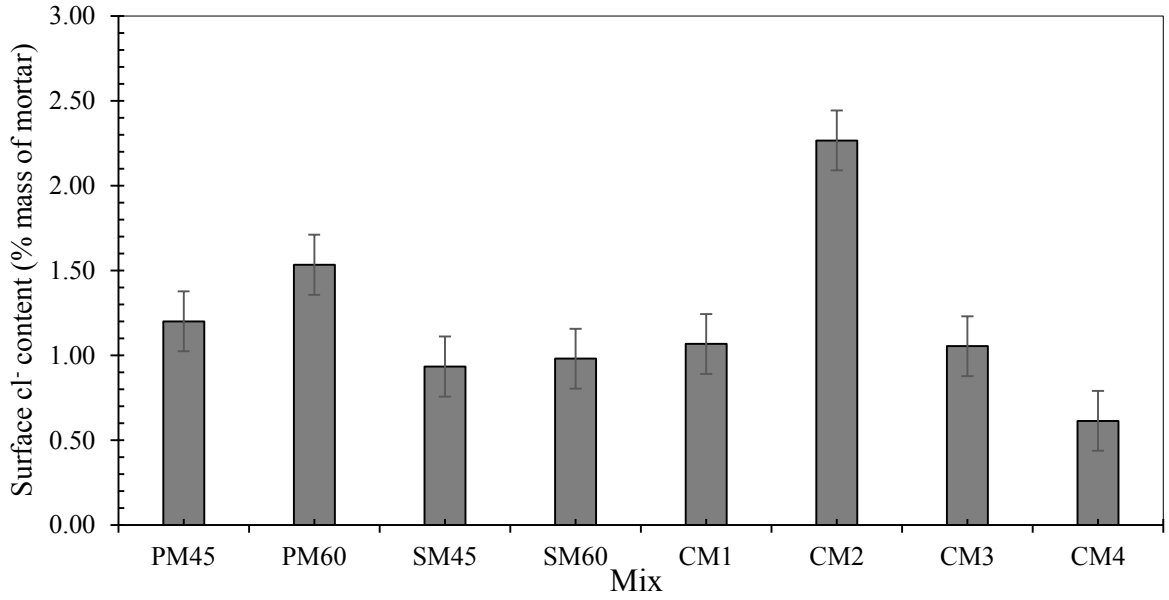

Figure 4.2: Surface chloride content of the mortar mixes (error bars indicate standard deviations)

It can be seen from Figure 4.1, that the diffusion coefficients were virtually the same in all the mortar mixes. The negligible variability in the diffusion coefficients of the mortar mixes could not be accounted for based on the reviewed literature. Further investigation is recommended to study this phenomenon. However, the fact that the commercial mortar mixes tend to be made within a carefully controlled environment could help ensure consistency in their diffusion coefficients. The differences in performance of the mortar mixes with regard to chloride diffusion seem to be more evident only in surface chloride content values (Figure 4.2), in which CM2 mix recorded the highest surface chloride content while CM4 mix had the lowest. Among the laboratory-made mixes, CEM II mixes (PM45 and PM60) recorded higher values of Cs than CEM II/GGBS mixes (SM45 and SM60). A detailed discussion of these results is presented in Section 4.2.3.

4.2.2 Chloride conductivity

The chloride conductivity test provides a measure of chloride diffusivity in cement based materials. It is sensitive to variations in the pore structure and the type of binder. In this test, the ionic flux is generated by conduction, driven by a potential difference of 10 V across the two opposite faces of the disc specimen (Alexander, 2004). Figure 4.3 shows the chloride conductivity values for the various mortar mixes used in the investigation. The test results are discussed in Section 4.2.3.

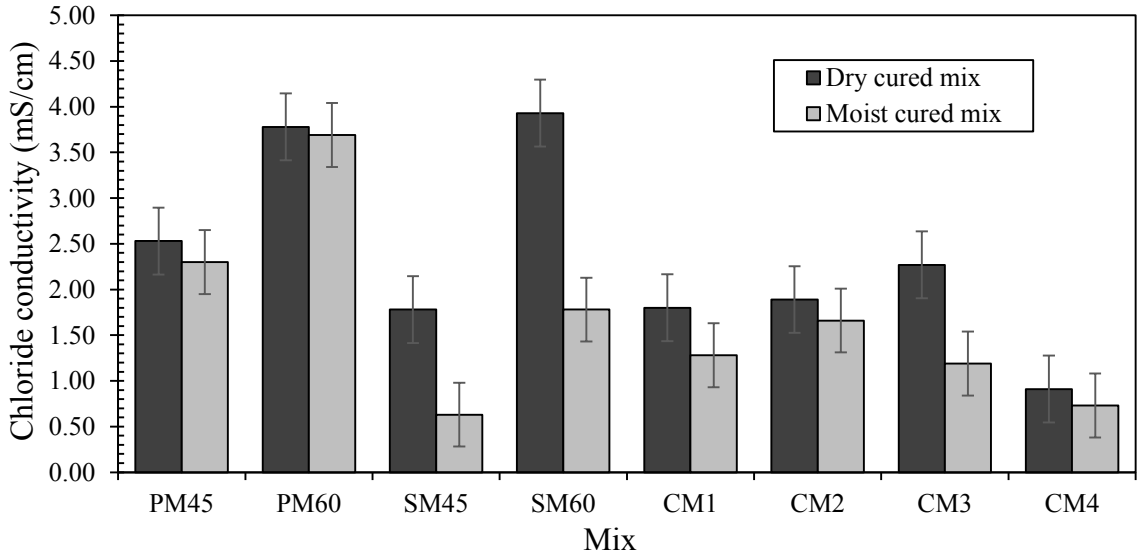

Figure 4.3 Chloride conductivity of the mortar mixes used in this study (error bars indicate standard deviations)

From Figure 4.2, it can be observed that the chloride conductivity values were generally lower in the commercial mortar mixes than in the laboratory-made mixes. Dry cured SM60 specimens had the highest chloride conductivity, while moist cured SM45 specimens recorded the lowest chloride conductivity among the laboratory mixes, indicating the highest resistance to chloride ingress. Section 4.2.3 presents a detailed discussion of these results.

4.2.3 General discussion of chloride-ion resistance results

The effects of varying the curing conditions (only for chloride conductivity specimens), w/b ratio, and binder type are discussed in the following subsections.

4.2.3.1 Influence of water/binder ratio

From Figure 4.1, it can be seen that for similar type of binder, specimens with w/b ratio of 0.60 (PM60 and SM60) recorded slightly higher chloride diffusion coefficients compared to specimens with w/b ratio of 0.45 (PM45 and SM45). Similarly, it can be inferred from Figure 4.2 that an increase in w/b ratio across the entire range of laboratory-made mixes and across the two curing regimes resulted in an increase in their chloride conductivity regardless of binder type. For CEM II and CEM II/GGBS specimens, the percentage increase in diffusion coefficients, surface chloride content and chloride conductivity with increase in w/b ratios in specimens with w/b ratios of 0.45 to 0.60 is presented in Table 4.3.

Table 4.3: Percentage increase in diffusion coefficients, surface chloride content and chloride conductivity with increase in w/b ratios in specimen with w/b ratios of 0.45 to 0.60.

Specimens	**CEM II**	**CEM II/GGBS**
% increase in diffusion coefficient	7	4
% increase in surface chloride content	28	6
% increase in cl^- conductivity (dry cured)	49	121
% increase in cl^- conductivity (moist cured)	60	183

The increase in diffusion coefficient and surface chloride content with an increase in w/b ratio is consistent with literature and can be attributed to the increased porosity that results from the high water binder ratio (Halamickova *et al.*, 1995; Dinku and Reinhardt, 1997). The w/b ratio controls the initial spacing of cement particles (see Section 2.4.1 for detailed review). A decrease in the w/b ratio would result in closely spaced cement particles in fresh

mortar and subsequently reduced size, connectivity and tortuosity of the capillary pores in hardened mortars (Glass, 2003; Kunthongkeaw *et al.*, 2006; Roziere *et al*., 2009). The overall effect is a denser pore structure with reduced penetrability to chloride ions, thus a reduction in the rate of ionic diffusion. This results in lower diffusion coefficient as well as reduced chloride conductivity.

From Figure 4.2, it seems that the surface chloride content of the laboratory-made mixes is mainly influenced by the type of binder used. Therefore, it (C_s) will be discussed in Section 4.2.3.3, which deals with the influence of binder type on chloride ingress.

4.2.3.2 Influence of curing regime

It can be observed that the chloride conductivity of dry cured mixes were generally higher than those of moist cured specimens across the entire set of mixes (Figure 4.3). More specifically, it can be observed that the effect of curing was more pronounced in CEM II/GGBS mixes than those with CEM II (see Table 4.3). The greatest percentage reduction in chloride conductivity was observed in specimens with SCMs (120.79% and 182.54% for dry and moist cured specimens respectively). From these results, it can be observed that the effect of curing on chloride conductivity is more pronounced in mixes with SCMs. The lower chloride conductivity in moist cured specimens (compared to dry cured specimens) can be attributed to continued cementing reactions (hydration) in the presence of water, which resulted in the formation of the expansive hydration products that filled up the capillary pores and voids (Atis, 2003). The effect is reduced size and connectivity of pores, resulting in a densified microstructure, therefore lower rate of electrical conductivity (Halamickova *et al.*, 1995; Grassl *et al.*, 2010).

A study by Bentur and Mitchell (2008) in which the durability performance was quantified by chloride diffusivity also showed that improved curing practice enhances concrete durability. Similar results were observed by Martys and Ferraris (1997). These results give a clear indication that better curing practice significantly slows down the deterioration of concrete structures due chloride-induced steel corrosion.

4.2.3.3 Influence of binder type

Comparing the surface chloride content among the laboratory-made mixes, it can be observed (Figure 4.2) that the addition of GGBS resulted in a decrease in the surface chloride content.

The lower values of C_s in CEM II/GGBS specimens compared to CEM II specimens is unexpected. Higher C_s values would be expected in mixes containing GGBS due to increased chloride binding capacity in the test specimens. Further investigation is therefore recommended to study this phenomenon. Among the commercial mortars, the inclusion of SCMs such as silica fume could further complicate the chloride penetration results.

It is noticeable that for similar w/b ratios, slag specimens recorded generally lower conductivity values compared to CEM II specimens with the exception of dry cured SM60 (Figure 4.3). The reduction in diffusion coefficient due to the addition of GGBS is consistent with literature and can be attributed to chloride binding effects and increased cementing reactions, which result in densification of the pore structure (Baroghel-Bouny *et al.*, 2009). Also, comparing the percentage increase in diffusion coefficients and chloride conductivity across the two types of binder (see Table 4.3), it can be observed that mixes with 50% GGBS experienced a greater increase in chloride conductivity (121% and 183% in dry and moist cured specimens respectively) and lower increase in diffusion coefficient (4%) and surface chloride content (6%). The subsequent reduction in size and connectivity of the pores impedes the transport of chloride ions, thus decreasing the rate of chloride diffusion as well as chloride conductivity (Poulsen, 1995; Khunthongkeaw *et al.*, 2006; Pack *et al.*, 2010). Furthermore, GGBS has the beneficial effect of filling up the pores, thus densifying the microstructure of concretes and mortars.

In addition, it has been shown that the addition of GGBS increases the chloride binding capacity of mortars and concretes (see Section 2.5.3). The effects of chloride binding were not investigated in this study. Nevertheless, literature reports that chloride binding reduces the amount of free chlorides in the pore solution, thus reducing the depth of chloride penetration. This subsequently reduces the rate of diffusion and conductivity (Tang and Nilsson, 1995; Stanish *et al.*, 2000; Kropp, 2005). Caballero *et al.* (2012) observed similar results using rapid chloride migration (RCM) test on mortar specimens containing Portland (CEM I) and blast furnace slag (CEM III/B) cements with constant w/b ratio. Similar results were also observed in the study by Delagrave (1997).

4.2.4 Correlation between chloride diffusion and chloride conductivity

The results obtained from specimens of the same mix, tested with different methods (bulk diffusion and CCI tests) are compared in this section. Figure 4.4 shows scatter plots of chloride conductivity versus diffusion coefficient.

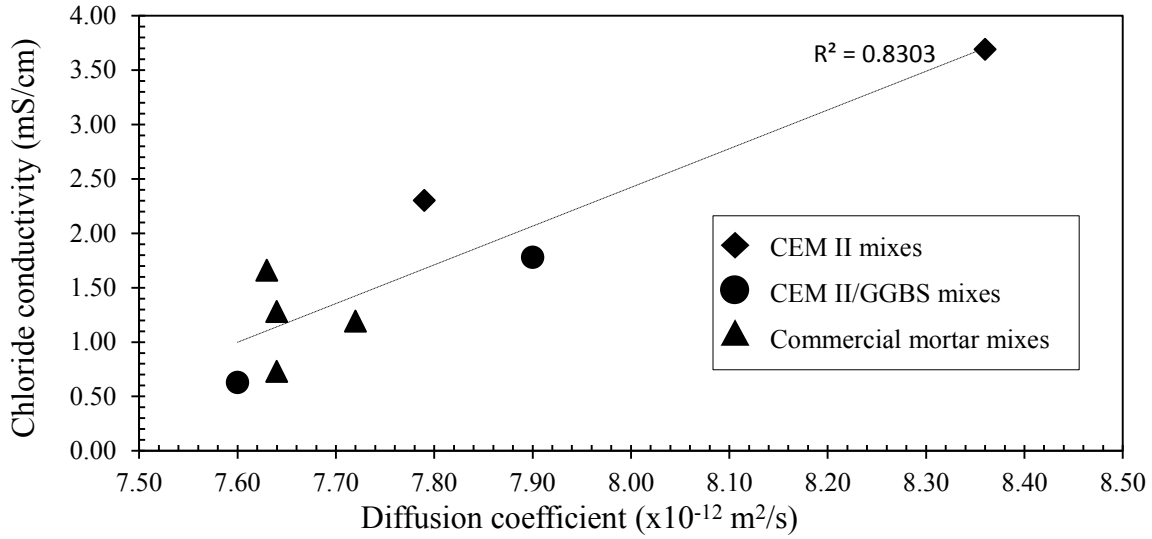

Figure 4.4: Chloride conductivity versus diffusion coefficient of the mixes

It can be seen from Figure 4.4 that chloride conductivity results correlate reasonably well with chloride diffusion coefficients. A 'very good' linear correlation with a correlation coefficient of (R =) 0.9112 was obtained. This indicates that electrical (chloride) conductivity, as characterized by the CCI test in this investigation, may offer a reasonable measure of resistance to chloride ingress in patch repair mortars. Although chloride conductivity is not the same as chloride diffusivity, it provides a measure of the mobility of chloride ions (Caballero *et al.*, 2012). It is important to note that the two methods are based on different transport mechanisms: migration for CCI test, and ionic diffusion for bulk diffusion test, yet the results are comparable. The reasonable correlation can be attributed to the fact that both electrical conductivity and rate of chloride diffusion in cement-based materials largely depend on the size, connectivity and tortuosity of the pores (Basheer *et al.*, 2001; Alexander and Thomas, 2015). Similar correlation might therefore be expected between the diffusion coefficient obtained from bulk diffusion test and results of other methods that essentially measure electrical conductivity or resistivity, such as the rapid chloride permeability test (RCPT). A recent study by Caballero et al. (2012) further confirms this.

However, as highlighted by Alexander and Thomas (2015) several factors may independently influence these material properties. For example, electrical conductivity of the pore solution essentially influences conductivity, whereas the volume and the chloride binding capacity of cement hydrates (cement paste) largely influence the rate of chloride diffusion. Therefore, the prediction of chloride ingress from the electrical properties of mixes ought to be implemented within the range where reasonable correlation can be established (Alexander and Thomas, 2015).

4.3 Carbonation resistance measurements

The results of the accelerated carbonation tests (ACT) and the OPI tests are discussed in the following sections. The experimental results that will be largely discussed are carbonation depth (d_c) for ACT, and oxygen permeability index (OPI value) and coefficient of permeability (k-value) for OPI test.

4.3.1 Accelerated carbonation depth

Figure 4.5 shows the carbonation depths of the mixes after 12 weeks of exposure in the carbonation chamber. The test results are discussed in Section 4.3.3.

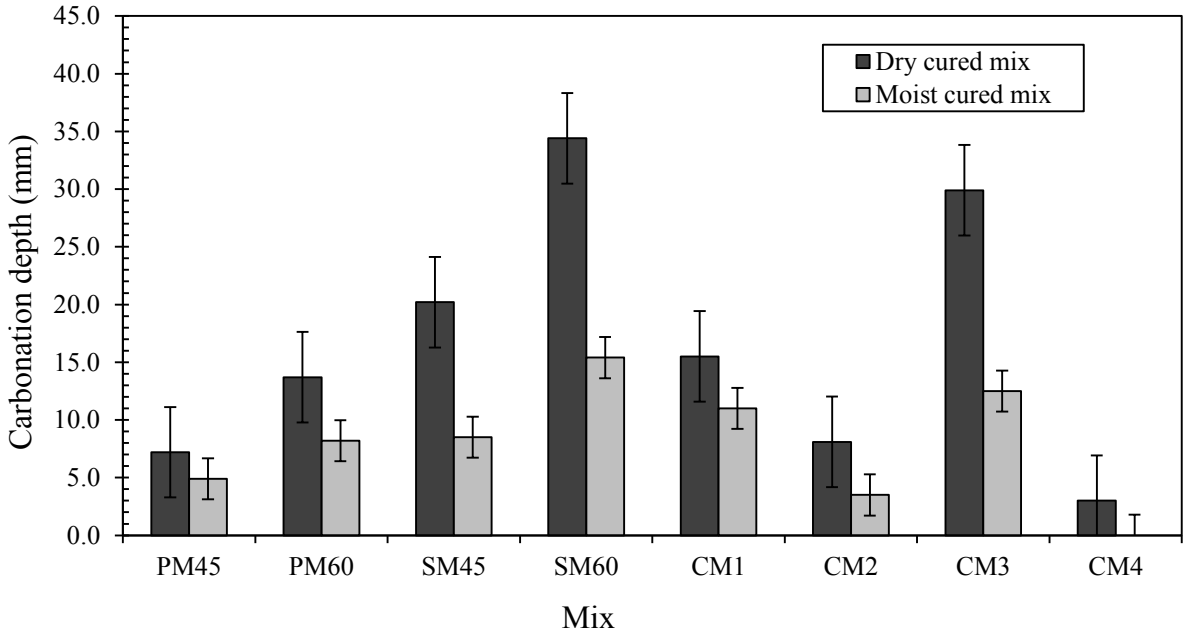

Figure 4.5: Carbonation depth measurements of mortar mixes after 12 weeks of exposure in the carbonation chamber (error bars indicate standard deviations)

From Figure 4.5 it can be noted that SM60 had the highest carbonation depths while CM4recorded the lowest carbonation depth, with no depth recorded in 7-day moist cured CM4 specimens. Furthermore, it can be inferred that across the entire set of laboratory-made mixes, CEM II/GGBS mixes experienced higher carbonation depths than CEM II mixes. These results are discussed in Section 4.3.3.

4.3.2 Oxygen permeability

The OPI test is sensitive to curing conditions, w/b ratio and binder type as will be seen in the following sections. The OPI value is a logarithmic value ranging from 8 to 11, with the higher index implying less permeable concrete (Alexander, 2004). Figure 4.6 shows the OPI results of the mortar specimens, obtained by measuring the pressure decay of oxygen passed through disc specimens. The OPI value is the negative logarithm of the Darcy's coefficient of permeability (*k*-value) presented in Figure 4.7. For this reason, the *k*-value gives a more significant evaluation in terms of numerical differences among the mixes, compared to the OPI values (Beushausen and Alexander, 2008). The coefficient of permeability would thus better evaluate the statistical significance of the different permeability values. These results are discussed in Section 4.3.3.

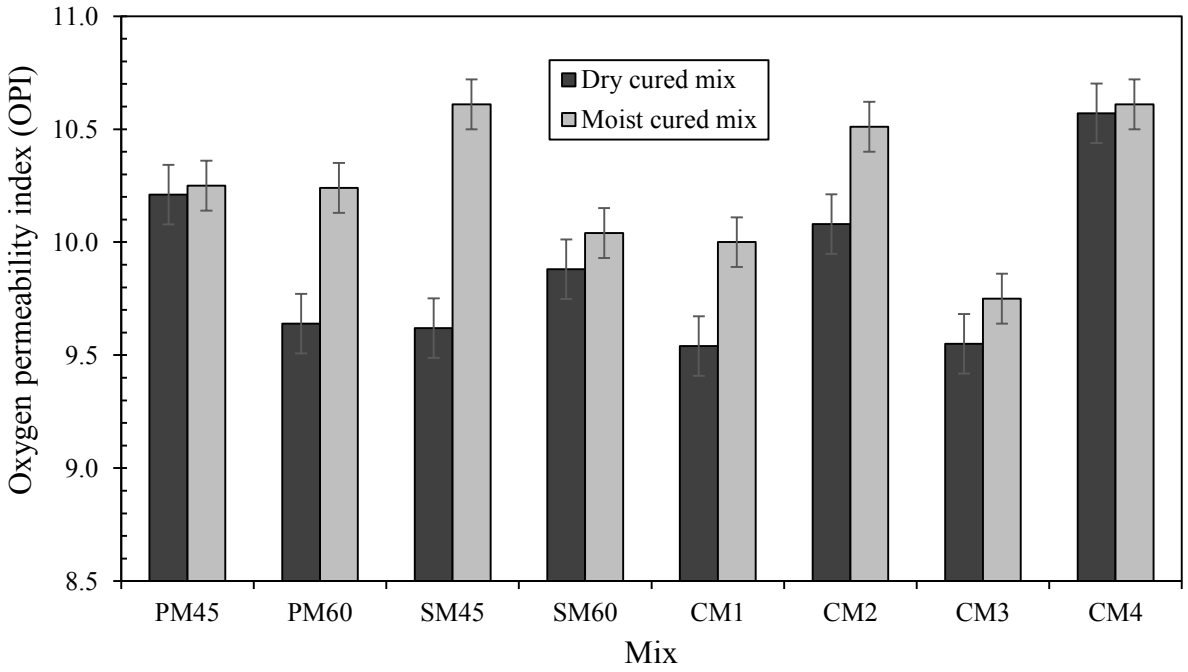

Figure 4.6: OPI results of the mortar mixes used (error bars indicate standard deviations)

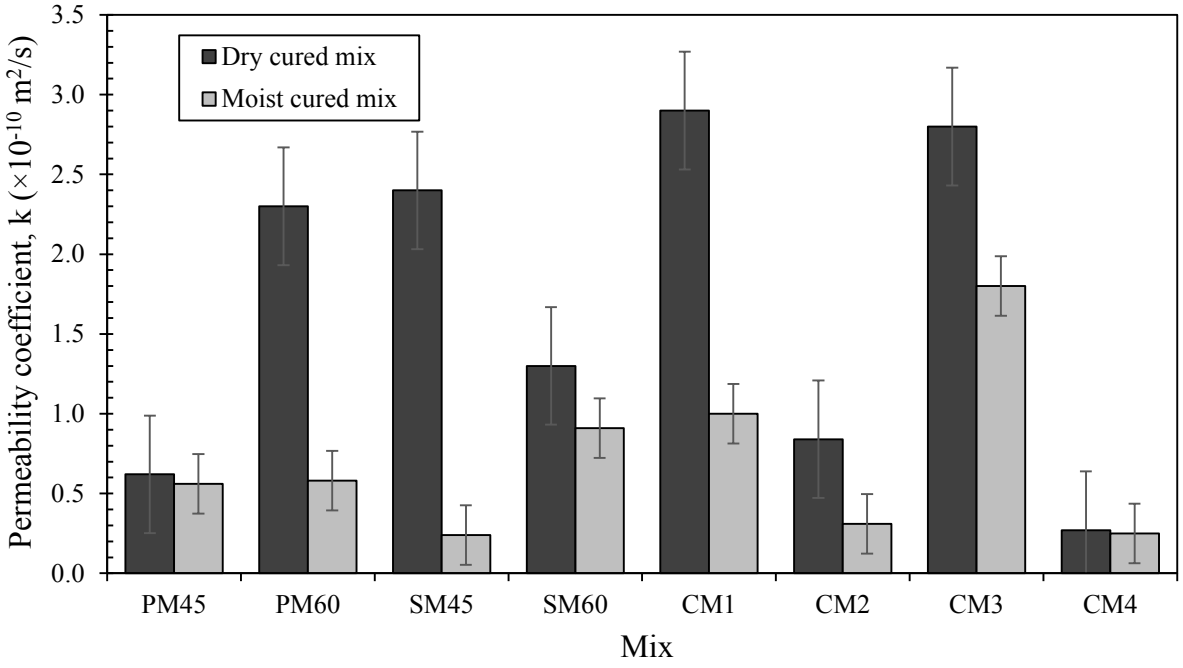

Figure 4.7: Permeability coefficients obtained from the OPI values of the mixes (error bars indicate standard deviations)

CM4 and moist cured SM45 specimens recorded the highest OPI values while dry cured CM1 specimen had the lowest OPI value (Figure 4.6). In terms of the *k*-value, the trend in OPI-values was reversed as expected (Figure 4.7). It should be noted the OPI value is inversely proportional to the *k*-value. Section 4.3.3 presents a detailed discussion of these results.

4.3.3 General discussion of carbonation resistance results

The effects of varying the curing conditions, w/b ratio, and binder type are discussed in the following subsections.

4.3.3.1 Influence of water/binder ratio

From Figure 4.5, it can be seen that for a similar type of binder, higher carbonation depths were recorded on specimens with a w/b ratio of 0.60 (PM60 and SM60) compared to specimens with a w/b ratio of 0.45 (PM45 and SM45). Also, the OPI value was generally lower in specimens with a w/b ratio of 0.60 (PM60 and SM60) compared to specimens with a w/b ratio of 0.45 (PM45 and SM45), for similar types of binder (Figure 4.6). The higher

depths of carbonation and lower OPI values in specimens of higher w/b ratio can be attributed to increased porosity. Literature reports that an increase in w/b ratio increases the initial spacing between cement particles, thus increasing the size, connectivity and tortuosity of capillary pores in hardened mortars (Kunthongkeaw *et al.*, 2006; Roziere *et al*., 2009).

The rate of diffusion of CO_2 is one of the key factors that control the rate of carbonation, thus a higher rate of diffusion generally results in increased depths of carbonation. These findings are consistent with the results of the study by Kunthongkeaw *et al*. (2006) who observed a better carbonation resistance in fly ash specimens with a lower w/b ratio compared to a higher w/b ratio. Costa and Appleton (2001) also showed the significance of w/b ratio on the rate of carbonation. The water not consumed in the hydration reaction will remain in the pore space, thus increasing penetrability when the mortar dries out. The effect is an increased rate of diffusion of carbon dioxide and increased oxygen permeability in mortars, when all the other factors (such as temperature, relative humidity and CO_2 concentration) are kept constant. Similar results were observed by Dinku and Reinhardt (1997) in their study on gas permeability coefficients of concretes with different w/b ratios.

4.3.3.2 Influence of curing regime

The depths of carbonation were generally lower in moist cured specimens compared to dry cured specimens (Figure 4.5). Also noticeable is the larger difference in carbonation depths between the two curing conditions in slag specimens compared to PC specimens. From Figure 4.6 it can be seen that the moist cured specimens recorded higher OPI values than the dry cured specimens.

The lower depths of carbonation and higher OPI values in moist cured specimens can be attributed to continued hydration in the presence of curing water as highlighted in Section 4.2.3, which densifies the pore structure. A denser microstructure is less permeable, thus lower rate of diffusion of carbon dioxide and lower oxygen permeability (Grassl *et al.*, 2010). The overall effect of a densified microstructure is a reduced rate of carbonation, as well as higher OPI values. Dinku and Reinhardt (1997) also observed the beneficial effects of curing on carbonation depths. Similar results were obtained by Kubens *et al*. (2003) using the Torrent air permeability method on specimens subjected to dry curing, different durations of alternating water curing, and different durations of curing in a water bath

The wide difference in carbonation depth between the two curing conditions on slag mortar can be attributed to the beneficial effects of curing on slag specimens, due to increased cementing reactions (PC hydration and GGBS pozzolanic reactions), which significantly reduce porosity. It is clear that proper curing practice significantly slows down the deterioration of concrete structures due to carbonation-induced steel corrosion.

4.3.3.3 Influence of binder type

For a similar w/b ratio, the slag specimens (SM45 and SM60) recorded greater depths of carbonation than the PC specimens (PM45 and PM60), as shown in Figure 4.5. The higher depths of carbonation in slag specimens can be attributed to a number of reasons. Firstly, the slower rate of pozzolanic reaction in blended cements reduces the rate of filling the pores and voids. Also, replacing Portland cement with GGBS significantly reduces the alkaline reserves (calcium silicate hydrate and calcium hydroxide), which are involved in the chemical reactions that lead to carbonation. A reduction in these hydrates increases the rate of carbonation, thus the higher depths of carbonation in slag specimens (Papadakis, 2000; Penttala, 2009). As can be seen from Figure 4.6 there is no clear trend showing the effect of binder type on the OPI results.

4.3.4 Correlation between carbonation depth and oxygen permeability

The results obtained from specimens of the same mix, tested with different methods (accelerated carbonation and OPI tests) are compared in this section. Figure 4.8 shows a scatter plot of the carbonation coefficients of the mixes measured after 12 weeks of exposure versus permeability coefficients of the mixes. The carbonation coefficients were calculated from the carbonation depths measured after 12 weeks of exposure in the carbonation chamber, using the square-root-of-time law. An example calculation is shown below:

Square-root-of-time law: $x = A\sqrt{t}$

This implies, carbonation coefficient: $A = \frac{x}{\sqrt{t}}$

where: x is the carbonation depth (mm),
A is carbonation coefficient (mm/√day),
t is exposure period.

Measured carbonation depth for dry cured PM45 after 12 weeks (84 days): 7.2mm

Thus, carbonation coefficient of dry cured PM45 mix: $A = \frac{7.2}{\sqrt{84}} = 0.786$ mm/√day

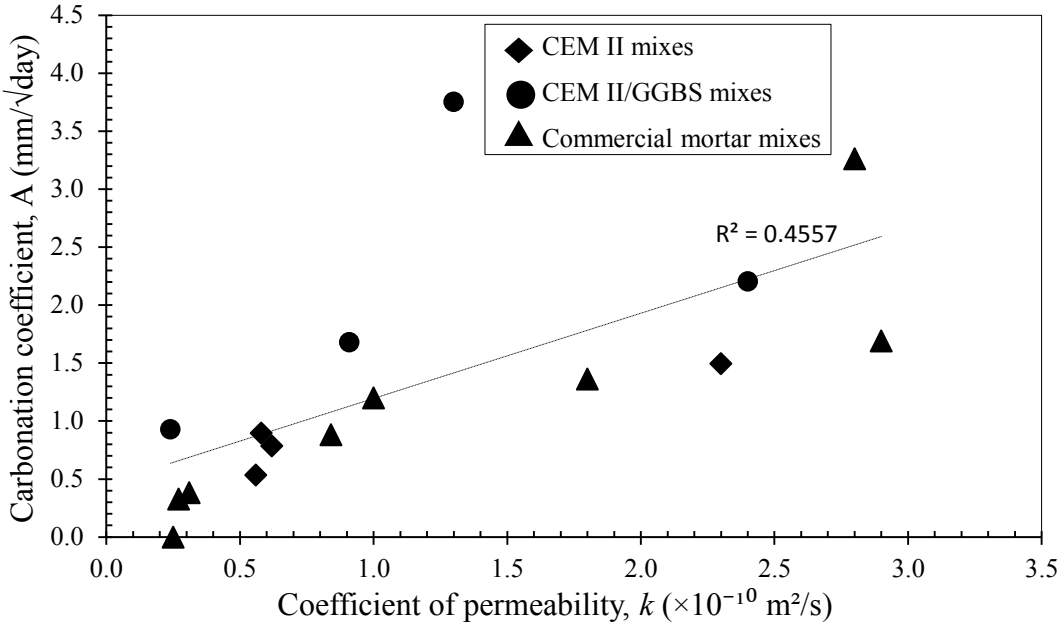

Figure 4.8: Carbonation coefficient after 12 weeks of exposure versus coefficient of permeability (*k*-value from OPI)

Figure 4.9 shows the relationship between carbonation coefficient and OPI for all the mixes after 12 weeks of exposure in the carbonation chamber.

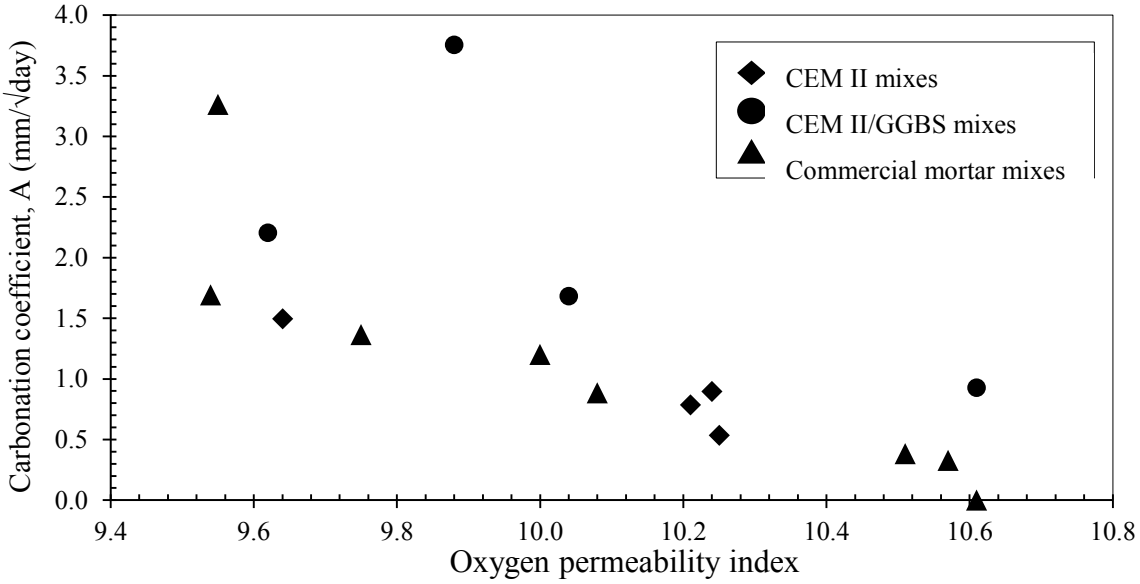

Figure 4.9: Carbonation coefficient versus OPI for all the mortar mixes after 12 weeks of exposure

From Figure 4.8, it can be seen that the carbonation coefficient correlates well with the coefficient of permeability. A 'good' linear correlation with a correlation coefficient of (R =) 0.6751 was obtained. This indicates that oxygen permeability as characterized by the OPI test may provide a reasonable measure of carbonation resistance of patch repair mortars. Even though the two test methods are based on different transport mechanisms (CO_2 diffusion in accelerated carbonation test, and oxygen permeability in OPI test), the results are comparable. The good correlation between accelerated carbonation test and OPI test on mortar specimens can be attributed to the fact that both oxygen permeability and the rate carbonation in cement based materials mainly depend on size, connectivity and tortuosity of the pores (Basheer *et al.*, 2001). Similar relationship might also be expected when depths of carbonation obtained from the accelerated carbonation test are compared with results of other methods that measure gas flow through specimens, such as the torrent permeability test (TPT).

It can also be seen that the results for CEM II/GGBS mixes lie "above" the other results (Figure 4.9), highlighting the fact that permeability alone is not a sufficient indicator for carbonation. Using different binder types results in a "shift" of the correlation curve (see Section 4.3.3 for a detailed discussion on effects of binder type on carbonation). However, within each binder-specific curve, the near-straight line indicates a good correlation, hence OPI is a useful tool to predict carbonation as long as the influence of the binder type (and hence the pore chemistry) is considered.

It is important to note that several factors may independently influence these parameters. It has been reported, for example, that the amount of carbonatable materials (cement hydrates) significantly influences the rate of carbonation, whereas the presence of moisture significantly reduces gas permeability. Therefore, as mentioned by Alexander and Thomas (2015), the prediction of carbonation depth from the gas permeability properties of mixes ought to be implemented within the range where reasonable correlation has been established.

4.4 Closure

The test results indicate that good correlations exist between (i) electrical conductivity and rate of chloride diffusion, and (ii) oxygen permeability and rate of carbonation. The good correlations can primarily be attributed to the fact that these material properties largely depend on the pore structure (particularly the size, connectivity and tortuosity of the pores).

These results also show that the durability performance of patch repair mortars, in terms of chloride and carbonation resistance, depends on material factors such as w/b ratio, curing type and binder type, which directly influence penetrability. The test results presented in this chapter will be used in the next chapter to develop service life prediction models for the mortar mixes used in this study.

CHAPTER 5: SERVICE LIFE PREDICTION

5.1 Introduction

In this chapter, empirical models based on Fickian equations are used to predict chloride ingress and carbonation in the mortars mixes used in this study. From these models, profiles showing the advancement of carbonation depth and the penetration of chloride ions with time are developed using the experimental results presented in Chapter 4. The theoretical basis of these empirical models as well as the assumptions made with regard to some important empirical parameters are also presented. It is important to note that the mean values presented (particularly for the effective diffusion coefficients, D_{eff} and the surface chloride content, C_s) are averages of three readings.

5.2 Prediction of chloride ingress

Fick's second law of diffusion has been shown to provide a reasonable estimation of the variation of chloride ions with depth in cement-based materials exposed to chloride ions. Equation 5.1 (solution to Fick's second law) is valid for constant diffusion coefficient, D_{eff} and surface chloride content C_s (symbols are as given in Section 2.5.1). However, it has been reported that D_{eff} and C_s change with time. Thus using a constant D_{eff} and C_s for long-term prediction of chloride ingress would significantly underestimate the actual service life. To obtain a more precise estimation in the long term, time-dependent D_{eff} and C_s ought to be incorporated in Equation 5.1 (Boddy *et al.*, 1999; Costa and Appleton, 1999a, 1999b). The following subsections present these time-dependent parameters as well as the assumptions made with regard to important empirical parameters such as the chloride threshold values.

$$C(x,t) = C_s\left[1 - erf\left(\frac{x}{2\sqrt{D_{eff}\,t}}\right)\right] \qquad (5.1)$$

5.2.1 Time-dependent chloride diffusion coefficient

The change in chloride diffusion coefficient over time can be described by the power function expressed in Equation 5.2. The aging factor (m) shown in the equation accounts for the

decrease in diffusion coefficient with time (Mangat and Molloy, 1994; Maage *et al*., 1996; Costa and Appleton, 1999b).

$$D(t) = D_1 t^{-m} \qquad (5.2)$$

where: $D(t)$ is the diffusion coefficient after exposure time, t,
D_1 is the diffusion coefficient after one year, if t is expressed in years,
m is the aging factor.

Factors influencing the aging factor (m) include the type of binder used, the w/b ratio and the exposure conditions (Luping and Gulikers, 2007; Rooij *et al*., 2007). Costa and Appleton (1999b) mention that the aging factor is greater in concrete of poor quality, implying a higher rate of reduction of the diffusion coefficient compared to concrete of higher quality. This subsequently suggests that the reduction in diffusion coefficient with time is greater when chloride penetration is higher. Studies by Bamforth (1999) and Maage *et al*. (1999) showed a significant decrease in effective diffusivity with the addition of SCMs. This reduction corresponded to m-values ranging from 0.6 to 0.8. For Portland cement (PC) concrete, Bamforth (1999) observed a value of 0.25. Typical values from literature are presented in Table 5.1.

Table 5.1: Values of aging coefficient, m as published in various literatures

Reference	**Aging coefficient (*m*-value)**	
Gehlen, 2000	0.45	
Polder and Rooij, 2005	0.48	
Viser and Polder, 2006	0.23 – 0.38	
Costa and Appleton, 1999b	Spray zone	0.43 – 0.51
	Tidal zone	0.6
	Atmospheric zone	0.36 – 0.42

The time-dependent diffusion coefficients of the mortar mixes used in this study were estimated using Equation 5.2. The m-values for the various binders are not yet well established. However, it was assumed that a value of 0.30 would simulate severe exposure conditions, which would necessitate patch repairs due to chloride-induced corrosion of steel. It is important to note that this section serves as a framework for modelling chloride ingress

in patch repair mortars, and further studies, which may include chemical analyses, should aim at quantifying the *m*-values for the various types of binders in order to improve the accuracy of service life predictions. Table 5.2 presents one-year predictions of the time-dependent effective diffusion coefficients of the mortar specimens. The predicted coefficients (D_1) were calculated from the chloride diffusion coefficients (D_{eff}) obtained from the chloride profiles of the specimens. The D_1-values will be incorporated in the empirical model for long-term prediction of chloride penetration in Section 5.2.5. As mentioned in Chapter 4, the little distinctions in diffusion coefficients (which have consequently caused little distinctions in D_1-values) could not be accounted for based on studied literature, and therefore, a further study of this phenomenon was recommended.

Table 5.2: One-year predictions of the effective diffusion coefficients using Equation 5.2

Mix	Mean D_{eff} ($\times 10^{-12}$ m²/s)	Std. dev. of D_{eff}	D_1 (1 year prediction)
PM45	8.27	0.18	2.88
PM60	8.66	0.29	3.02
SM45	7.68	0.05	2.67
SM60	8.03	0.14	2.80
CM1	7.74	0.08	2.69
CM2	7.95	0.17	2.77
CM3	7.77	0.05	2.71
CM4	7.59	0.13	2.64

** One-year prediction values of time-dependent diffusion coefficient calculated from the experimentally obtained effective diffusion coefficients (D_{eff}).*

5.2.2 Time-dependent surface chloride content

The change in surface chloride content, C_s with time can be described using Equation 5.3. An empirical coefficient (n) shown in the equation accounts for the increase in C_s with time. The main factor affecting the time-dependent surface chloride content (C_1) is the exposure condition. Severe exposure conditions would lead to higher values of C_1. Thus, the initial value (C_s) would increase over time in attenuated manner (Swamy *et al.*, 1994; Costa and Appleton, 1999b; Luping and Gulikers, 2007).

$$C_s(t) = C_1 t^n \tag{5.3}$$

where: $C_s(t)$ is the surface chloride content after time t,

C_1 is the surface chloride content after one year, if t is expressed in years,

n is an empirical coefficient.

The time-dependent surface chloride content of the mortars mixes used in this study were estimated using Equation 5.3. The empirical coefficients for mortars are not yet well established. However, it was assumed that a value of 0.60 would simulate severe exposure conditions that would necessitate patch repairs due to chloride-induced corrosion of steel. As mention earlier, further studies should be conducted to quantifying this parameter for the various types of binders in order to improve the accuracy of service life predictions.

Table 5.3: Empirical coefficients for various exposure conditions (Costa and Appleton, 1999b)

Exposure condition	***n***	**Mean *n***	**Std. dev. of *n***
Spray zone	0.47	0.49	0.02
	0.51		
	0.48		
Tidal zone	0.37	0.37	-
Atmospheric zone	0.54	0.61	0.08
	0.69		
	0.59		

Table 5.4 presents one-year predictions of the time-dependent surface chloride contents of the mortar specimens, calculated from equation 5.3. The predicted values (C_1) were calculated from the values of surface chloride content (C_s) obtained from the chloride profiles of the specimens. In all the specimens, chloride content was expressed in percentage by mass of binder. The binder content of the commercial mortars was estimated as shown in Section 5.2.4 due to the absence of information regarding their composition. The C_1-values will be incorporated in the empirical model for long-term prediction of chloride penetration in Section 5.2.5.

Table 5.4 One-year predictions of the surface chloride content using Equation 5.3

Mix	Mean C_s (% by mass of binder)	Std. dev of C_s	C_1 (% by mass of:)	
			Binder	Mortar
PM45	5.33	0.21	12.70	2.86
PM60	8.23	0.32	19.60	3.64
SM45	3.02	0.41	7.18	2.21
SM60	5.15	0.30	12.26	2.33
CM1	5.10	0.10	12.14	2.55
CM2	11.33	0.31	26.98	5.4
CM3	4.17	0.12	9.92	2.5
CM4	1.28	0.06	3.06	1.45

** One-year prediction values of time-dependent surface chloride content calculated from the experimentally obtained surface chloride content (C_s). C_1 expressed as % by mass of mortar was calculated from the C_s values presented in Table 4.2 (Section 4.2.1).*

5.2.3 Chloride threshold values

Several values of the critical chloride threshold have been reported in literature. Some of these values are presented in Table 5.5. To obtain better estimates of expected service life, the following chloride threshold values were deemed reasonable:

i) Laboratory-made mortars: 0.53% and 0.41% for CEM II and CEM II/GGBS specimens respectively. These values were obtained by Scott (2004), who studied the chloride threshold values of South African binders. Thus, they can be assumed as better estimates of the chloride threshold values in this study since both experiments were conducted in the same region and with similar binder types.
ii) Commercial mortar mixes: 0.4%, which is widely accepted as the critical chloride content that can initiate reinforcement corrosion (Costa and Appleton, 1999b).

Table 5.5: Chloride threshold values as presented in various publications

Reference	Binder type	Chloride threshold (% by mass of binder)
Alonso *et al*., 2000	Portland cement (PC)	1.24 – 3.08
Lambert *et al.*, 1991	PC and sulphate resisting PC	1.0 – 3.0
Scott, 2004	PC	0.53
	Slag	0.41
Trejo and Pillai, 2003	PC	0.02 – 0.24
Costa and Appleton, 1999b	Generally assumed in Europe	0.4

5.2.4 Estimation of binder content in commercial mortars

The chloride content in cement-based materials is often expressed in percentage by mass of binder. However, information regarding the constituents (binder content) of the commercial mortars is often absent. For the purpose of consistency, the binder content of the commercial mortars was estimated using the 28-day compressive strength and water content. The w/b ratios of the commercial mortars were inferred from their 28-day compressive strength using Figure 5.1 (graph of compressive strength versus w/b ratio of CEM II specimens). The binder content was thereafter calculated from the estimated w/b ratio and the volume of water used to prepare the mix. An example calculation is shown below:

28-day compressive strength of CM3 specimen = 44.8 MPa

Estimated w/b ratio (see Figure 5.1) = 0.56

Water content = 261 *l*/m^3

$$\text{Thus, binder content} = \frac{\text{water content}}{w/b\ ratio} = \frac{261}{0.56} = 467\ \text{kg/m}^3$$

The calculated binder content may not be entirely accurate since it does not take into account the effects of modification by polymers, synthetic fibre reinforcement, and the addition of silica fume and other chemicals to some of the commercial mortars. However, the effects of modification have been assumed minimal, and thus ignored for the purpose of this study.

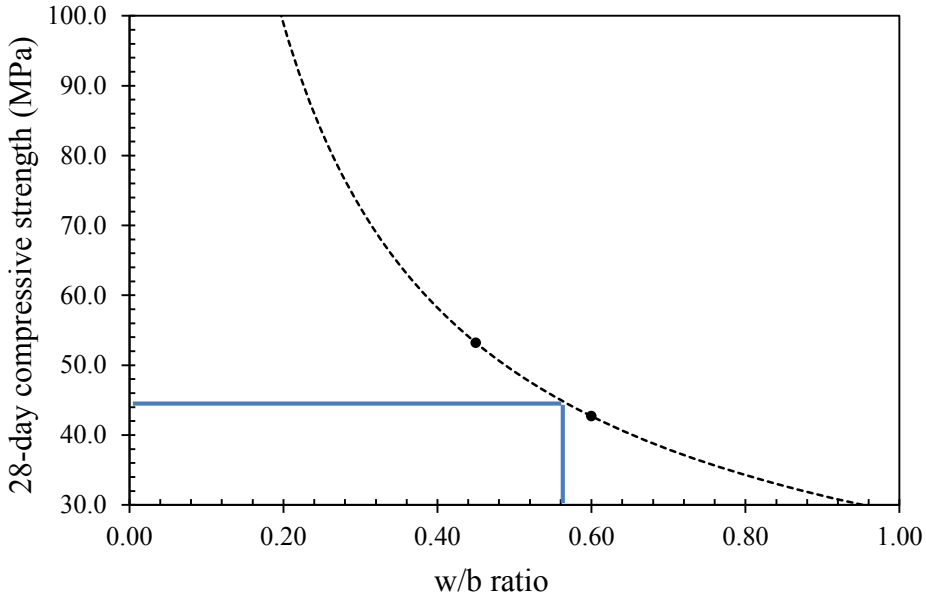

Figure 5.1: 28-day compressive strength versus w/b ratio for the CEM II mortar specimens

Note: In cement-based materials, the relationship between compressive strength and w/b ratio is usually depicted by a curve (as shown in Figure 5.1), thus using the plots, a similar correlation curve was assumed.

The assumed binder contents of the commercial mortars used in this investigation are presented in Table 5.6.

Table 5.6: Estimated binder contents of the commercial mortars

Mix	Compressive strength (MPa)	Estimated w/b ratio	Water content (l/m^3)	Binder content (kg/m^3)
CM1	38.7	0.68	283	417
CM2	36.7	0.72	253	352
CM3	44.8	0.56	261	467
CM4	82.2	0.26	282	1084

5.2.5 Prediction profiles for chloride ingress

The time-dependent parameters (D_1 and C_1) estimated in Sections 5.2.1 and 5.2.2 were used in the empirical model for predicting chloride ingress (see Equation 5.4) (Costa and Appleton, 1999b). From this equation, chloride penetration profiles that can be used to

predict chloride ingress in the mortar mixes used in this study were developed (see Figure 5.2 and Figure 5.3).

$$C(x,t) = C_1 t^n \left[1 - erf\left(\frac{x}{2\sqrt{D_1 t^{1-m}}} \right) \right] \tag{5.4}$$

The parameters x, t and D_1 are expressed in mm, years and mm^2/year respectively. Substituting the previously calculated values (D_1 and C_1) and assumed values (m and n) into Equation 5.4, for each mortar mix, gives the equations presented in Table 5.7.

Table 5.7: Equations for modelling chloride ingress for the mortar mixes used in this study

Mix ID	Equation
PM45	$C(x,t) = 12.70t^{0.60}\left[1 - erf\left(\frac{x}{2\sqrt{2.881t^{1-0.30}}} \right) \right]$
PM60	$C(x,t) = 19.60t^{0.60}\left[1 - erf\left(\frac{x}{2\sqrt{3.02t^{1-0.30}}} \right) \right]$
SM45	$C(x,t) = 7.18t^{0.60}\left[1 - erf\left(\frac{x}{2\sqrt{2.67t^{1-0.30}}} \right) \right]$
SM60	$C(x,t) = 12.26t^{0.60}\left[1 - erf\left(\frac{x}{2\sqrt{2.80t^{1-0.30}}} \right) \right]$
CM1	$C(x,t) = 12.14t^{0.60}\left[1 - erf\left(\frac{x}{2\sqrt{2.69t^{1-0.30}}} \right) \right]$
CM2	$C(x,t) = 26.98t^{0.60}\left[1 - erf\left(\frac{x}{2\sqrt{2.77t^{1-0.30}}} \right) \right]$
CM3	$C(x,t) = 9.92t^{0.60}\left[1 - erf\left(\frac{x}{2\sqrt{2.71t^{1-0.30}}} \right) \right]$
CM4	$C(x,t) = 3.06t^{0.60}\left[1 - erf\left(\frac{x}{2\sqrt{2.64t^{1-0.30}}} \right) \right]$

Figure 5.2 and 5.3 present chloride penetration profiles showing the rate of accumulation of chloride ions at cover depths of 30 mm and 40 mm respectively, for all the mortar mixes used. These cover depths were selected because they are commonly applied in RC structures. The effects of varying curing regimes was not investigated since the upper surface (20mm) of the specimens was cut to determine the initial chloride content (in accordance with ASTM C1556-04), thus eliminating the influence of curing. For this reason, only the moist cured specimens were used in the analysis.

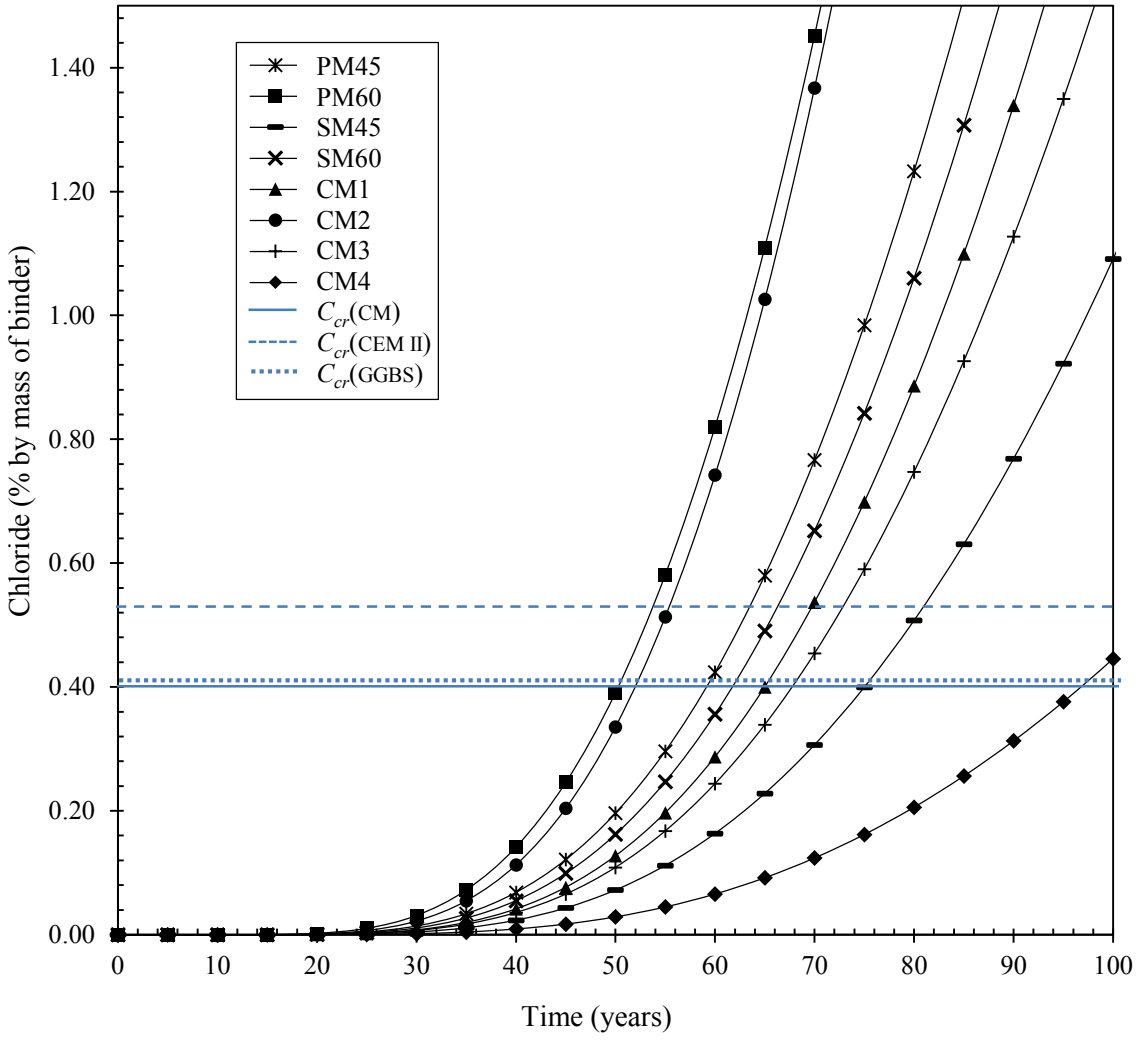

Figure 5.2: Chloride penetration profiles showing the rate of accumulation of chloride ions at a cover depth of 30 mm, for all the mortar mixes used.

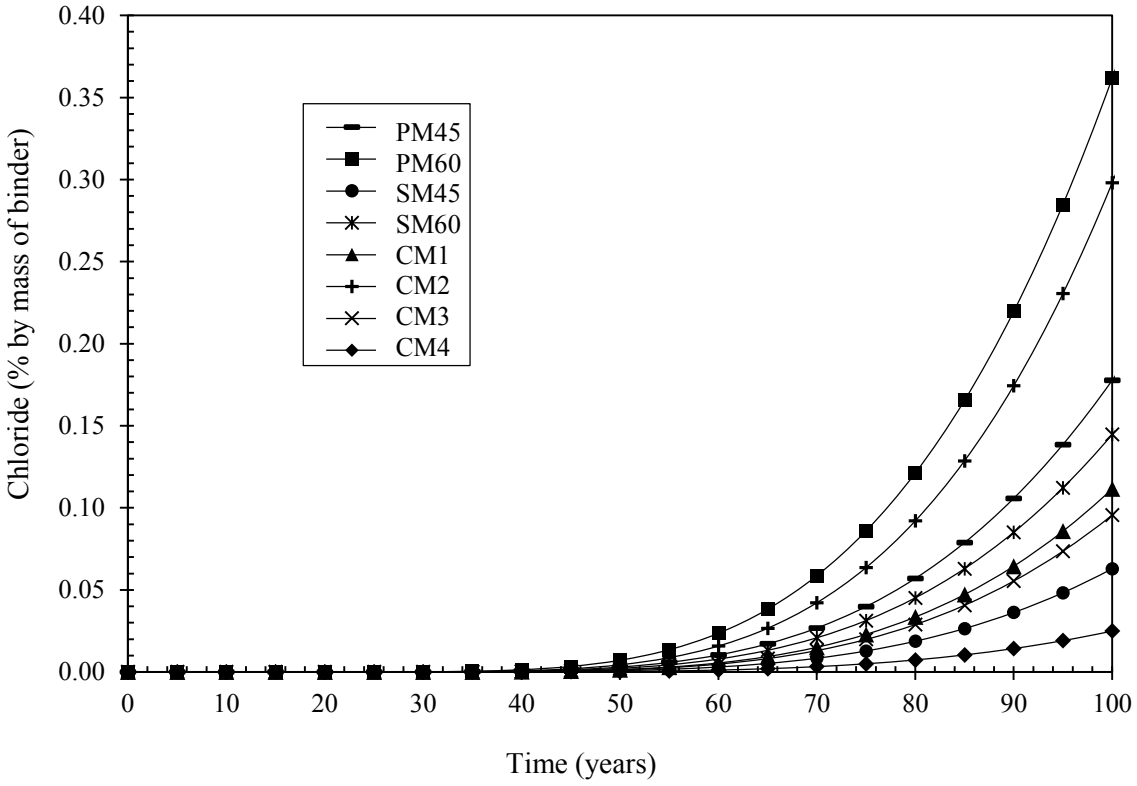

Figure 5.3: Chloride penetration profiles showing the rate of accumulation of chloride ions at a cover depth of 40 mm, for all the mortar mixes used.

From Figure 5.2, the time taken to reach the chloride threshold value (time to steel depassivation) for each mortar mix, at a cover depth of 30 mm, could approximately be predicted as follows: PM45 – 62 years, PM60 – 54 years, SM45 – 74 years, SM60 – 62 years, CM1 – 64 years, CM2 – 52 years, CM3 – 68 years, CM4 – 96 years. These trends are as expected, and are discussed below. As seen in Figure 5.3, the chloride threshold values were however not reached for all the mortar mixes, at a cover depth of 40 mm, within a reference time of 100 years.

Comparing the profiles for the accumulation of chloride ions at a cover depth of 30 mm in laboratory-made mortar mixes (Figure 5.2 and 5.3), it can be predicted that steel depassivation would occur in the shortest time in PM60, while it would take the longest time in SM45. This can be attributed to two main reasons. Firstly, the higher w/b ratio (0.60) results in higher porosity (see Section 4.2.3.1), thus increased rate of diffusion of chloride ions. Consequently, this increases the rate of accumulation of chloride ions at a particular cover depth (Halamickova *et al.*, 1995; Dinku and Reinhardt, 1997). Secondly, the beneficial effects of GGBS, such as pore filling, chloride binding and increased cementing reactions

(see Section 4.2.3.3) result in densification of the microstructure and reduction in chloride diffusivity (Poulsen, 1995; Baroghel-Bouny *et al.*, 2009; Pack *et al.*, 2010). This also explains why, in general, CEM II/GGBS specimens outperformed CEM II specimens

Among the commercial repair mortars, the profile of CM4 showed the best resistance to chloride ingress, with CM2 displaying the worst performance. Apart from CM2, the commercial repair mortars generally outperformed the laboratory-made mortars. This can be attributed to the fact that these commercial mortars are specially manufactured under controlled conditions to be sufficiently impenetrable.

Generally, the accumulation of chloride ions were predicted to begin after 25 to 30 years at 30 mm cover depth (Figure 5.2), and 40 to 50 years at 40 mm cover depth (Figure 5.3), after which the rate of accumulation increases rapidly in both cases. This broadly implies that an additional 10 mm cover thickness would delay the onset of accumulation of chloride ions by about 20 years, highlighting the significance of cover depth on the durability of concrete structures.

5.3 Prediction of carbonation

The rate of carbonation in cement-based materials can be predicted using the square-root-of-time law (derived from Fick's second law of diffusion), which is often applied to relate the depth of carbonation with time (see Section 2.5.5.3). The square-root-of-time law assumes a constant diffusion coefficient for carbon dioxide. However, literature reports that the diffusion coefficient of carbon dioxide varies with, among other factors, time, depth and moisture content in the pores (Kropp, 1995; Costa and Appleton, 2001; Czarnecki and Woyciechowski, 2015). Thus, the empirical law is limited by this assumption. However, it provides a reasonable estimation of the rate of development of carbonation depth in cement-based materials.

5.3.1 Carbon dioxide concentration

In this analysis, a constant carbon dioxide concentration of 800 ppmv was deemed reasonable for severe natural exposure conditions where patch repairs due to carbonation-induced corrosion of steel would be expected. Table 5.8 presents the carbon dioxide concentrations for various exposure conditions in parts per million by volume (ppmv). These values are based on research by Grimmond *et al*. (2002), Idso *et al*. (2002) and Westerdahl *et al*. (2005).

Table 5.8: Carbon dioxide concentration in ppmv based on land use.

Condition	Description	ppmv
Severe	Highways, industrial areas and areas close to CO_2 sources	700-900
Moderate	City centers, urban areas with high densities	500-600
Mild	Rural areas and urban areas with low densities	390-450

5.3.2 Relationship between accelerated and natural carbonation depths

Equation 5.5 outlined by Bahador and Cahyadi, (2009) can be used to relate accelerated carbonation depth and natural carbonation depth.

$$\frac{x_{ac}}{x_{nc}} = \sqrt{\frac{[CO_2]_{ac}}{[CO_2]_{nc}}} \qquad (5.5)$$

where: x_{ac} is carbonation depth in accelerated test,
x_{nc} is carbonation depth in natural condition,
$[CO_2]_{ac}$ is CO_2 concentration in accelerated test,
$[CO_2]_{nc}$ is CO_2 concentration in natural condition.

Khunthongkeaw *et al*. (2006) proposed a linear equation (Equation 5.6) from a plot of natural depth versus accelerated depth, which can be used to relate carbonation depths measured from natural exposure conditions with those obtained from accelerated carbonation test.

$$x_{nc,t_1} = A \cdot x_{ac_1} \cdot \sqrt{t} \qquad (5.6)$$

where: $x_{nc,t1}$ is carbonation depth in natural environment for t months,
x_{ac1} is carbonation depth of same material in accelerated test after one month of exposure,
t is the exposure time in natural environment (months),
A is the correlation factor between $x_{nc,t1}$ and x_{ac1} (slope of the graph).

Assuming a constant rate of carbonation, the one-month accelerated carbonation depths (x_{ac1}) were inferred from the 12-weeks accelerated carbonation depths measured in the laboratory. Thereafter, the natural carbonation depths (after one month of exposure, $x_{nc,t1}$), expected to correspond with the one-month accelerated carbonation depths were calculated using Equation 5.5. Table 5.9 presents a summary of the abovementioned calculations.

Table 5.9: A summary of one-month (31 days) accelerated carbonation depths and the corresponding natural carbonation depths

Mix	CO_2 conc., nc. (ppmv)	CO_2 conc., ac. (ppmv)	Carbonation depth, ac. (mm)		Carbonation depth, nc. (mm)
			84 days	31 days	
PM45_D	800	20000	7.2	2.6	0.5
PM45_M	800	20000	4.9	1.8	0.4
PM60_D	800	20000	13.7	4.9	1.0
PM60_M	800	20000	8.2	2.9	0.6
SM45_D	800	20000	20.2	7.2	1.4
SM45_M	800	20000	8.5	3.0	0.6
SM60_D	800	20000	34.4	12.3	2.5
SM60_M	800	20000	15.4	5.5	1.1
CM1_D	800	20000	15.5	5.5	1.1
CM1_M	800	20000	11.0	3.9	0.8
CM2_D	800	20000	8.1	2.9	0.6
CM2_M	800	20000	3.5	1.3	0.3
CM3_D	800	20000	29.9	10.7	2.1
CM3_M	800	20000	12.5	4.5	0.9
CM4_D	800	20000	3.0	1.1	0.2
CM4_M	800	20000	0.0	0.0	0.0

Note: D represents dry cured specimens

M represents moist cured specimens

nc. denotes natural exposure conditions (projected one-month carbonation depths)

ac. denotes accelerated conditions (one-month carbonation depths)

To determine the correlation factor, A (Equation 5.6) between the natural and the accelerated carbonation depths, the projected natural carbonation depths (one-month - $x_{nc,t1}$) were plotted against the inferred accelerated carbonation depths (one-month - x_{ac1}) as shown in Figure 5.4. A correlation factor of 0.2 (slope of the graph) was obtained for the selected natural exposure conditions (CO_2 concentration of 800ppmv and 75% RH).

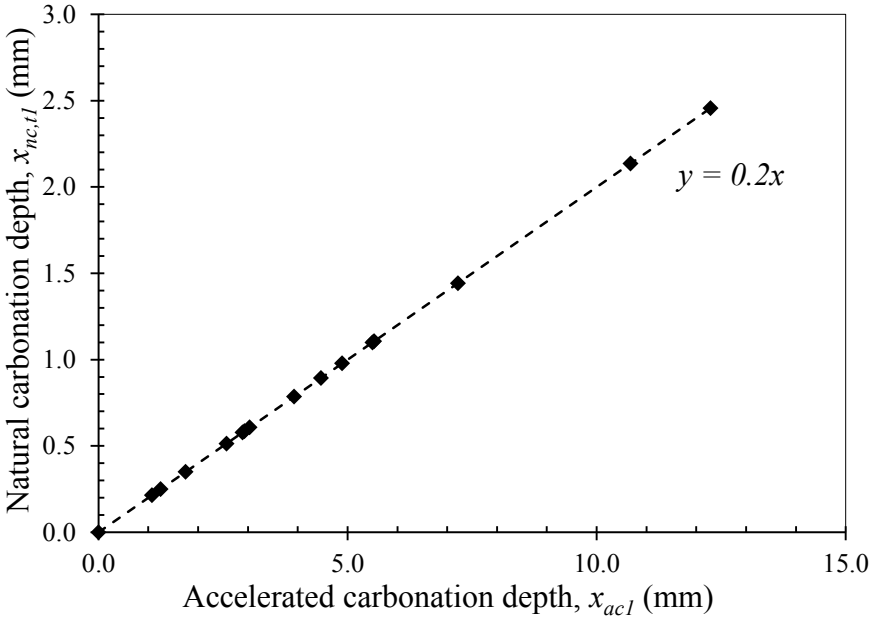

Figure 5.4: Linear relationship between one-month natural carbonation depth and one-month accelerated carbonation depth (*nc*. of 75% RH and 800ppmv CO_2 concentration)

As mentioned by Khunthongkeaw *et al*. (2006), the correlation factor depends entirely on the exposure conditions since the specimens are assumed to be of similar material composition and subsequently, same pore structure. Therefore, it can be assumed that the accelerated carbonation depths may be used to predict reasonable natural carbonation depths.

5.3.3 Prediction profiles for carbonation depth

Profiles that can be used to predict the depth of carbonation in the mortar mixes used in this study were developed from Equation 5.7 (see Figure 5.5 to 5.6). The symbols are similar to those of Equation 5.6.

$$x_{nc,t_1} = 0.2 \cdot x_{ac_1} \cdot \sqrt{t} \qquad (5.7)$$

Figure 5.6 and 5.7 present the carbonation depth profiles showing the rate of advancement of carbonation front in the laboratory-made mortar mixes and the commercial mortar mixes respectively.

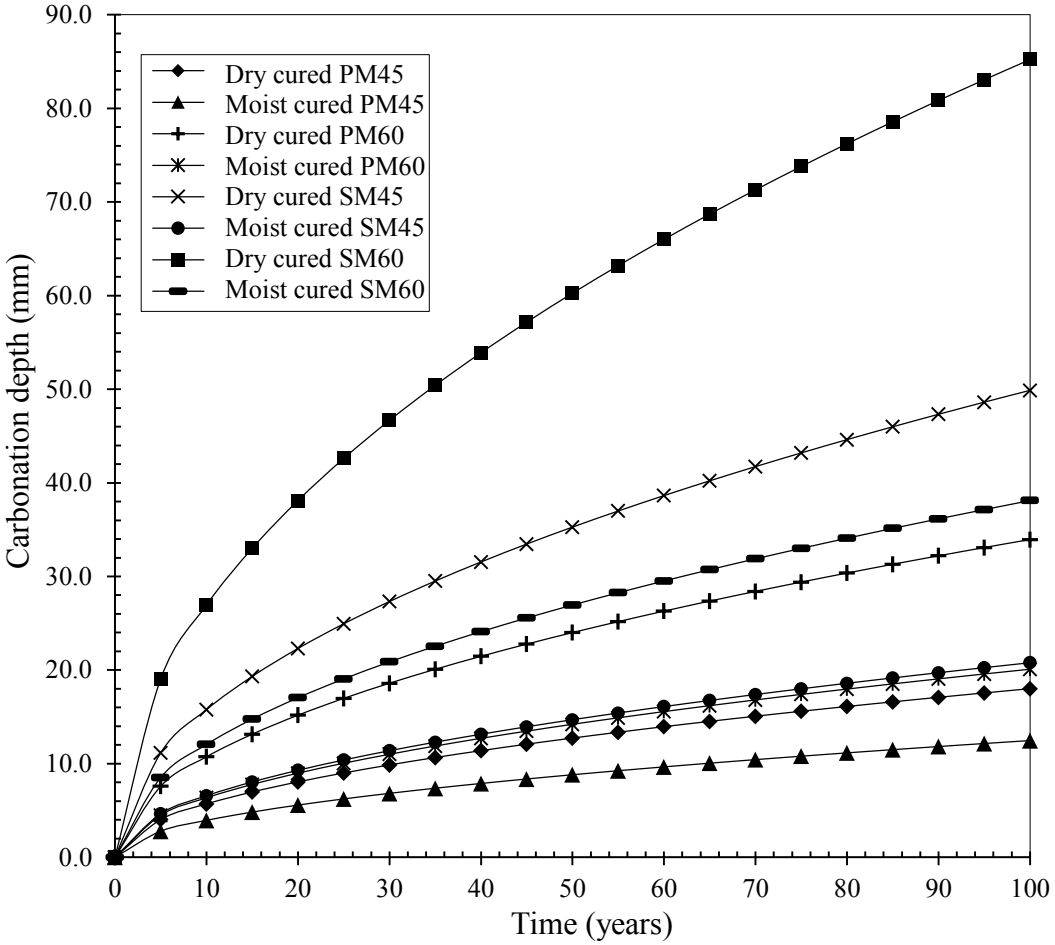

Figure 5.5: Carbonation depth profiles showing the predicted carbonation depths in the laboratory-made mortar mixes

Comparing the prediction profiles for development of carbonation depth among the laboratory-made mortars (Figure 5.5), it can be seen that the highest rate of carbonation was predicted in dry cured SM60 mix, while the lowest was predicted in moist cured PM45. This is consistent with literature and it can be attributed to three main reasons. Firstly, the higher w/b ratio (0.60) results in higher porosity (see Section 4.3.3.1), thus increased rate of diffusion of CO_2. Consequently, the rate of carbonation increases, resulting in greater depths of carbonation (Costa and Appleton, 2001; Kunthongkeaw *et al.*, 2006; Roziere *et al.*, 2009). Secondly, moist curing enhances cementing reactions which result in densification of the pore structure of mortar (see Section 4.3.3.2), thus reducing the penetrability of CO_2 gas (Dinku and Reinhardt, 1997; Kubens *et al.*, 2003; Grassl *et al.*, 2010). This reduces the rate of carbonation. Thirdly, the substitution of CEM II with GGBS reduces alkaline reserves (carbonatable components) which are in the carbonation reactions, thus increasing the rate of carbonation (see Section 4.3.3.3) (Papadakis, 2000; Penttala, 2009).

It can also be observed that for each mix, improved resistance to carbonation was predicted in moist cured specimens compared to dry cured specimens (Figure 5.5). This was expected and as already mentioned, it can be attributed to enhanced cementing reactions in the presence of water. In addition, the better carbonation resistance in CEM II specimens compared to CEM II/GGBS specimens has been attributed to more alkaline reserves which reduce the rate of carbonation.

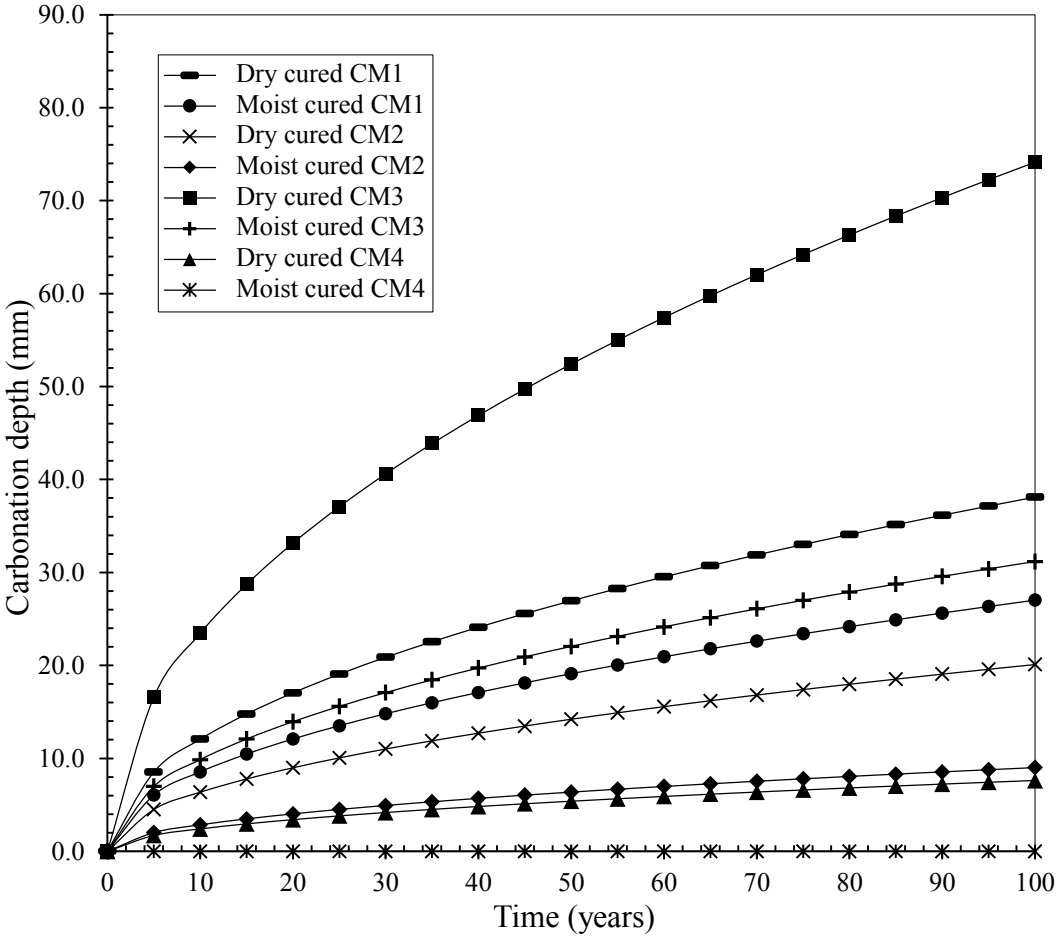

Figure 5.6: Carbonation depth profiles showing the predicted carbonation depths in the commercial mortar mixes

From Figure 5.6, it is noticeable that the worst resistance to carbonation was predicted in dry cured CM3 while moist cured CM4 outperformed all the other commercial mortar mixes. In addition, the prediction results show rapid development of carbonation depths for all mortars (Figure 5.5 and 5.6) in the initial service life (in the first 4 to 6 years), after which the rate of carbonation reduces gradually. This is can be attributed to further cementing reactions that continue to densify the pore structure of cement-based materials, thus increasing their

resistance to carbonation. In addition, the reduction in the rate of carbonation can be ascribed to the precipitation of $CaCO_3$ on the pore walls (see Section 2.6.3), which continually reduces the size and connectivity of pores, thus slowing down the rate of carbon dioxide diffusion (Bentz *et al.*, 1999; Penttala, 2009). It is also evident that, for each mix, moist cured specimens were predicted to outperform dry cured specimens, due to improved pore structure (refining of microstructure) as a result of curing.

5.4 Closure

Models that may be used to predict carbonation (Figure 5.5 and 5.6) and chloride ingress (Figure 5.2 and 5.3) in the mortar mixes used have been developed in this chapter. These models are based on the experimental results presented in Chapter 4, as well as reasonable assumptions made. Generally, the trends in the durability performance of the various mortar mixes were as expected. However, it should be noted that the proposed models presented in this study essentially serve as framework for modelling carbonation and chloride ingress in patch repair mortars. This is due to the fact that these models are based on many assumptions that ought to be verified/modified in future research. The evaluation of 'carbonatability' as well as chemical analysis of the materials should be considered in future work for better modelling results. The next chapter presents the conclusions of this study as well as recommended future work in this area.

CHAPTER 6: CONCLUSIONS AND RECOMMENDATIONS

6.1 Introduction

This study aimed at investigating the durability performance, in terms of resistance to chloride penetration and carbonation, of selected patch repair mortars. The study was motivated by the need to consider material properties that directly influence the transport of aggressive species such as chloride ions, rather than compressive strength, when prescribing patch repair mortars. These material properties include chloride conductivity, chloride diffusion coefficient, gas permeability and carbonation coefficient. While much research effort in concrete repair has been directed towards, among other properties, bond strength and cracking resistance of concrete repair materials, little effort has been put in the repair material properties that directly relate to durability. This poses a challenge in quantifying the durability performance of patch repair mortars, since these material properties are essential input parameters for most of the durability prediction models. This study contributes towards addressing this challenge. The essential findings of this study, in light of the research objectives, are summarised in this chapter. In the *Recommendations* section, the various aspects of this study that need further work are presented.

6.2 Summary of the major findings

The following conclusions, can be drawn from the experimental results and service life prediction models.

6.2.1 Effect of curing on penetration resistance

Moist curing was observed to increase the penetration resistance of the repair mortars tested in this study. The chloride conductivity, permeability coefficients (from OPI values) and carbonation depths of moist cured specimens were lower than those of the dry cured specimens. This was attributed to continued cementing reactions that densify the microstructure, in the presence of curing water. The improved penetration resistance due to curing implies that better curing methods would be beneficial to the durability of concrete repairs in practice. By increasing the penetration resistance of patch repair mortars, better

curing methods could delay or prevent the onset of reinforcement corrosion, thus increasing the remaining service life of repaired RC structures.

6.2.2 Effect of water/binder ratio on penetration resistance

An increase in water/binder ratio resulted in reduced penetration resistance of the mortar specimens. Specimens with higher w/b ratios recorded greater chloride diffusion coefficients, chloride conductivity, permeability coefficients and carbonation depths. This was ascribed to increased initial spacing of cement particles in fresh mortar, which results in increased size and connectivity of the capillary pores in hardened mortars. This implies that the use of sufficient w/b ratios in patch repair mortars could be beneficial to the durability of concrete repairs.

6.2.3 Effect of binder type on penetration resistance

The addition of GGBS was observed to increase chloride resistance of the mortar specimens. The chloride conductivity of CEM II/GGBS specimens were lower than those of CEM II specimens, except for dry cured SM60, which suffered poor curing practice and excessive w/b ratio. The increased chloride resistance was attributed to the beneficial chloride binding effects of GGBS, and increased cementing reactions that result in densification of the pore structure. These results suggest that the addition of SCMs such as GGBS and silica fume in patch repair mortars could improve the durability of concrete repairs in marine environments and structures exposed to de-icing salts.

On the contrary, the addition of GGBS resulted in reduced carbonation resistance of the mortar specimens. Greater depths of carbonation were observed on GGBS/CEM II specimens compared to CEM II specimens. This was attributed to the reduction in the alkaline reserves (calcium silicate hydrate and calcium hydroxide formed as a result of hydration of CEM II) that take part in carbonation reactions, due to the partial replacement of CEM II. This implies that the addition of some SCMs such as GGBS could aggravate the durability performance of patch repair mortars in environments with high carbon dioxide concentrations, such as urban and industrial areas.

6.2.4 Correlations between material transport properties

A comparison was drawn between the results of bulk diffusion test (BDT) and chloride conductivity index (CCI) test. A 'very good' correlation, with a linear correlation coefficient of 0.9112 was observed between diffusion coefficients (from BDT) and chloride conductivity values (from CCI test). The observed correlation was attributed to the fact that both electrical conductivity and rate of chloride diffusion are mainly governed by the size, connectivity and tortuosity of the capillary pores. This suggests that CCI values could provide reasonable measure of chloride resistance in patch repair mortars.

Similarly, the results of accelerated carbonation test (ACT) and oxygen permeability index (OPI) test were compared. The correlation between carbonation coefficients (from ACT) and permeability coefficients (from OPI test) was observed to be 'good', with a linear correlation coefficient 0.6751. The 'good' correlation was attributed to the fact that both oxygen permeability and rate of carbonation largely depend on the pore structure of cement-based materials. Thus, the OPI values could provide reasonable measure of carbonation resistance in patch repair mortars. However, since several factors may independently influence these transport properties in each case, the measures of carbonation and chloride resistance should be obtained within the range where reasonable correlations can been established.

6.2.5 Modelling of chloride penetration and carbonation

Modelling of chloride penetration and carbonation for the patch repair mortars used in this study was based on Fickian equations. Several assumptions, which should be verified and/or modified in future research, were made to simulate severe exposure conditions that would necessitate patch repairs. These included an aging factor (m) of 0.30, an empirical coefficient (n) of 0.60, chloride threshold values of 0.53% (CEM II), 0.41% (CEM II/GGBS) and 0.4% (commercial mortars), and estimation of binder content in commercial mortars using their compressive strength (see section 5.2.4), for the prediction of chloride ingress. In carbonation prediction, a carbon dioxide concentration of 800 ppmv was assumed. The following can be drawn from the modelled prediction profiles:

i) Chloride penetration could be predicted based on the solution to Fick's second law of diffusion. As expected, the chloride penetration profiles predicted a longer duration to steel depassivation in CEM II/GGBS specimens than in CEM II specimens, due to chloride binding and pore filling effects of GGBS. Also, a higher w/b ratio was

predicted to reduce the duration to steel depassivation, which was attributed to increased porosity. The observed trends are quite favourable considering the many assumptions made in developing the chloride penetration profiles. Comparing the prediction profiles for 30 mm and 40 mm cover depths, it was observed that an additional 10 mm would delay the onset of accumulation of chloride ions at the level of steel by about 20 years (see Figure 5.2 and 5.3), underscoring the significance of cover depth on the durability of RC structures.

ii) Carbonation depths could be predicted based on the square-root-of-time law. From the carbonation depth prediction profiles (see Figure 5.5 and 5.6), improved carbonation resistance was observed with: reduced w/b ratio, due to reduced porosity; moist curing, due to continued cementing reactions that densify the microstructure; and the exclusion of GGBS, which maintained the amount of alkaline reserves that reduce the rate of carbonation. In addition, rapid development of carbonation depths was predicted in the initial service life (in the first 4 -6 years), after which the rate of carbonation reduced gradually. This was attributed to further cementing reactions as the patch repair mortars mature, as well as the precipitation of calcium carbonate ($CaCO_3$) on the walls of the capillary pores, thus reducing their size and connectivity.

The above-mentioned conclusions suggest that, more reliable predictions of chloride penetration and carbonation depths could be attained with the Fickian equations used, with well-established input parameters. This study did not quantify/verify the input parameters such as m, n and CO_2 concentration, but future research should determine these values for better modelling results. In real life, chloride penetration and carbonation in these patch repair mortars may occur differently from what is presented in this study. This is due to the several assumptions made as well as some laboratory results that were rough estimates (i.e. surface chloride content and chloride diffusion coefficients). However, these modelling results would prove useful as framework for evaluating the penetration resistance of patch repair mortars, and are subject to further improvement.

6.3 Recommendations

The aspects of this study that need further work for improved results include the following:

i) Detailed results should be obtained on the chemical and phase properties of the binders used in the study. This may include the evaluation of ‘carbonatability’ of

materials to improve the results of carbonation modelling. Measurement of vital material properties such as porosity and pore-size distribution are also recommended to shed more light on the transport properties of materials.

ii) The profile intervals used for chloride profiling in bulk diffusion test was quite coarse. Future research should consider finer profile interval (such as 2mm) and longer duration of testing (such as 90 days) to minimize errors on the surface chloride content (C_s) and chloride diffusion coefficient (D_{eff}). In addition, superior modelling techniques such as FEM should be considered when developing service life prediction profiles.

iii) As already mentioned, future study should quantify the assumed input parameters to the Fickian equations, i.e. the aging factor (m) and the empirical coefficient (n).

iv) Though useful results were obtained from the eight mortar specimens and a small range of experimental variables, there is need to increase the number of test specimens as well as consider a wide range of experimental variables such as w/b ratios, curing methods, binder types and exposure conditions.

v) Further work should consider formulating the models based on the DI approach, using the durability indexes.

vi) The little distinctions in chloride diffusion coefficients (Chapter 4) could not be accounted for based on studied literature, thus further investigation was recommended to study this phenomenon.

REFERENCES

AFREM Technical report. (1999). AFREM test procedures concerning chlorides in concrete: Extraction and titration methods. *Materials and Structures*. 32:230-234.

Ahmad, S. (2003). Reinforcement corrosion in concrete structures, its monitoring and service life prediction – a review. *Cement and Concrete Composites*. 25:459-471.

Alexander, M. G., Mackechnie, J. R. and Ballim, Y. (1999). Guide to the use of durability indexes for achieving durability in concrete structures. University of Cape Town and Witswatersrand, Research Monograph no. 2.

Alexander, M. G. (2004). Durability indexes and their use in concrete engineering. In *International RILEM Symposium on Concrete Science and Engineering: A Tribute to Arnon Bentur*. Ed: K. Kovler, J. Marchand, S. Mindess and J. Weiss. RILEM Publications SARL.

Alexander, M. G. and Mackechnie, J. R. (2004). A pragmatic prediction model for chloride ingress into concrete. In *RILEM Report 38: Testing and Modelling Chloride Ingress into Concrete*. Eds: C. Andrade and J. Kropp. RILEM Publications S.A.R.L, pp. 277-289.

Alexander, M. G., Stanish, K. and Ballim, Y. (2006). Performance-based durability design and specification: Overview of the South African approach. *Proceedings of the "International RILEM Workshop on Durability Indicators"*. March 2006. Madrid.

Alexander, M. G., Ballim, Y. and Stanish, K. (2008). A framework for use of durability indexes in performance-based design and specifications for reinforced concrete structures. *Materials and Structures*. 41:921-936.

Alexander, M. G. and Beushausen, H. (2009). Performance-based durability testing, design and specification in South Africa: latest developments. In *Excellence in Concrete Construction through Innovation*. Eds: Limbachiya and Kew. London, UK: Taylor and Francis Group. Pp 429-434.

Alexander, M. and Thomas, M. (2015). Service life prediction and performance testing – Current developments and practical application. *Cement and Concrete Research.* 78:155-164.

Alonso, C., Andrade, C., Castellote, M. and Castro, P. (2000). Chloride threshold values to depassivate reinforcing bars embedded in a standardized OPC mortar. *Cement and Concrete Research*. 30(7):1047-1055.

Andrade, C., Polder, R. and Basheer, M. (2007). Non-destructive methods to measure ion migration. In *RILEM Report 40: Non-destructive evaluation of the penetrability and thickness of the concrete cover*. Eds: R. Torrent and L. F. Luco. RILEM Publications S.A.R.L, pp. 91-112.

Arya, C. and Wood, L. A. (1995). The relevance of cracking in concrete to corrosion of reinforcement. Concrete Society Technical Report No 44. In *Concrete Repair Manual*, 2nd ed. Eds: B. L. Schmick and A. Pollington. Pp. 555-584.

Arya, C. and Ofori-Darko, F. K. (1996). Influence of crack frequency on reinforcement corrosion in concrete. *Cement and Concrete Research*. 26(3):345-353.

ASTM C1556-04. (2004). Standard Test Method for Determining the Apparent Chloride Diffusion Coefficient of Cementitious Mixtures by Bulk Diffusion. ASTM International, USA.

ASTM C1152/C1152M-04. (2012). Standard Test Method for Acid-Soluble Chloride in Mortar and Concrete. ASTM International, USA.

Atis, C. D. (2003). Accelerated carbonation and testing of concrete made with fly ash. *Construction and Building Materials*. 17:147-152.

Badaoui, A., Badaoui, M. and Kharchi, F. (2013). Probabilistic analysis of reinforced concrete carbonation depth. *Material Sciences and Applications.* 4:205-215.

Bahador, S. D. and Cahyadi, J. H. (2009). Modelling of carbonation of PC and blended cement concrete. *The Institution of Engineers Singapore Journal*, 2:59-67.

Ballim, Y., Alexander, M. G., Beushausen, H. D. and Moyo, P. (2008). Reflections on future needs in concrete durability research and development. *Proceedings of the 2nd International Conference on Concrete Repair, Rehabilitation and Retrofitting (ICCRRR)*. Eds: M. G. Alexander, H.-D. Beushausen, F. Dehn and P. Moyo. 24-26 November 2008. Cape Town: South Africa. pp. 67-74.

Ballim, Y., Alexander, M. and Beushausen, H. (2009). Durability of concrete. In *Fulton's Concrete Technology*, 9th ed. Ed: G. Owens. Midrand, South Africa: Cement and Concrete Institute, pp. 155-188.

Bamforth, P. B. (1999). The derivation of input data for modeling chloride ingress from eight-year UK coastal exposure trials. *Magazine of Concrete Research*. 51(2):87-96.

Baroghel-Bouny, V., Kinomura, K., Thiery, M. and Moscardelli, S. (2011). Easy assessment of durability indicators for service life prediction or quality control of concretes with high volumes of supplementary cementitious materials. *Cement and Concrete Composites*. 33:832-847.

Baroghel-Bouny, V., Nguyen, T. Q. and Dangla, P. (2009). Assessment and prediction of RC structure service life by means of durability indicators and physical/chemical models. *Cement and Concrete Composites*. 31:522-534.

Basheer, L., Kropp, J. and Cleland, D. J. (2001). Assessment of the durability of concrete from its permeation properties: a review. *Construction and Building Materials*. 15:93-103.

Bentur, A. and Mitchell, D. (2008). Material performance lessons. *Cement and Concrete Research*. 38:259-272.

Bentz, D. P., Clifton, J. R., Ferraris, C. F. and Garboczi, E. J. (1999). Transport properties and durability of concrete: literature review and research plan. NISTIR 6395. Building and Fire Research Laboratory. Gaithersburg, Maryland.

Beushausen, H. and Alexander, M. G. (2008). The South African durability index tests in an international comparison. *Journal of the South African Institution of Civil Engineering.* 50(1):25-31.

Beushausen, H. and Alexander, M. (2009). Concrete repair. In *Fulton's Concrete Technology*, 9th ed. Ed: G. Owens. Midrand, South Africa: Cement and Concrete Institute, pp. 393-409.

Beushausen, H. and Chilwesa, M. (2013). Assessment and prediction of drying shrinkage cracking in bonded mortar overlays. *Cement and Concrete Research*. 53:256-266.

Bickley, J. A., Hooton, R. D. and Hover, K. C. (2006a). Performance specifications for durable concrete, current practice and limitations. *Concrete International.* Pp. 51-57.

Bickley, J., Hooton, R. D. and Hover, K. C. (2006b). Preparation of a performance-based specification for cast-in-place concrete. RMC Research Foundation.

Bjegovic, D., Serdar, M., Oslakovic, I. S., Jacobs, F., Beushausen, H., Andrade, C., Monteiro, A. V., Paulini, P. and Nanukuttan, S. (2015). Test methods for concrete durability indicators. In *RILEM TC 230-PSC, Performance-Based Specifications and Control of Concrete Durability*. Pp. 51-106.

Blagojevic, A., Fennis, S. and Walraven, J. C., (2012). Impact of cracks on chloride-induced corrosion and durability of reinforced concrete structures - a literature review. In: *Fifth International PhD Student Workshop on Durability of Reinforced Concrete*, Finland.

Boddy, A., Bentz, E., Thomas, M. D. A. and Hooton, R. D. (1999). An overview and sensitivity study of a multimechanistic chloride transport model. *Cement and Concrete Research*. 29:827-837.

British Standard (BS). (2005). BS-EN 1504-3 – *Products and systems for the protection and repair of concrete structures-Definitions, requirements, quality control and evaluation of conformity-Part 3: Structural and non-structural repair*. London: British Standards.

BS EN 206-1:2000. Concrete. Specification, performance, production and conformity. London: British Standards Institution, 2000.

Buenfeld, N. R., Shurafa-Daoudi, M.-T. and McLoughlin, I. M. (1997). Chloride transport due to wick action in concrete. In *Chloride Penetration into Concrete, Proceedings of the International RILEM Workshop*. Eds: L.-O. Nilsson and J. P. Ollivier. St-Remy-les-Chevreuse. Pp. 315-324.

Building Research Establishment (1998). Digest 434, Corrosion of reinforcement in concrete: electrochemical monitoring. In *Concrete Repair Manual*, 2nd ed. Eds: B. L. Schmick and A. Pollington. Pp. 431-442.

Caballero, J., Polder, R. B., Leegwater, G. A. and Fraaij, A. L. A. (2012). Chloride penetration into cementitious mortar at early age. *HERON*. 57(3):185-196.

Carcasses, M., Abbas, A., Ollivier, J. P. and Verdier, J. (2002). An optimised preconditioning procedure for gas permeability measurement. *Materials and Structures*. 35:22-27.

CEB-FIP Model Code 1990, Final Draft, (1991). CEB Bulletin d'Information pp. 203-205, Lausanne.

Cement and Concrete Institute (C&CI). (2009). Cementitious materials for concrete - standards, selection and properties. Midrand, South Africa: Cement and Concrete Institute.

Chang, C. and Chen, J. (2006). The experimental investigation of concrete carbonation depth. *Cement and Concrete Research*. 36:1760-1767.

Chilwesa, M. (2012). Assessing the age at cracking of concrete repair mortars/overlays subjected to restrained drying shrinkage. MSc Thesis, University of Cape Town.

Costa, A. and Appleton, J. (1999a). Chloride penetration into concrete in marine environment – Part I: Main parameters affecting chloride penetration. *Materials and Structures*. 32:252-259.

Costa, A. and Appleton, J. (1999b). Chloride penetration into concrete in marine environment – Part II: Prediction of long-term chloride penetration. *Materials and Structures*. 32:354-359.

Costa, A. and Appleton, J. (2001). Concrete carbonation and chloride penetration in a marine environment. *Concrete Science and Engineering*. 3:242-249.

Czarnecki, L. and Woyciechowski, P. (2015). Modelling of concrete carbonation; is it a process unlimited in time and restricted in space? *Bulletin of the Polish Academy of Sciences, Technical Sciences*. 63(1):43-54.

Decatoire, R., Larrard, T., Yalamas, T., Schoefs, F. and Elachachi, S. M. (2014). Stochastic evaluation of carbonation depth and predictions updating. *7th European Workshop on Structural Health Monitoring*. 8-11 July 2014. Nantes: France.

Decter, M. H. (1997). Durable concrete repair – importance of compatibility and low shrinkage. *Construction and Building Materials*. 11(5-6):267-273.

Delagrave, A., Bigas, J. P., Ollivier, J. P., Merchand, J. and Pigeon, M. (1997). Influence of the interfacial zone on the chloride diffusivity of mortars. *Advanced Cement Based Materials.* 5:86-92.

Dinku, A. and Reinhardt, H. W. (1997). Gas permeability coefficient of cover concrete as a performance control. *Materials and Structures*. 30:387-393.

Djerbi, A., Bonnet, S., Khelidj, A. and Baroghel-bouny, V., (2008). Influence of traversing crack on chloride diffusion into concrete. *Cement and Concrete Research*. 38:877-883.

DuraCrete (1998). Compliance testing for probabilistic design purposes – Evaluation report. Contract BRPR-CT95-0132, Project BE95-1347. Document BE95-1347/R7. The European Union – Brite EuRam III. Gouda, The Netherlands.

Garboczi, E. J. and Bentz, D. P. (1996). Modelling of the microstructure and transport properties of concrete. *Construction and Building Materials*. 10(5):293-300.

Gehlen, C. (2000). Probabilistische Lebensdauerbemessung von Stahlbetonbauwerken, Deutscher Ausschuss für Stahlbeton 510, Berlin.

Gergely, J., Bledsoe, J. E., Tempest, B. Q. and Szabo, I. F. (2006). Concrete diffusion coefficients and existing chloride exposure in North Carolina. North Carolina Department of Transportation, Research Project No. HWY-2004-12. Charlotte, USA: University of North Carolina at Charlotte.

Gjorv, O. E. (2009). *Durability design of concrete structures in severe environments*. London, UK: Taylor and Francis.

Glass, G. K. and Buenfeld, N. R. (2000). The influence of chloride binding on the chloride induced corrosion risk in reinforced concrete. *Corrosion Science*. 42:329-344.

Glass, G. K. (2003). Reinforcement corrosion. In *Advanced Concrete Technology, Concrete Properties*. Eds: J. Newman and B. S. Choo. Oxford, United Kingdom: Butterworth-Heinemann, pp. 9/1-9/27.

Grassl, P., Wong, H. S. and Buenfeld, N. R. (2010). Influence of aggregate size and volume fraction on shrinkage induced micro-cracking of concrete and mortar. *Cement and Concrete Research*. 40:85-93.

Grieve, G. (2009a). Cementitious materials. In *Fulton's Concrete Technology*, 9th ed. Ed: G. Owens. Midrand, South Africa: Cement and Concrete Institute, pp. 1-16.

Grieve, G. (2009b). Aggregates for concrete. In *Fulton's Concrete Technology*, 9th ed. Ed: G. Owens. Midrand, South Africa: Cement and Concrete Institute, pp. 25-54.

Grimmond, C. S. B. *et al*. (2002). Local-scale fluxes of carbon dioxide in urban environments: methodological challenges and results from Chicago. Environmental Pollution. 116:243-254.

Guneyisi, E., Gesoglu, M., Karaoglu, S. and Mermerdas, K. (2012). Strength, permeability and shrinkage cracking of silica fume and metakaolin concretes. *Construction and Building Materials*. 34:120-130.

Halamickova, P., Detwiler, R. J., Bentz, D. P. and Garboczi, E. J. (1995). Water permeability and chloride ion diffusion in Portland cement mortars: relationship to sand content and critical pore diameter. *Cement and Concrete Research*. 25(4):790-802.

Hamilton, H. R., Boyd, A. J. and Vivas, E. (2007). *Permeability of concrete - Comparison of conductivity and diffusion methods*. UF Project No. 00026899. Florida, USA: Engineering and Industrial Experiment Station, University of Florida.

Hassanein, N. M. (1997). The application of neutral networks to service life prediction of concrete structures. *PhD thesis*, Imperial College, London.

Hearn, N., Hooton, R. D. and Mills, R. H. (1994). Pore structure and permeability. In *ASTM STP 169C*. Philadelphia, U.S.A.: ASTM International, pp. 240-262.

Hearn, N. (1998). Self-sealing, autogenous healing and continued hydration: What is the difference? *Materials and Structures*. 31:563-567

Hearn, N., Hooton, R. D. and Nokken, M. R. (2006). Pore structure, permeability, and penetration resistance characteristics of concrete. In *ASTM STP 169D: Significance of tests and properties of concrete and concrete-making materials*. Eds: J. F. Lamond and J. H. Pielert. Philadelphia, U.S.A.: ASTM International, pp. 238-252.

Heiyantuduwa, R. and Alexander, M. G. (2009). Studies on prediction models for concrete durability. In *Concrete Repair, Rehabilitation and Retrofitting II*. Eds: Alexander *et al*.. London: Taylor and Francis Group. pp. 303-309.

Hong, K. and Hooton, R. D. (1999). Effects of cyclic chloride exposure on penetration of concrete cover. *Cement and Concrete Research*. 29:1379-1386.

Houst, Y. F. (1996). The role of moisture in the carbonation of cementitious materials. *Internationale Zeitschrift fur Bauintstandsetzen 2*. 1:49-66.

Hyde, G. W. and Smith, W. J. (1889). Results of experiments made to determine the permeability of cements and cement mortars. *Permeability of Cements, etc.* 128(3):199-207.

ICRI Technical Guidelines (1996). Guide for selecting and specifying materials for repair of concrete surfaces. Guideline No. 03733. In *Concrete Repair Manual*, 2nd ed. Eds: B. L. Schmick and A. Pollington. Pp. 835-868.

Idso, S. B., Idso, C. D. and Balling, R. C. (2002). Seasonal and diurnal variations of near-surface atmospheric CO_2 concentration within a residential sector of the urban CO_2 dome of Phoenix, AZ, USA. *Atmospheric Environment*. 36:1655-1660.

Itim, A., Ezziane, K. and Kadri, E. (2011). Compressive strength and shrinkage of mortar containing various amounts of mineral additions. *Construction and Building Materials*. 25:3603-3609.

Kellerman, J. (2009). Manufacture and handling of concrete. In *Fulton's Concrete Technology*, 9th ed. Ed: G. Owens. Midrand, South Africa: Cement and Concrete Institute, pp. 229-250.

Khunthongkeaw, J., Tangtermsirikul, S. and Leelawat, T. (2006). A study on carbonation depth prediction for fly ash concrete. *Concrete and Building Materials*. 20:744-753.

Kollek, J. J. (1989). The determination of the permeability of concrete to oxygen by the Cembureau method. A recommendation. *Materials and Structures.* 22:225-230.

Kovacs, T. (2000). Deterioration of reinforced concrete repair mortar layers. *Periodica Polytechnica Ser. Civ. Eng.* 44(2):197-206.

Kropp, J. (1995). Relations between transport characteristics and durability. In *Performance criteria for concrete durability*. Eds: J. Kropp and H. K. Hilsdorf. RILEM. Pp. 97-137.

Kropp, J. (1999a). concrete durability – an approach towards performance testing. *Materials and Structures*. 32:163-173.

Kropp, J. (1999b). Preconditioning of concrete test specimens for the measurement of gas permeability and capillary absorption of water. *Materials and Structures*. 32:174-179.

Kropp, J. (2005). Chlorides in concrete. In *RILEM Report 12: Performance Criteria for Concrete Durability*. Eds: J. Kropp and H. K. Hilsdorf. London, United Kingdom: E & FN Spon.

Kropp, J. and Alexander, M. (2007). Transport mechanisms and reference tests. In *RILEM Report 40: Non-destructive evaluation of the penetrability and thickness of the concrete cover*. Eds: R. Torrent and L. F. Luco. RILEM Publications S.A.R.L, pp. 13-34.

Kubens, S., Wasserman, A. and Bentur, A. (2003). Non destructive air permeability tests to assess the performance of the concrete cover. *Internationalen Baustofftagung ibausil, 24*. 27 September 2003, pp.1231-1238.

Lafhaj, Z., Goueygou, M.,Djerbi, A. and Kaczmarek, M. (2006). Correlation between porosity, permeability and ultrasonic parameters of mortar with variable water/cement ratio and water content. *Cement and Concrete Research.* 36:625-633.

Lambert, P., Page G. L. and Vassie P. R. (1991). Investigations of reinforcement corrosion, Electrochemical monitoring of steel in chloride-contaminated concrete. *Materials and Structures*. 24:351-358.

Life-365 Service Life Prediction Model™ and computer program for predicting the service life and life-cycle costs of reinforced concrete exposed to chlorides. (2008).

Lindvall, A. (2000). Probabilistic, performance based service life design of concrete structures – environmental actions and response. In *RILEM Report 19: Testing and Modelling the Chloride Ingress into Concrete*. Eds: C. Andrade and J. Kropp. RILEM Publications S.A.R.L, pp. 277-289.

Loser, R., Lothenbach, B., Leemann, A. and Tuchschmid, M. (2010). Chloride resistance of concrete and its binding capacity – Comparison between experimental results and thermodynamic modelling. *Cement and Concrete Composites*. 32:34-42.

Luco, L. F., Fischli, M. and Podvoiskis, J. (2007). Transport mechanisms and reference tests. In *RILEM Report 40: Non-destructive evaluation of the penetrability and thickness of the concrete cover*. Eds: R. Torrent and L. F. Luco. RILEM Publications S.A.R.L, pp. 133-155.

Luo, R., Cai, Y., Wang, C. and Huang, X. (2003). Study of chloride binding and diffusion in GGBS concrete. *Cement and Concrete Research*. 33:1-7.

Luping, T. and Gulikers, J. (2007). On the mathematics of time-dependent apparent chloride diffusion coefficient in concrete. *Cement and Concrete Research*. 37:589-595.

Maage, J., Helland, M., Poulsen, E., Vennesland, O. and Carlsen, J. E. (1996). Service life prediction of existing structures exposed to marine environment. *ACI Material Journal*. 93(6):602-608.

Maage, M., Helland, S. and Carlsen, J. E. (1999). Chloride penetration into concrete with lightweight aggregates. Brite EuRam project BE96-3942. AK Gouda, The Netherlands.

Mackechnie, J. R. and Alexander, M. G. (2002). Durability predictions using early-age durability index testing. University of Cape Town.

Mackechnie, J. R. and Alexander, M. G. (2004). Rapid assessment of chloride resistance of concrete using the chloride conductivity test. *The Indian Concrete Journal*.

Mangat, P. S. and Molloy, B. T. (1994). Prediction of long-term chloride concentration in concrete. *Ibid*. 27:338-346.

Marsavina, L., Audenaert, K., Schutter, G., Faur, N. and Marsavina, D. (2009). Experimental and numerical determination of the chloride penetration in cracked concrete. *Construction and Building Materials*. 23:264-274.

Marsh, B. (2003a). Curing. In *Advanced Concrete Technology, Concrete Properties*. Eds: J. Newman and B. S. Choo. Oxford, United Kingdom: Butterworth-Heinemann, pp. 3/1-3/15.

Marsh, B. (2003b). Specification and achievement of cover to reinforcement. In *Advanced Concrete Technology, Concrete Properties*. Eds: J. Newman and B. S. Choo. Oxford, United Kingdom: Butterworth-Heinemann, pp. 14/1-14/9.

Martin-Perez, B. (1999). *Service life modelling of RC highway structures exposed to chlorides*. PhD Thesis. University of Toronto.

Martin-Perez, B., Zibara, H., Hooton, R. D. and Thomas, M. D. A. (2000). A study of the effect of chloride binding on service life predictions. *Cement and Concrete Research*. 30:1215-1223.

Martys, N. S. and Ferraris, C. F. (1997). Capillary transport in mortars and concrete. *Cement and Concrete Research*. 27(5):747-760.

Masuku, C. (2009). Tensile relaxation of bonded concrete overlays. MSc Dissertation. University of Cape Town.

Mehta, P. K. and Monteiro, P. J. M. (2006). *Concrete microstructure, properties and materials*, 3rd ed. USA: McGraw-Hill.

Miyagawa, T. (1991). Durability design and repair of concrete structures: chloride corrosion of reinforcing steel and alkali-aggregate reaction. *Magazine of Concrete Research*. 43(156):155-170.

Nilsson, L.-O. (2003). Durability concept; pore structure and transport processes. In *Advanced Concrete Technology, Concrete Properties*. Eds: J. Newman and B. S. Choo. Oxford, United Kingdom: Butterworth-Heinemann, pp. 8/3-8/29.

Nilsson, L.-O. (2009). Models for chloride ingress into concrete – from Collepardi to today. *International Journal of Modelling, Identification and Control*. 7(2):129-134.

Nokken, M., Boddy, A, Hooton, R. D. and Thomas, M. D. A. (2006). Time dependent diffusion in concrete – three laboratory studies. *Cement and Concrete Research.* 36: 200-207.

NordTest, (1984). NTBuild 208: *Concrete, hardened: chloride content*. 2nd ed. NORDTEST. Espoo, Finland.

NordTest, (1989). NTBuild 357: *Concrete, repairing materials and protective coating: Carbonation resistance*. NORDTEST. Espoo, Finland.

NordTest, (1995). NTBuild 443: *Concrete, hardened: Accelerated chloride penetration*. NORDTEST. Espoo, Finland.

O'Brien, F. E. M. (1947). The control of humidity by saturated salt solutions. *British Electrical and Allied Industries Research Association*. London, United Kingdom.

Oh, B. H. and Jang, S. Y. (2007). Effects of material and environmental parameters on chloride penetration profiles in concrete structures. *Cement and Concrete Research*. 37:47-53.

Otieno, M. B., Alexander, M. G. and Beushausen, H.-D., (2009). Corrosion propagation in cracked and uncracked concrete. In *Concrete Repair, Rehabilitation and Retrofitting II.* Eds: Alexander *et al*., London, United Kingdom: Taylor and Francis. pp. 339-344.

Otieno, M., Beushausen, H. and Alexander, M. (2012). Prediction of corrosion rate in reinforced concrete structures – a critical review and preliminary results. *Materials and Corrosion*. 63(9):777-790.

Pacheco-Torgal, F., Abdollahnejad, Z., Miraldo, S., Baklouti, S. and Ding, Y. (2012). An overview on the potential of geopolymers for concrete infrastructure rehabilitation. *Construction and Building Materials*. 36:1053-1058.

Pack, S., Jung, M., Song, H., Kim, S. and Ann, Y. (2010). Prediction of time dependent chloride transport in concrete structures exposed to a marine environment. *Cement and Concrete Research*. 40:302-312.

Papadakis, V. G., Vayenas, C. G. and Fardis, M. N. (1991). Fundamental modelling and experimental investigation of concrete carbonation. *ACI Materials Journal*. 88(4):363-373.

Papadakis, V. G. (2000). Effect of supplementary cementing materials on concrete resistance against carbonation and chloride ingress. *Cement and Concrete Research*. 30:291-299.

Papadakis, V. G. and Tsimas, S. (2002). Supplementary cementing materials in concrete. Part I: efficiency and design. *Cement and Concrete Research*. 32:1525-1532.

Pease, J. B., (2010). Influence of concrete cracking on ingress and reinforcement corrosion. *PhD Thesis*, Technical University of Denmark.

Penttala, V. (2009). Causes and mechanisms of deterioration in reinforced concrete. In *Failure, distress and repair of concrete structures*. Ed: N. Delatte. Cambridge, United Kingdom: Woodhead Publishing Limited, pp. 3-31.

Polder, R., Andrade, C., Elsener, B., Vennesland, O., Gulikers, J., Weidert, R. and Raupach, M. (2000). Test methods for on-site measurement of resistivity of concrete. *Materials and Structures*. 33:603-611.

Polder, R. B. (2001). Test methods for on-site measurement of resistivity of concrete – A RILEM TC-154 technical recommendation. *Construction and Building Materials*. 15:125-131.

Polder, R. B. and Rooij, M. R. (2005). Durability of marine concrete structures – field investigations and modelling. *HERON*. 50(3):133-153.

Poulsen, E. (1995). Chloride profiles, analysis and interpretation of observations. AEC laboratory, 20 Staktoften. DK-2850 Vedbæk, Denmark.

Poursaee, A. and Hansson, C. M., (2008). The influence of longitudinal cracks on the corrosion protection afforded reinforcing steel in high performance concrete. *Cement and Concrete Research*. 38:1098-1105.

Rao, G. A. (1998). Influence of silica fume replacement of cement on expansion and drying shrinkage. *Cement and Concrete Research*. 28(10):1505-1509.

Raupach, M. (2006). Concrete repair according to the new European standard EN 1504. RWTH, Aachen ibac.

Richardson, M. G. (2002). *Fundamentals of durable concrete, modern concrete technology*. London, United Kingdom: Spon Press.

RILEM TC 116-PCD: Permeability of concrete as a criterion of its durability. *Materials and Structures*. 32:174-179.

RILEM recommendations TC56-MHM: Hydrocarbon Materials. (1988). CPC-18 Measurement of hardened concrete carbonation depth.

Rooij, M. R. and Polder, R. B. (2005). Durability of marine concrete structures. *CUR Report 215*.

Rooij, M. R., Polder, R. B. and Oosten, H. H. (2007). Validation of service life performance of in situ concrete by TEM and RCM measurements. *HERON*. 52(4):225-238.

Roziere, E., Loukili, A. and Cussigh, F. (2009). A performance based approach for durability of concrete exposed to carbonation. *Construction and Building Materials*. 23:190-199.

Russell, D., Basheer, P. A. M., Rankin, G. I. B. and Long, A. E. (2001). Effect of relative humidity and air permeability on prediction of the rate of carbonation of concrete. *Proceedings of the Institution of Civil Engineers – Structures & Building 146.* 3:319-326.

Safehian, M. and Ramezanianpour, A. A. (2013). Assessment of service life models for determination of chloride penetration into silica fume concrete in the severe marine environmental condition. *Construction and Building Materials.* 48:287-294.

Savija, B. (2014). Experimental and numerical investigation of chloride ingress in cracked concrete. *PhD Thesis*. Technische Universiteit Delft.

Scott, A. N. (2004). The influence of binder type and cracking on reinforcing steel corrosion in concrete. *PhD Thesis*. University of Cape Town.

Shukla, K. N. and Pillai, R. G. (2015). Modelling of chloride diffusion coefficient in concrete with supplementary cementitious materials. *Proceedings of the 4th International Conference on Concrete Repair, Rehabilitation and Retrofitting (ICCRRR 2015)*. Eds: F. Dehn, H.-D. Beushausen, M. G. Alexander and P. Moyo. 5-7 October 2015. Leipzig: Germany. pp. 83-90.

Sisomphon, K. and Franke, L. (2007). Carbonation rates of concretes containing high volume of pozzolanic materials. *Cement and Concrete Research.* 37:1647-1653.

South African National Standards. SANS 5863:2006. Concrete tests-compressive strength of hardened concrete. Pretoria: South African Bureau of Standards.

Saraswathy, V. and Song, H. (2008). Evaluation of cementitious repair mortars for corrosion resistance. *Portugaliae Electrochimica Acta*. 26(5):417-432.

Sika South Africa (Pty) Ltd. (2010). Product Data Sheet: *Sikacrete-214*. 6th edition. Version no. 01.10. South Africa.

Sika South Africa (Pty) Ltd. (2012a). Product Data Sheet: *Sika MonoTop-612*. 21/02/2012 edition. Identification no.: 010302040010000004. South Africa.

Sika South Africa (Pty) Ltd. (2012b). Product Data Sheet: *Sika MonoTop-615HB*. 21/02/2012 edition. Identification no.: 010302040010000033. South Africa.

Sika South Africa (Pty) Ltd. (2012c). Product Data Sheet: *SikaRep LW*. 21/02/2012 edition. Identification no.: 010302020010000027. South Africa.

Stanish, K. D., Hooton, R. D. and Thomas, M. D. A. (2000). Testing the chloride penetration resistance of concrete: a literature review. FHWA Contract DTFH61-97-R-00022. University of Toronto, Ontario, Canada.

Stanish, K. and Thomas, M. (2003). The use of bulk diffusion tests to establish time-dependent concrete chloride diffusion coefficients. *Cement and Concrete Research*. 33:55-62.

Streicher, P. E. and Alexander, M. G. (1995). A chloride conduction test for concrete. *Cement and Concrete Research*. 25(6):1284-1294.

Swamy, R. N., Hamada, H. and Laiw, J. C. (1994). Acritical evaluation of chloride penetration into concrete in marine environment. In *Corrosion and Corrosion Protection of Steel in Concrete, Proceedings of an International Conference*. University of Sheffield, England. Pp. 404-419.

Tamimi, A. K., Abdalla, J. A. and Sakka, Z. I. (2008). Prediction of long term chloride diffusion of concrete in harsh environment. *Construction and Building Materials*. 22:829-836.

Tang, L. and Nilsson, L.-O. (1993). Chloride binding capacity and binding isotherms of OPC pastes and mortars. *Cement and Concrete Research*. 23:247-259.

Tang, L. and Nilsson, L.-O. (1995). A new approach to the determination of pore distribution by penetrating chlorides into concrete. *Cement and Concrete Research*. 25(4):695-701.

Tang, L. and Nilsson, L.-O. (2000). Current development and verification of the numerical model ClinConc for predicting chloride penetration into concrete. In *RILEM Report 19: Testing and modelling the chloride ingress into concrete*. Eds: C. Andrade and J. Kropp. RILEM Publications S.A.R.L, pp. 305-316.

Tang, L. (2007). Service life modelling. In *RILEM Report 38: Durability of self-compacting concreter*. Eds: G. De Schutter and K. Audenaert. RILEM Publications S.A.R.L, pp. 163-172.

Tang, L. (2008). Engineering expression of the ClinConc model for prediction of free and total chloride ingress in submerged marine concrete. *Cement and Concrete Research*. 38:1092-1097.

Tang, L. and Sørensen, H. E. (2001). Precision of the Nordic test methods for measuring the chloride diffusion/migration coefficients of concrete. *Materials and Structures*. 34:479-485.

Tang, S. W., Yao, Y., Andrade, C. and Li, Z. J. (2015). Recent durability studies on concrete structure. *Cement and Concrete Research*. 78:143-154.

Teply, B., Chroma, M. and Rovnanik, P. (2010). Durability assessment of concrete structures: reinforcement depassivation due to carbonation. *Structure and Infrastructure Engineering*. 6(3):317-327.

Theodosiou, G. (2009). Reinforcement. In *Fulton's Concrete Technology*, 9th ed. Ed: G. Owens. Midrand, South Africa: Cement and Concrete Institute, pp. 265-272.

Thiery, M., Villain, G., Dangla, P. and Platret, G. (2007). Investigation of the carbonation front shape on cementitious materials: Effects of the chemical kinetics. *Cement and Concrete Research*. 37:1047-1058.

Thiery, M., Baroghel-Bouny, V. and Cremona, C. (2008). An engineering approach to the problem of natural carbonation accompanied by drying-wetting cycles. *International RILEM Symposium on Concrete Modelling –CONMOD'08.* 26-28 May 2008. Delft, Netherlands.

Thomas, M. D. A. and Bentz, E. C. (2001). Life 365: Computer program for predicting the service life and life-cycle costs of reinforced concrete exposed to chlorides. American Concrete Institute, Committee 365, Service life prediction. Detroit, Michigan.

Thomas, M. D. A. and Skalny, J. (2006). Chemical resistance of concrete. In *ASTM STP 169D: Significance of tests and properties of concrete and concrete-making materials.* Eds: J. F. Lamond and J. H. Pielert. Philadelphia, U.S.A.: ASTM International, pp. 253-273.

Torrent, R., Alexander, M. and Kropp, J. (2007a). Introduction and problem statement. In *RILEM Report 40: Non-destructive evaluation of the penetrability and thickness of the concrete cover*. Eds: R. Torrent and L. F. Luco. RILEM Publications S.A.R.L, pp. 1-11.

Torrent, R., Basheer, M. and Goncalves, A. F. (2007b). Non-destructive methods to measure gas permeability. In *RILEM Report 40: Non-destructive evaluation of the penetrability and thickness of the concrete cover*. Eds: R. Torrent and L. F. Luco. RILEM Publications S.A.R.L, pp. 35-70.

Torrent, R., Denarie, E., Jacobs, F., Leemann, A. and Teruzzi, T. (2012). Specification and site control of the permeability of the cover concrete: The Swiss approach. *Materials and Corrosion.* 63(12):1127-1133.

Trejo, D. and Pillai, R. G. (2003). Accelerated chloride threshold testing: Part I - ASTM A-615 and A-706 reinforcement, *ACI Materials Journal*, 100(6):519-527.

University of Cape Town and University of the Witwatersrand, (2010). Durability Index Testing Procedure Manual. Ver. 2.0.

Vanier, D. J. (2001). Why industry needs asset management tools. *Journal of Computing in Civil Engineering*. 15(1):35-43.

Vaysburd, A. M., Carino, N. J. and Bissonette, B. (2000). Predicting the performance of concrete repair materials. In *Summary of Repair Workshop*. April 26-27, 1999. New Hampshire.

Visser, J. H. M. and Polder, R. B. (2006). Concrete binder performance evaluation in service life design. In *ConcreteLife'06 – International RILEM-JCI Seminar on Concrete Durability and Service Life Planning: Curing, Crack Control, Performance in Harsh Environments*. March 2006, Israel. Pp 14-16.

Walraven, J. C. (2008). Design for service life: How should it be implemented in future codes. *Proceedings of the 2nd International Conference on Concrete Repair, Rehabilitation and Retrofitting (ICCRRR)*. Eds: M. G. Alexander, H.-D. Beushausen, F. Dehn and P. Moyo. 24-26 November 2008. Cape Town: South Africa. pp. 3-10.

Webb, S. W. and Pruess, K. (2003). The use of Fick's Law for modelling trace gas diffusion in porous media. *Transport in Porous Media*. 51:327-341.

Wegen, G., Polder, R. B. and Breugel, K. (2012). A guideline for service life design of structural concrete – A performance based approach with regard to chloride induced corrosion. *HERON*. 57(3):153-167.

Westerdahl, D. *et al*. (2005). Mobile platform measurements of ultrafine particles and associated pollutant concentrations on freeways and residential streets in Los Angeles. *Atmospheric Environment*. 39:3597-3610.

Wong, H. S., Zobel, M., Buenfeld, N. R. and Zimmerman, R. W. (2009). Influence of the interfacial transition zone and microcracking on the diffusivity, permeability and sorptivity of cement-based materials after drying. *Magazine of Concrete Research*. 61(8):571-589.

Yang, C. C. and Cho, S. W. (2003). An electrochemical method for accelerated chloride migration test of diffusion coefficient in cement-based materials. *Materials Chemistry and Physics*. 81:116-125.

Zibara, H. (2001). *Binding of external chlorides by cement paste*. PhD Thesis. University of Toronto.

Appendix A: Experimental results

Detailed results of the experiments performed in this investigation are presented in this section.

A.1 Grading curves for fine aggregate

Figure A.1 and Figure A.2 show the grading curves of Philippi dune sand and crusher sand respectively. The two aggregates were mixed at 50/50.

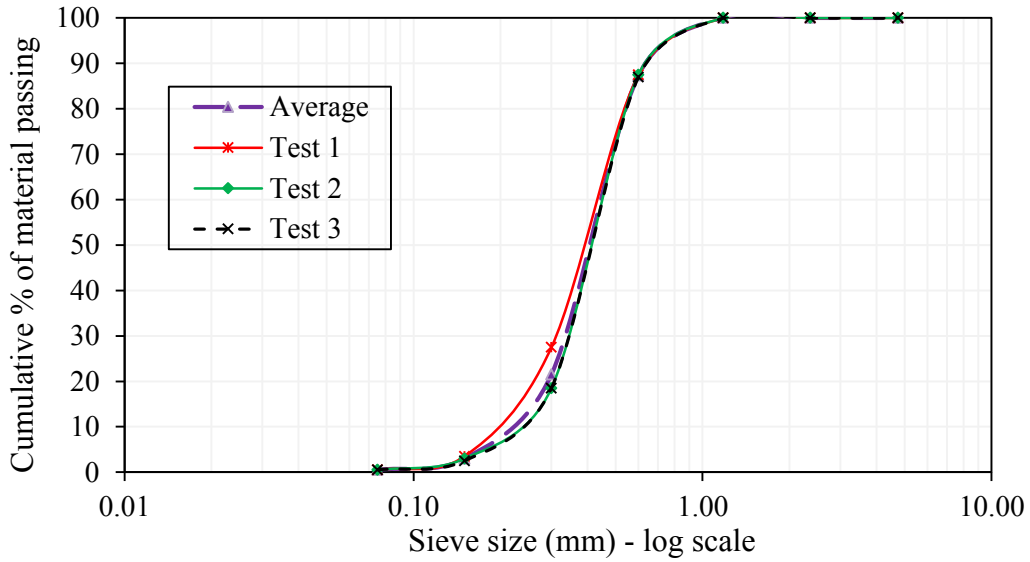

Figure A.1: Grading curve of Philippi dune sand

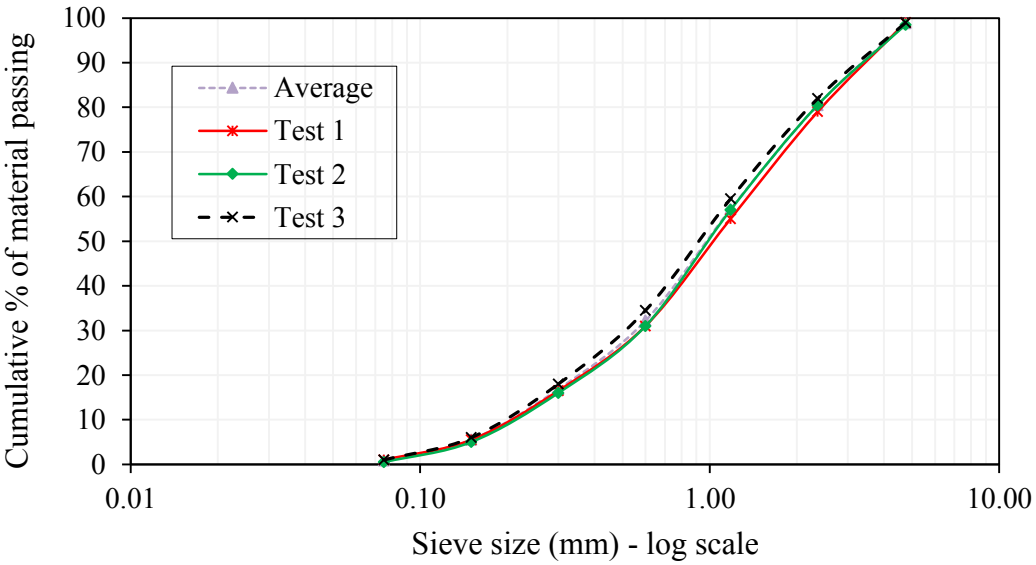

Figure A.2: Grading curve of crusher sand

A.2 Compressive strength results

Table A.1 shows the density and compressive strength of the mixes after 7 and 28 days of curing in water bath at 23 ± 2 °C. A summary of the results of compressive strength is presented in Figure A.3.

Table A.1: Compressive strength test results

Mix ID	Age (days)	Average*		Std. Dev.
		Density (kg/m³)	Strength (MPa)	
PM45	7	2211.7	46.1	0.3
	28	2208.3	53.2	1.0
PM60	7	2188.3	33.3	0.3
	28	2208.3	42.7	0.7
SM45	7	2220.0	30.8	0.4
	28	2236.7	52.7	1.0
SM60	7	2211.7	17.3	0.3
	28	2215.0	32.2	0.4
CM1	7	2020.0	11.3	0.3
	28	2010.0	38.7	0.6
CM2	7	1801.7	12.2	0.2
	28	1805.0	36.2	0.5
CM3	7	1853.3	10.8	0.4
	28	1856.7	44.8	1.2
CM4	7	2251.7	25.7	0.2
	28	2268.3	82.8	0.9

**Average denotes the arithmetic mean of 3individual readings*

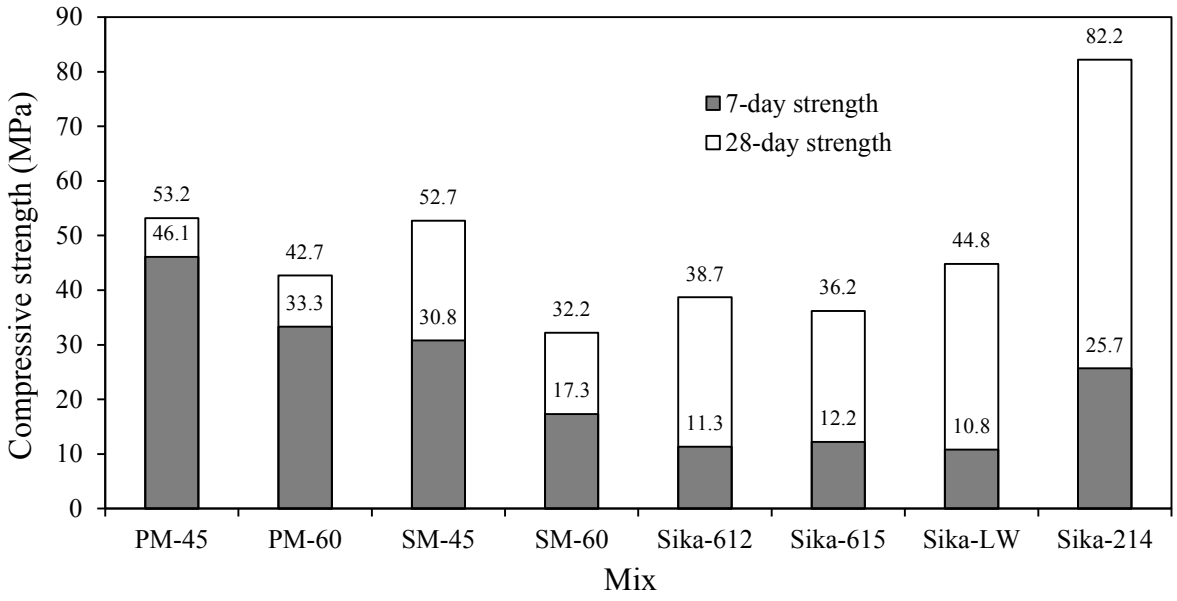

Figure A.3: 7-day and 28-day compressive strength results

A.3 Chloride conductivity test results

Table A.2: Chloride conductivity values of the mortar mixes

Mix ID	Dry cured	Moist cured
PM45	2.53	2.30
PM60	3.78	3.69
SM45	1.78	0.63
SM60	3.93	1.78
CM1	1.80	1.28
CM2	1.89	1.66
CM3	2.27	1.19
CM4	0.91	0.73

A.4 Bulk diffusion test results

Figure A.4 to Figure A.7 present the chloride profiles for the mortar mixes. Chloride content in laboratory-made mixes are expressed in chlorides by mass of binder while in commercial mortars it is expressed in chlorides by mass of mortar.

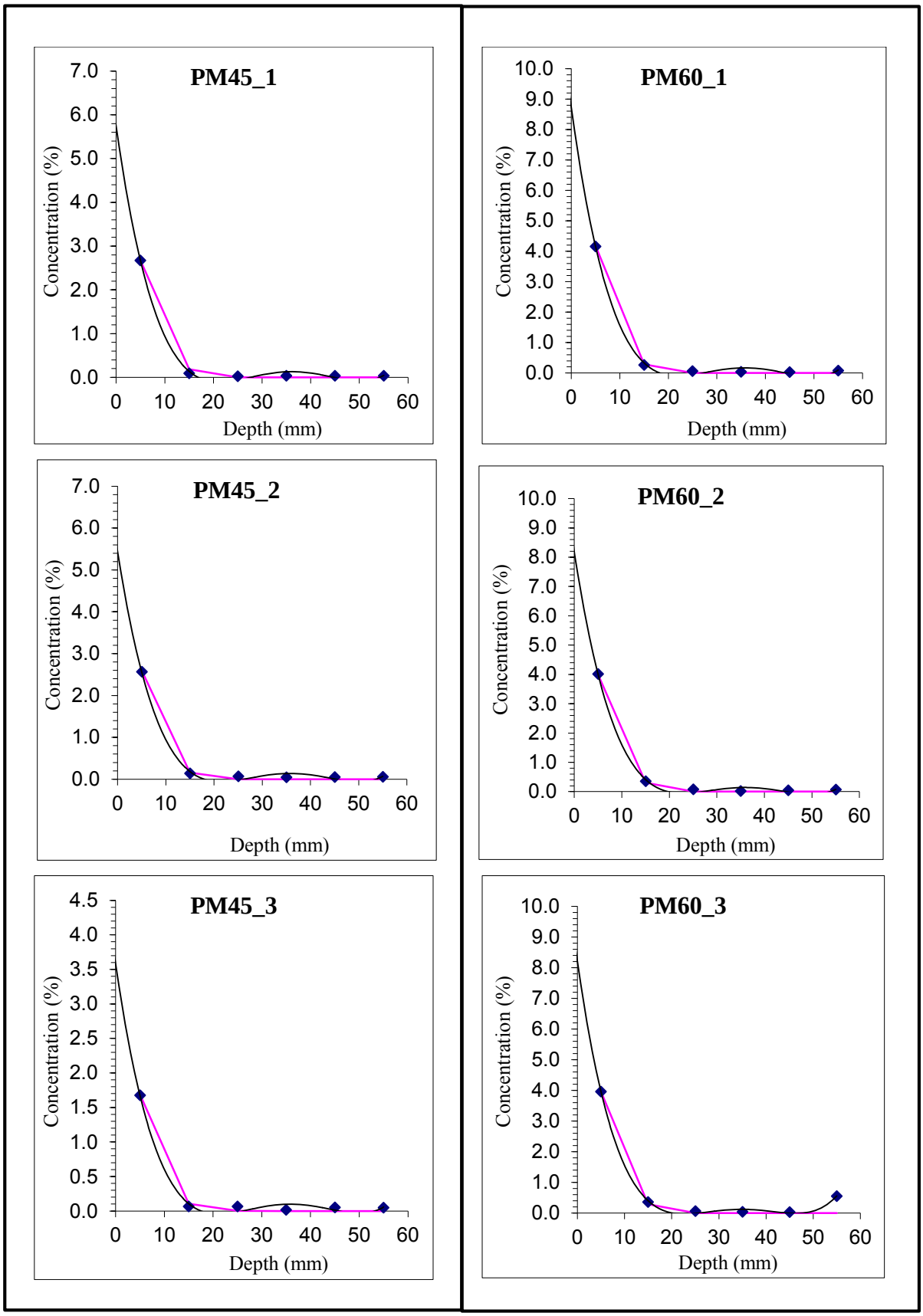

Figure A.4: Chloride profiles for (a) PM45 specimens and (b) PM60 specimens

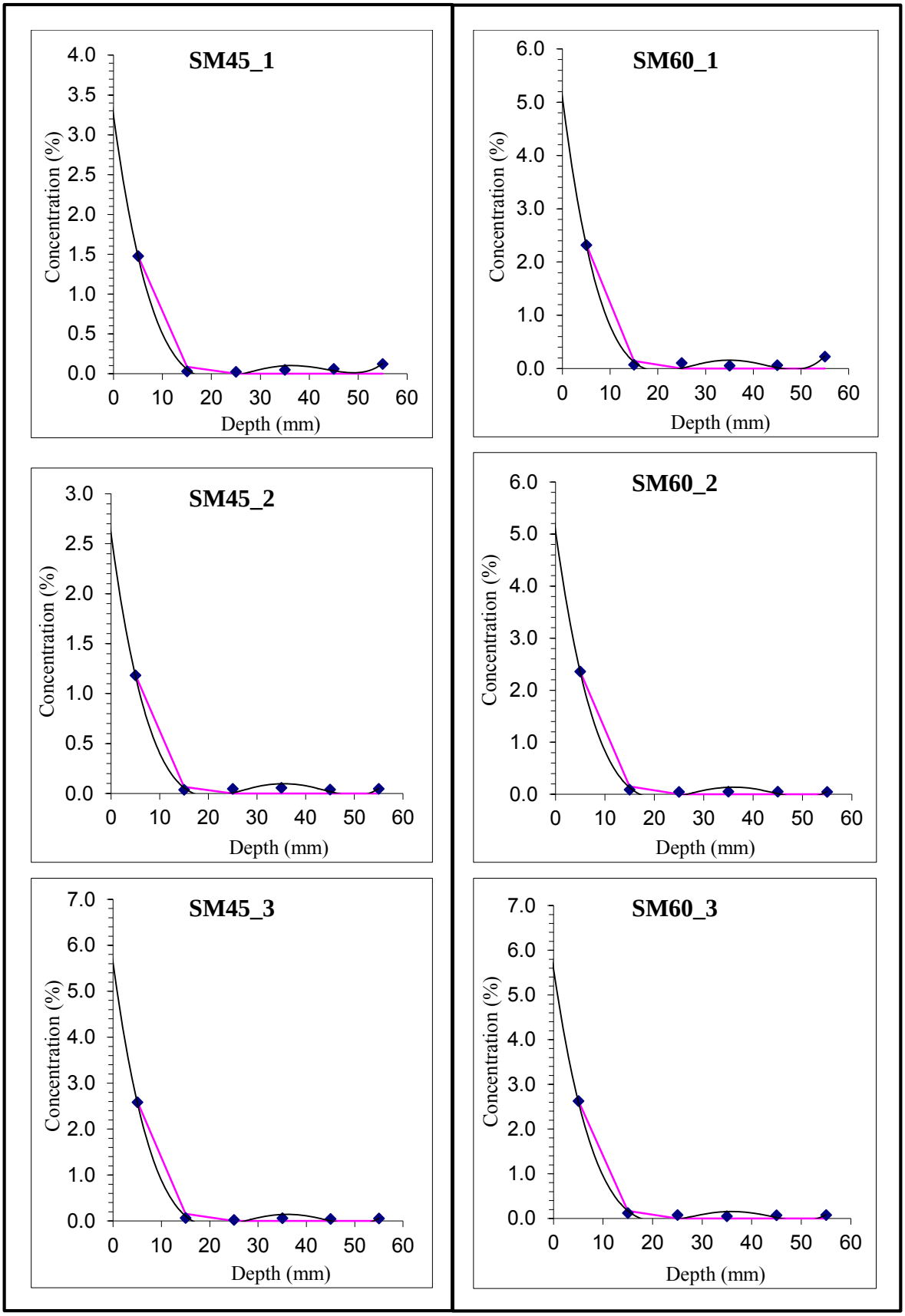

Figure A.5: Chloride profiles for (a) SM45 specimens and, (b) SM60 specimens

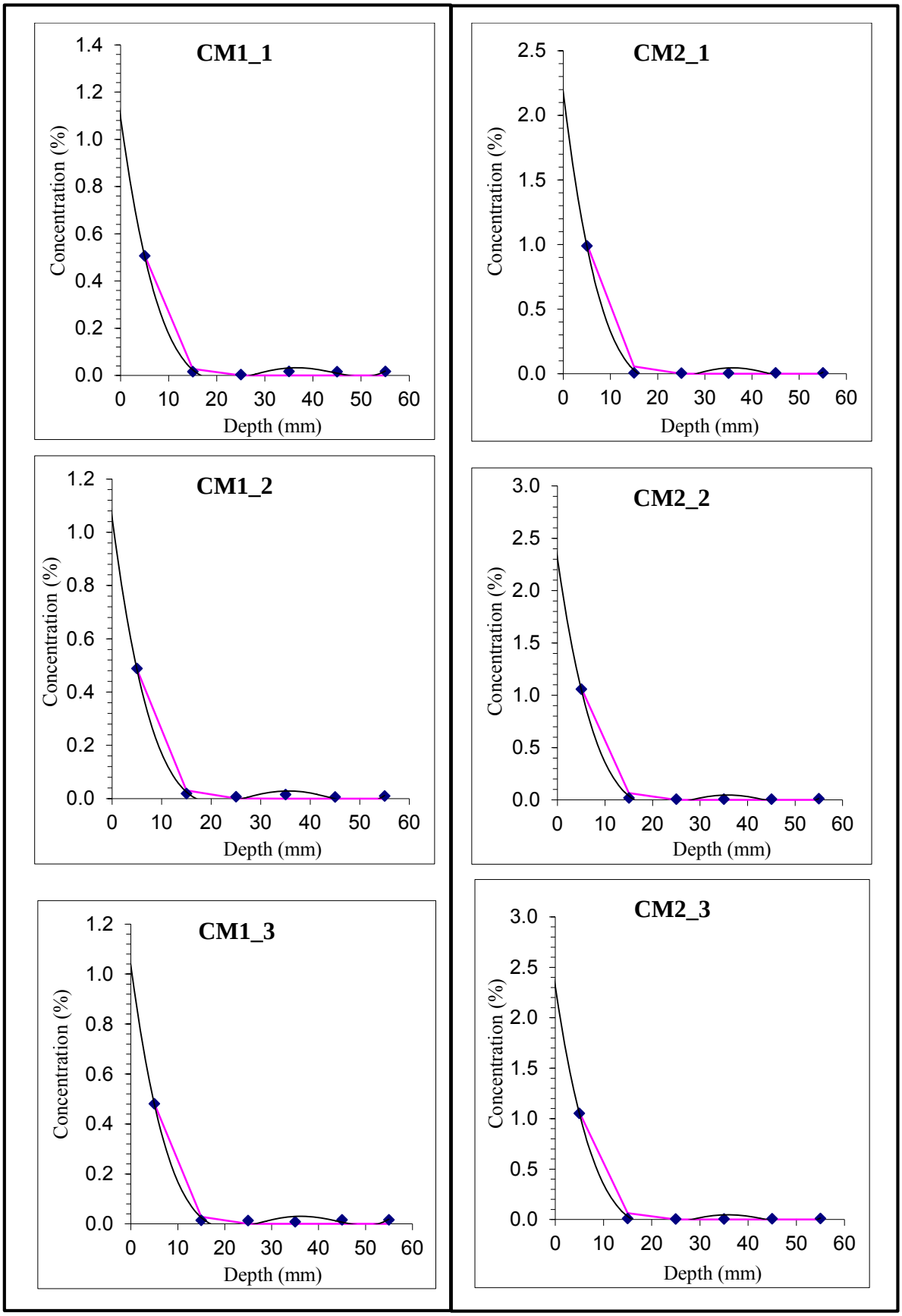

Figure A.6: Chloride profiles for (a) CM1 specimens and, (b) CM2 specimens specimens

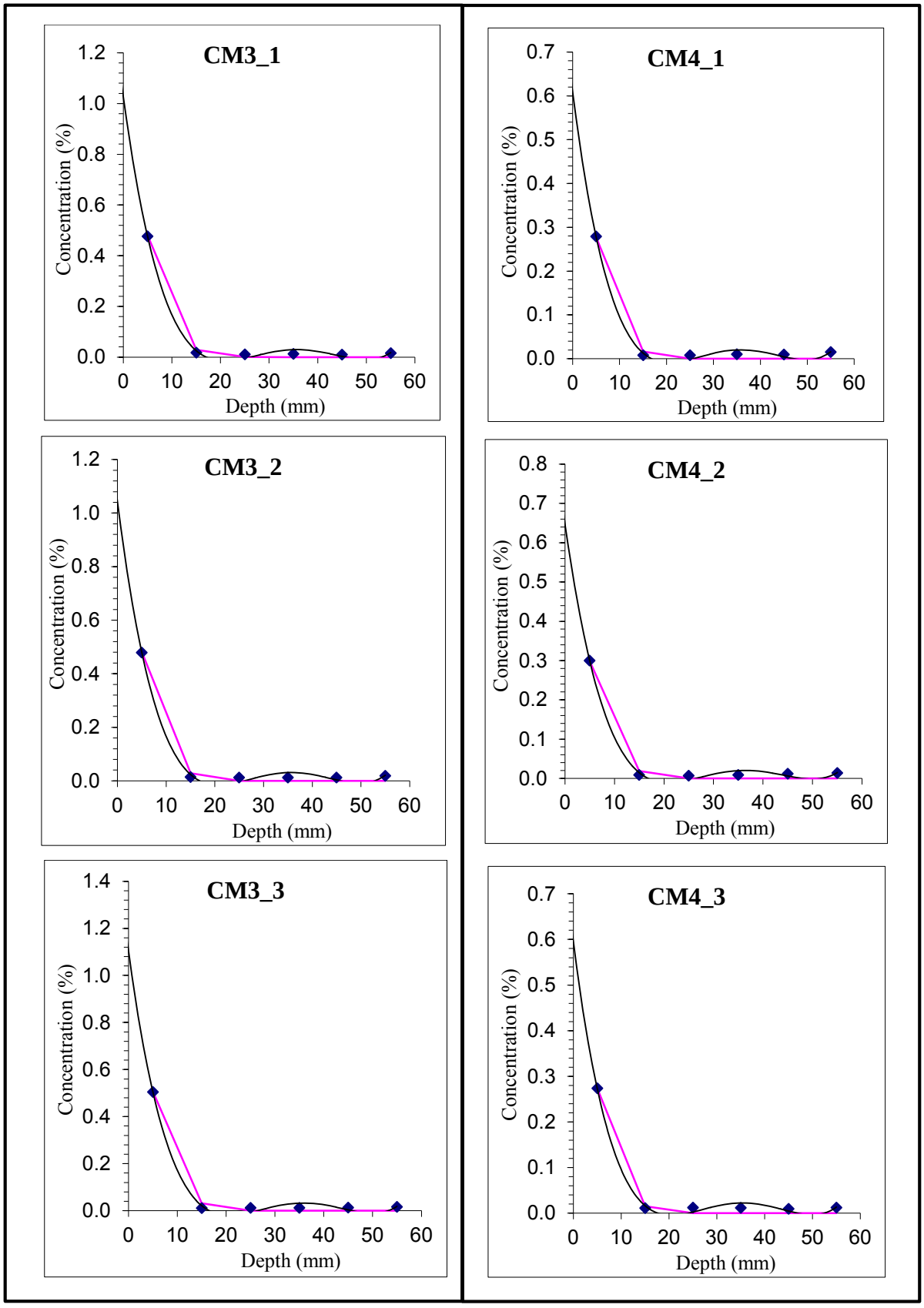

Figure A.7: Chloride profiles for (a) CM3 specimens and, (b) CM4 specimens

A.5 Accelerated carbonation test results

Table A.3 and A.4 presents the results of carbonation depth measurement in the laboratory-made and the commercial mortar mixes respectively.

Table A.3: Carbonation depth measurements of the laboratory-made mortar mixes after 12 weeks of exposure in the carbonation chamber.

Mix	Curing regime	Sample No.	12 weeks carbonation depth (mm)						
			1	2	3	4	Avg1	Avg2	Std.dev.
PM45	Dry	1	7.5	8.0	6.5	7.5	7.4	**7.2**	**0.2**
		2	8.0	7.0	7.0	6.5	7.1		
		3	8.0	6.0	6.5	7.5	7.0		
	Moist	1	5.0	4.5	4.5	6.0	5.0	**4.9**	**0.1**
		2	4.5	5.0	4.5	6.0	5.0		
		3	4.5	5.0	5.0	4.5	4.8		
PM60	Dry	1	15.0	14.5	14.0	15.5	14.8	**13.7**	**0.9**
		2	13.0	11.5	14.0	13.5	13.0		
		3	12.5	15.0	13.0	12.5	13.3		
	Moist	1	8.5	8.0	6.5	9.5	8.1	**8.2**	**0.6**
		2	8.5	8.0	7.5	6.5	7.6		
		3	8.5	9.0	8.0	10.0	8.9		
SM45	Dry	1	20.5	21.5	20.0	19.5	20.4	**20.2**	**0.6**
		2	20.0	18.5	19.5	20.0	19.5		
		3	20.5	20.0	21.5	20.5	20.6		
	Moist	1	11.0	10.0	9.0	9.5	9.9	**8.5**	**1.2**
		2	8.0	7.5	8.5	7.0	7.8		
		3	8.5	8.0	8.0	7.5	8.0		
SM60	Dry	1	34.5	35.5	36.0	36.5	35.6	**34.4**	**1.2**
		2	33.0	32.0	33.5	34.5	33.3		
		3	34.5	33.5	34.0	35.0	34.3		
	Moist	1	14.5	15.0	15.0	15.5	15.0	**15.4**	**0.4**
		2	15.5	16.0	16.5	15.5	15.9		
		3	16.0	15.0	15.5	15.0	15.4		

Table A.4: Carbonation depth measurements of the commercial mortar mixes after 12 weeks of exposure in the carbonation chamber.

Mix	Curing regime	Sample No.	12 weeks carbonation depth (mm)						
			1	2	3	4	Avg1	Avg 2	SD
CM1	Dry	1	15.5	16.0	17.0	17.0	16.4	**15.5**	**0.9**
		2	15.5	14.5	12.5	15.5	14.5		
		3	15.5	15.0	16.5	15.5	15.6		
	Moist	1	11.5	13.0	11.5	9.0	11.3	**11.0**	**0.4**
		2	11.0	9.5	12.5	9.0	10.5		
		3	11.0	9.0	13.0	11.5	11.1		
CM2	Dry	1	9.0	8.0	8.0	9.0	8.5	**8.1**	**0.5**
		2	7.5	8.0	9.0	8.5	8.3		
		3	7.0	8.0	8.5	7.0	7.6		
	Moist	1	4.0	3.0	3.5	3.0	3.4	**3.5**	**0.1**
		2	3.5	3.0	4.5	3.5	3.6		
		3	4.0	3.0	3.5	3.0	3.4		
CM3	Dry	1	32.5	29.0	29.5	35.0	31.5	**29.9**	**1.4**
		2	26.0	31.0	26.5	33.5	29.3		
		3	30.0	28.0	28.5	29.0	28.9		
	Moist	1	12.0	12.5	14.0	13.0	12.9	**12.5**	**0.4**
		2	12.0	12.5	13.0	12.5	12.5		
		3	11.5	12.5	13.5	11.0	12.1		
CM4	Dry	1	3.0	2.5	3.5	3.5	3.1	**3.0**	**0.2**
		2	3.0	3.0	2.5	3.5	3.0		
		3	3.0	2.5	3.0	2.5	2.8		
	Moist	1	0.0	0.0	0.0	0.0	0.0	**0.0**	**0.0**
		2	0.0	0.0	0.0	0.0	0.0		
		3	0.0	0.0	0.0	0.0	0.0		

Table A.5: Carbonation coefficients of the mortar mixes

Mix	Carbonation depth (mm)	Std. dev. of depth	Carbonation coeff. (mm/√day)
PM45_D*	7.2	0.2	0.786
PM45_M**	4.9	0.1	0.535
PM60_D	13.7	0.9	1.495
PM60_M	8.2	0.6	0.895
SM45_D	20.2	0.6	2.204
SM45_M	8.5	1.2	0.927
SM60_D	34.4	1.2	3.753
SM60_M	15.4	0.4	1.680
CM1_D	15.5	0.9	1.691
CM1_M	11.0	0.4	1.200
CM2_D	8.1	0.5	0.884
CM2_M	3.5	0.1	0.382
CM3_D	29.9	1.4	3.262
CM3_M	12.5	0.4	1.364
CM4_D	3.0	0.2	0.327
CM4_M	0.0	0.0	0.000

* *denotes dry cured specimens*

** *denotes moist cured specimens*

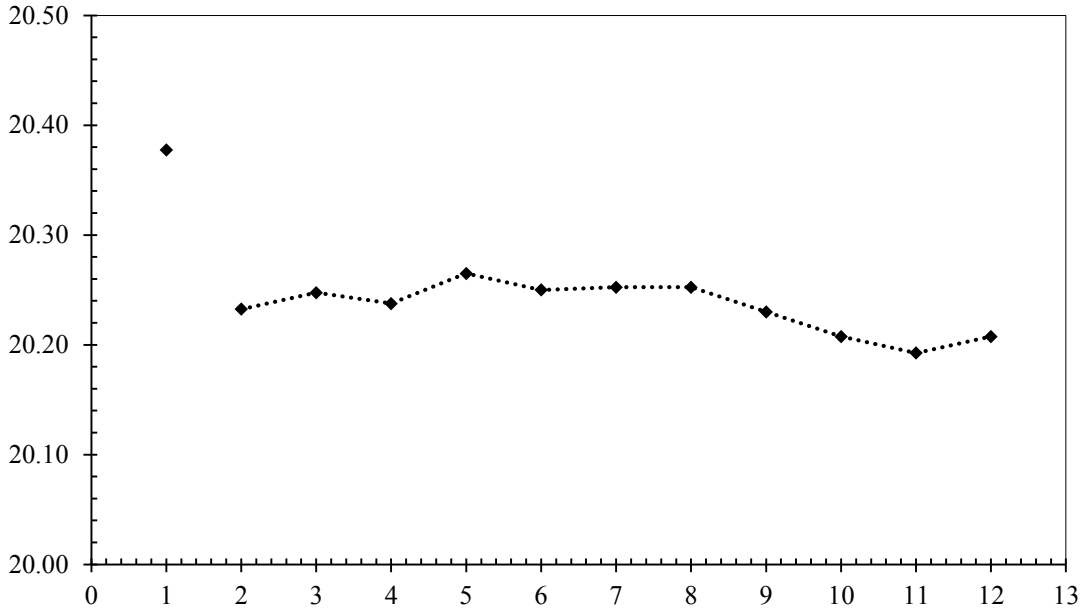

Figure A.8: Variation of temperature in the carbonation chamber

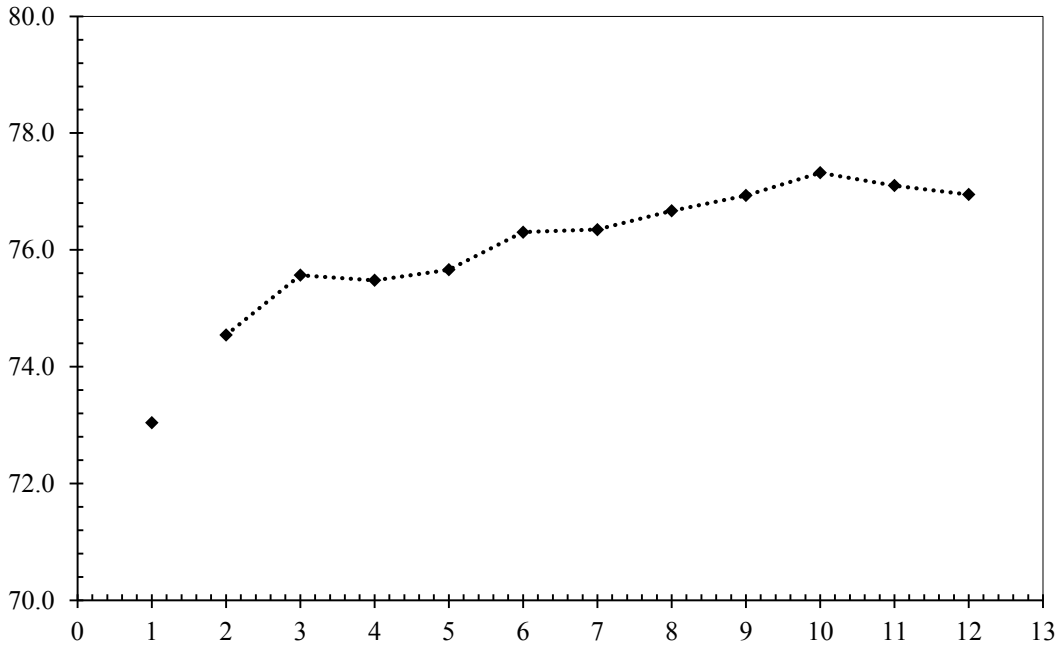

Figure A.9: Variation of relative humidity in the carbonation chamber

A.6 Oxygen permeability test results

Table A.6: OPI results showing the OPI values and the corresponding permeability coefficients of the mortar mixes.

Mix ID	Dry cured specimens		Moist cured specimens	
	OPI (log)	**k (x10^{-10} m/s)**	**OPI (log)**	**k (x10^{-10} m/s)**
PM45	10.21	0.62	10.25	0.56
PM60	9.64	2.30	10.24	0.58
SM45	9.62	2.40	10.61	0.24
SM60	9.88	1.30	10.04	0.91
CM1	9.54	2.90	10.00	1.00
CM2	10.08	0.84	10.51	0.31
CM3	9.55	2.80	9.75	1.80
CM4	10.57	0.27	10.61	0.25

Appendix B: Summarised procedures for tests and data analysis

B.1: Summarised procedure for potentiometric titration in bulk diffusion test

A. Reagents

i) Silver nitrate (0.1M $AgNO_3$) – dissolve 16.99 g in 1.0 litre of distilled water
ii) Nitric acid (1.0M HNO_3)
iii) Sodium acetate (NaOAc)

B. Test procedure

1. Mechanically grind the dry concrete/mortar sample to fine powder.
2. Place the powdered sample in a sealed Ziploc* bag.
3. Measure approximately 2.1 to 2.5 (to the nearest milligram) of the powdered sample.
4. Place the measured powdered sample (2.1 to2.5g) in a 100 mL plastic titration beaker and disperse with a little distilled water just to cover the sample.
5. Slowly add 2.0 mL of nitric acid to the sample and slowly swirl the beaker to bring the concrete powder into suspension.
6. Leave the solution to stand in the laboratory (temperature: 23 ˚C, relative humidity: 50%) for at least 30 minutes and then add 2.5 mL of NaOAc.
7. Fill the beaker to the 60 mL mark with distilled water and titrate using silver nitrate.
8. Run a blank test (using distilled water) following the procedure described above with the same reagents, but without sample i.e. without powdered concrete or mortar.
9. The titration is performed using a commercial Mettler Toledo DL50 automatic titration machine.
10. At the end of the titration process (when the end-point is reached), the machine will print out the results.

C. Results/Calculations

1. From the print-out obtained at the ned of the titration process, record the following values for each sample tested:
   a) Mass of sample (powder) used (g)
   b) Volume of $AgNO_3$ consumed (mL) – labelled "R1" in the print out
2. Use the Excel spreadsheet to compute the total chloride content as a percentage:
   a) By mass of the concrete or mortar sample, and
   b) By mass of cement in the concrete or mortar samples

B.2: Summarized procedure for regression analysis

The effective chloride diffusion coefficient (D_{eff}) and the surface chloride content (C_s) were estimated by regression analysis using an MS Excel spreadsheet template. Figure A.4 to A.7 show the results of this analysis. The guidelines specified in ASTM C1556-04 were followed as outlined below:

a) The chloride ion content (C_x) of the powder samples was determined by potentiometric titration (in mass %).
b) The measured chloride contents at each profile layer was plotted against the depth of profile as shown in Figure A.10, in an MS Excel spreadsheet template. The best-fit curve was then plotted on the same curve.

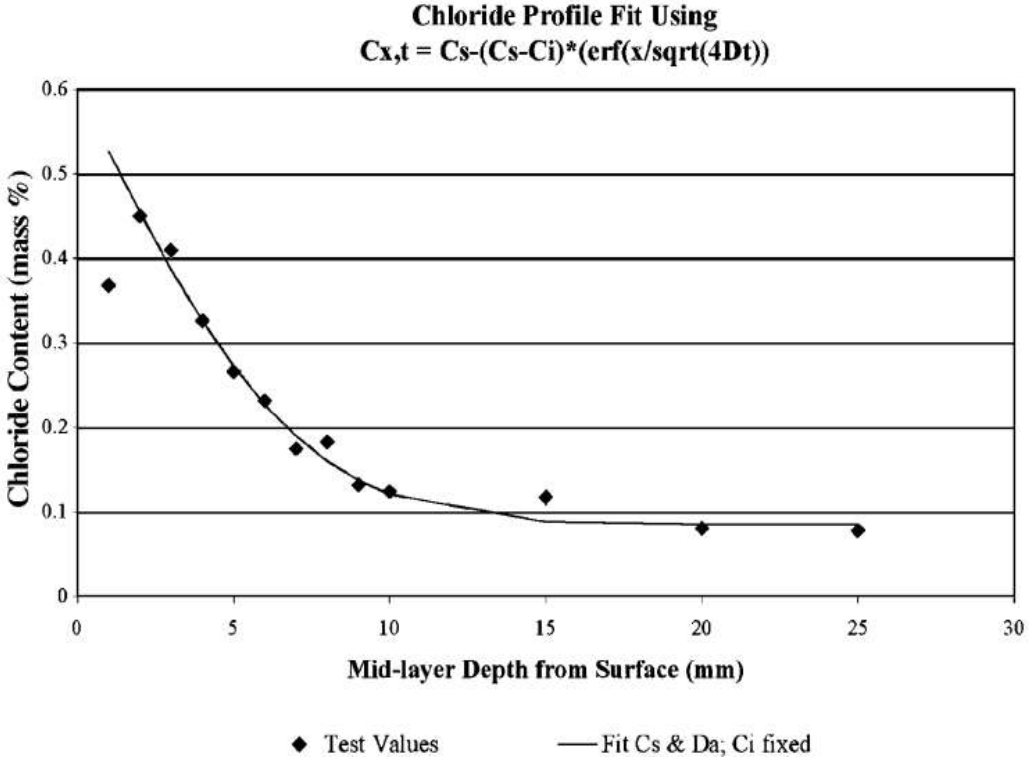

Figure A.10: A plot of chloride content versus profile depth

c) C_s was determined by projecting the curve backwards to estimate the most probable value of C_x at zero depth from the surface.
d) D_{eff} was calculated by the MS Excel spreadsheet template using the equation of Fick's second law of diffusion.

Appendix C: Salient details of the commercial repair products used

The details provided in this section are summarised from the manufacturer's product data sheets: Sika SA (Pty) Ltd., 2010, 2012a, 2012b and 2012c.

C.1 Sika® MonoTop®-612: Wet sprayed/hand placed fibre reinforced repair mortar

Product description:	Cementitious, polymer modified, low permeability mortar containing silica fume and synthetic fibre reinforcement.
Chemical base:	Cement and crystalline free silica aggregate
Density:	Approximately 2.1 kg/litre fresh mortar
Compressive strength:	(23 °C/50% RH) 10 N/mm^2 @ 1 day 40 N/mm^2 @ 28 day

C.2 Sika® MonoTop®-615 HB: High build repair and reprofiling mortar

Product description:	Cementitious, polymer modified, one component repair and reprofiling mortar containing silica fume.
Chemical base:	Cement and crystalline free silica aggregate
Density:	Approximately 1.65 kg/litre fresh mortar
Compressive strength:	(23 °C/50% RH) 35 – 40 N/mm^2

C.3 Sika® Rep LW: Non-sag patching and repair mortar

Product description:	One component, non-sag, cement based, multi-purpose patching and repair mortar.
Chemical base:	Cement and crystalline free silica aggregate
Density:	1.6 – 1.7 kg/litre
Compressive strength:	12 N/mm^2 @ 24 hours, 31 N/mm^2 @ 7 days, 43 N/mm^2 @ 28 days

C.4 Sikacrete®-214: Free-flowing structural repair concrete

Product description:	One component, free-flowing, high strength, cement based concrete with a maximum aggregate size of 9 mm.
Chemical base:	Cement, crystalline free silica, aggregate and additives
Density:	2.3 – 2.4 kg/litre
Compressive strength:	34 N/mm^2 @ 1 day, 55 N/mm^2 @ 7 days, 75 N/mm^2 @ 28 days

Appendix D: EBE Faculty: Assessment of Ethics in Research Projects

Any person planning to undertake research in the Faculty of Engineering and the Built Environment at the University of Cape Town is required to complete this form before collecting or analysing data.When completed it should be submitted to the supervisor (where applicable) and from there to the Head of Department. If any of the questions below have been answered YES, and the applicant is NOT a fourth year student, the Head should forward this form for approval by the Faculty EIR committee: submit to Ms Zulpha Geyer (Zulpha.Geyer@uct.ac.za; ChemEngBuilding, Ph021 650 4791).
NB: A copy of this signed form must be included with the thesis/dissertation/report when it is submitted for examination

This form must only be completed once the most recent revision EBE EIR Handbook has been read.

Name of Principal Researcher/Student: Ezekiel Kusimba Arito Department: Civil Engineering

Preferred email address of the applicant: arteze001@myuct.ac.za

If a Student: Degree: MSc Supervisor: Assoc. Prof. Beushausen

If a Research Contract indicate source of funding/sponsorship: CoMSIRU

Research Project Title: Performance requirements for patch repair mortars

Overview of ethics issues in your research project:

Question 1: Is there a possibility that your research could cause harm to a third party (i.e. a person not involved in your project)?	YES	NO X
Question 2: Is your research making use of human subjects as sources of data? If your answeris YES, please complete Addendum 2.	YES	NO X
Question 3: Does your research involve the participation of or provision of services to communities? If your answeris YES, please complete Addendum 3.	YES	NO X
Question 4: If your research is sponsored, is there any potential for conflicts of interest? If your answeris YES, please complete Addendum 4.	YES	NO X

If you have answered YES to any of the above questions, please append a copy of your research proposal, as well as interview schedules or questionnaires (Addendum 1) andplease complete further addenda as appropriate. Ensure that you refer to the EiR Handbook to assist in completing the documentation requirements for this form.

I hereby undertake to carry out my research in such a way that

- there is no apparent legal objection to the nature or the method of research; and
- the research will not compromise staff or students or the other responsibilities of the University;
- the stated objective will be achieved, and the findings will have a high degree of validity;
- limitations and alternative interpretations will be considered;
- the findings could be subject to peer review and publicly available; and
- I will comply with the conventions of copyright and avoid any practice that would constitute plagiarism.

Signed by:

	Full name and signature	Date
Principal Researcher/Student:	Ezekiel Kusimba Arito Signed	10/02/2016

This application is approved by:

Supervisor (if applicable):	Prof. Hans Beushausen Signed	10/02/2016
HOD (or delegated nominee): *Final authority for all assessments with NO to all questions and for all undergraduate research.*	Signed	11/2/16
Chair : Faculty EIR Committee For applicants other than undergraduate students who have answered YES to any of the above questions.		